THE UNIVERSITY OF
WARWICK

Library Declaration and Deposit Agreement

1. STUDENT DETAILS

Please complete the following:

Full name: ..... CARLOS ..... MORENO .....

University ID number: ..... 1153410 .....

2. THESIS DEPOSIT

2.1 Under your registration at the University, you are required to deposit your thesis with the University in BOTH hard copy and in digital format. The digital copy should normally be saved as a single pdf file.

2.2 The hard copy will be housed in the University Library. The digital copy will be deposited in the University's Institutional Repository (WRAP). Unless otherwise indicated (see 2.6 below), this will be made immediately openly accessible on the Internet and will be supplied to the British Library to be made available online via its Electronic Theses Online Service (EThOS) service.
[At present, theses submitted for a Master's degree by Research (MA, MSc, LLM, MS or MMedSci) are not being deposited in WRAP and not being made available via EthOS. This may change in future.]

2.3 In exceptional circumstances, the Chair of the Board of Graduate Studies may grant permission for an embargo to be placed on public access to the thesis **in excess of two years**. This must be applied for when submitting the thesis for examination (further information is available in the *Guide to Examinations for Higher Degrees by Research.*)

2.4 If you are depositing a thesis for a Master's degree by Research, the options below only relate to the hard copy thesis.

2.5 If your thesis contains material protected by third party copyright, you should consult with your department, and if appropriate, deposit an abridged hard and/or digital copy thesis.

2.6 Please tick one of the following options for the availability of your thesis (guidance is available in the *Guide to Examinations for Higher Degrees by Research)*:

☑ Both the hard and digital copy thesis can be made publicly available immediately

☐ The hard copy thesis can be made publicly available immediately and the digital copy thesis can be made publicly available after a period of two years (*should you subsequently wish to reduce the embargo period please inform the Library*)

☐ Both the hard and digital copy thesis can be made publicly available after a period of two years (*should you subsequently wish to reduce the embargo period please inform the Library*)

☐ Both the hard copy and digital copy thesis can be made publicly available after _____ (insert time period in excess of two years). **This option requires the prior approval of the Chair of the Board of Graduate Studies (see 2.3 above)**

The University encourages users of the Library to utilise theses as much as possible, and unless indicated below users will be able to photocopy your thesis.

☐ I **do not** wish for my thesis to be photocopied

3. GRANTING OF NON-EXCLUSIVE RIGHTS

Whether I deposit my Work personally or through an assistant or other agent, I agree to the following:

- Rights granted to the University of Warwick and the British Library and the user of the thesis through this agreement are non-exclusive. I retain all rights in the thesis in its present version or future versions. I agree that the institutional repository administrators and the British Library or their agents may, without changing content, digitise and migrate the thesis to any medium or format for the purpose of future preservation and accessibility.

4. DECLARATIONS

I DECLARE THAT:

- I am the author and owner of the copyright in the thesis and/or I have the authority of the authors and owners of the copyright in the thesis to make this agreement. Reproduction of any part of this thesis for teaching or in academic or other forms of publication is subject to the normal limitations on the use of copyrighted materials and to the proper and full acknowledgement of its source.

- The digital version of the thesis I am supplying is either the same version as the final, hard-bound copy submitted in completion of my degree once any minor corrections have been completed, or is an abridged version (see 2.5 above).

- I have exercised reasonable care to ensure that the thesis is original, and does not to the best of my knowledge break any UK law or other Intellectual Property Right, or contain any confidential material.

- I understand that, through the medium of the Internet, files will be available to automated agents, and may be searched and copied by, for example, text mining and plagiarism detection software.

- At such time that my thesis will be made publically available digitally (see 2.6 above), I grant the University of Warwick and the British Library a licence to make available on the Internet the thesis in digitised format through the Institutional Repository and through the British Library via the EThOS service.

- If my thesis does include any substantial subsidiary material owned by third-party copyright holders, I have sought and obtained permission to include it in any version of my thesis available in digital format and that this permission encompasses the rights that I have granted to the University of Warwick and to the British Library.

5. LEGAL INFRINGEMENTS

I understand that neither the University of Warwick nor the British Library have any obligation to take legal action on behalf of myself, or other rights holders, in the event of infringement of intellectual property rights, breach of contract or of any other right, in the thesis.

Please sign this agreement and ensure it is bound into the final hard bound copy of your thesis, which should be submitted to Student Reception, Senate House.

Student's signature: 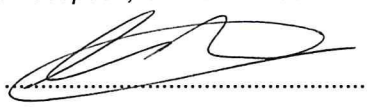 Date: 21/06/2016

Identification, Test and Performance Prediction of a Novel Energy Absorbing Mechanism for Railway Vehicles

by

Carlos Moreno

Innovation Report

Submitted to the University of Warwick

in partial fulfilment of the degree of

Doctor of Engineering

WMG

March 31, 2015

Abstract

Regulation requires railway energy absorbers to dissipate the collision energy and to prevent overriding. There is no industrial consensus about which energy absorbing mechanism is the most suitable for the crash conditions present in a collision between railway vehicles. There is scope for improving the existing designs or creating new concepts.

The combination of two energy absorption mechanisms, expansion and splitting of cylindrical tubes, was identified as an improved energy absorption mechanism. Quasi-static and dynamic testing of scaled splitting, expansion and expansion-splitting (hybrid) tubes was carried out to assess their force, stroke, energy absorption and oblique loading efficiency. In addition, the standard requires a calibrated numerical model of the energy absorber to predict its behaviour. The fracture strain of the tube and the coefficient of friction between the tube and the die are needed to build accurate numerical models. The fracture strain was measured using a Digital Image Correlation technique and a new methodology was developed to overcome its limitations. The inclusion of the fracture strain correctly predicted the deformation of the splitting specimens. The friction coefficient was adjusted until the energy absorption matched that observed during testing.

Quasi-static testing showed that the force efficiency was 80%, 100% and 90%, for the splitting, expansion and hybrid tubes respectively. The stroke efficiency was measured as 77%, 44% and 70%, respectively. The energy absorption efficiency of the hybrid tubes was assessed as 11% and 40% higher than that of the splitting and expansion tubes respectively. The testing also showed that the hybrid tubes were more insensitive than the expansion and splitting tubes to the application of oblique loading. More testing may be necessary to confirm this assertion. The results suggest that the hybrid energy absorbing mechanism could become a commercial energy absorber with improved performance over the existing solutions. The validation of the hybrid numerical models showed an accurate prediction of the test results.

A full-scale hybrid demonstrator has been tested and a patent of the hybrid concept applied for.

Declaration

This innovation report is submitted to the University of Warwick in support of my application for the degree of Engineering Doctorate. It has been composed by myself and has not been submitted in any previous application for any degree. The work presented (including data generated and data analysis) was carried out by the author.

Engineering Doctorate Mentors

Academic Mentors: Professor Richard Dashwood, Dr Darren Hughes

Industrial Mentor: Dr Terry Williams

Acknowledgements

I would like to express my deepest thanks to my supervisors Professor Richard Dashwood, Dr Darren Hughes and Dr Terry Williams for their assistance. I would like to thank the EPSRC, Warwick University and Oleo International for kindly funding this programme. I would also like to thank Dr Li Han for recruiting me for this programme.

Much gratitude to the following, who were so helpful and supportive: Richard Beaumont, Neill Raath, Sanjeev Sharma, Scott Taylor, Beth Middleton, Iain Masters, Sumit Hazra, Neil Reynolds, Dave Williams, the rest of the Materials and Manufacturing Group and the workshop staff.

To my parents Sebastian and Maria Dolores and my sister Eukene, to whom I owe so much.

Finally, to my loving wife Natallia and very best friends Sophia and Nikolai, without whom nothing would make sense.

Contents

List of Tables

List of Figures

Abbreviations

BS	British Standards
SEA	Specific Energy Absorption
FEA	Finite Element Analysis
DIC	Digital Image Correlation
DPH	Diamond Pyramid Hardness

1 Introduction to Railway Vehicles Energy Absorbers, Regulatory Requirements and Objectives of the Project

Fatalities and injuries are undesired consequences of transportation. In railway transportation accidents continue to happen, despite advances in active safety devices and methods designed to avoid accidents and crashes. Active safety is defined as those safety systems, such as signalling or brakes, which aim to prevent collisions. Therefore, railway vehicles are subject to strict crashworthiness regulations, which deal with railway passive safety. Passive safety is defined as those systems in place, such as energy absorbers, seatbelts, airbags or personal protective equipment, intended to protect passengers, drivers and goods in the case of a collision.

Crash energy management has been applied to railway vehicles since the 1970s. Before that, vehicle and passenger protection was achieved by means of adding stiffness to the vehicle structure. The vehicle was required to withstand a particular loading with negligible deformation, once the recoverable buffers had been exceeded. Without crash zones dissipating energy and transferring lower loads to the vehicle's compartment, damage would be primarily located at the point of impact. Therefore the crash might lead to fatalities and serious injuries, as the passenger area is crushed. Energy absorbers were introduced to dissipate energy and to protect the vehicle and passengers. Nowadays, energy absorbers are part of the standard crashworthiness requirements.

1.1 The Need for This Project

Any energy absorber for railway vehicles needs to comply with the current crashworthiness requirements. Standards BS EN 15227 (British Standards, 2010b) and 12663 (British Standards, 2010a) detail the railway vehicles crashworthiness requirements. The focus of the protective measures specified in BS EN 15227 is on the energy absorption requirements and overriding prevention. These requirements are quantified in terms of energy absorption by specifying that an approaching train unit must be able to maintain its integrity (and avoid overriding and derailment) when colliding with a stationary similar train unit at 36 km/h (worst case scenario). The determination of the energy involved in the collision requires the

knowledge of the train unit mass. Since there are many different train units and vehicles, the energy calculation needs to be performed 'ad hoc' for each train unit design.

Table 1 shows an estimate of energy absorption requirement for different leading vehicle masses. The magnitude of the railway collision energy absorption requirement is stated. For example, 2.6 MJ of energy needs to be dissipated on a 50 tonnes leading vehicle collision at 60 km/h.

	30t	**35t**	**40t**	**45t**	**50t**	**55t**	**60t**	**65t**
LEADING END (FRONT) [kJ]	1562	1822	2083	2343	2604	2864	3125	3385
INTERMEDIATE END [kJ]	640	747	854	960	1067	1174	1281	1388

Table 1: Energy absorption requirements for vehicles masses in a 60 km/h collision (Lu, 2002), located at the front end of the vehicle and at the intermediate interfaces

BS EN 12663 specifies the maximum loads which energy absorbers might transmit to the different railway vehicle structures. The maximum admissible longitudinal loads in buffers/couplings area are shown in Table 2.

LOCOMOTIVES	**PASSENGER ROLLING STOCK**				
CATEGORY L	**CATEGORY P-I**	**CATEGORY P-II**	**CATEGORY P-III**	**CATEGORY P-IV**	**CATEGORY P-V**
2000	2000	1500	800	400	200

Table 2: Loads transmitted to the buffers and/or coupler attachment [kN] (British Standards, 2010a)

A typical energy absorber dissipates energy through material plastic deformation. The energy dissipated is determined by the energy absorber reaction force and the device stroke. (Scholes, 1987) proposed an ideal force-displacement diagram, based on older load specifications, which a railway vehicle energy absorber should exhibit, Figure 1. For a Category P-I vehicle (Table 2), based on the 2000 kN limit load and the 2.6 MJ of collision energy at the leading end of a 50 tonnes rail vehicle, and assuming 100% force efficiency (mean to peak forces ratio), the length of the energy absorber must be about 1.3 m.

In addition, railway vehicles need to incorporate means of preventing overriding. Overriding is the undesirable situation when relative vertical movement between colliding railway vehicles occur. The underframe of one of the colliding vehicles may override the

underframe of the other. BS EN 15227 (British Standards, 2010b) requires that one wheelset of every vehicle bogie should keep in contact with the track throughout the collision. The magnitude of the transverse load that the energy absorber is subjected to is inherent to each particular colliding railway unit. However, although the standard does not specify the magnitude of the vertical load, a value of 150 kN is widely used in industry for anti-climbing energy absorber units design process, as stated by (Huss, 2005).

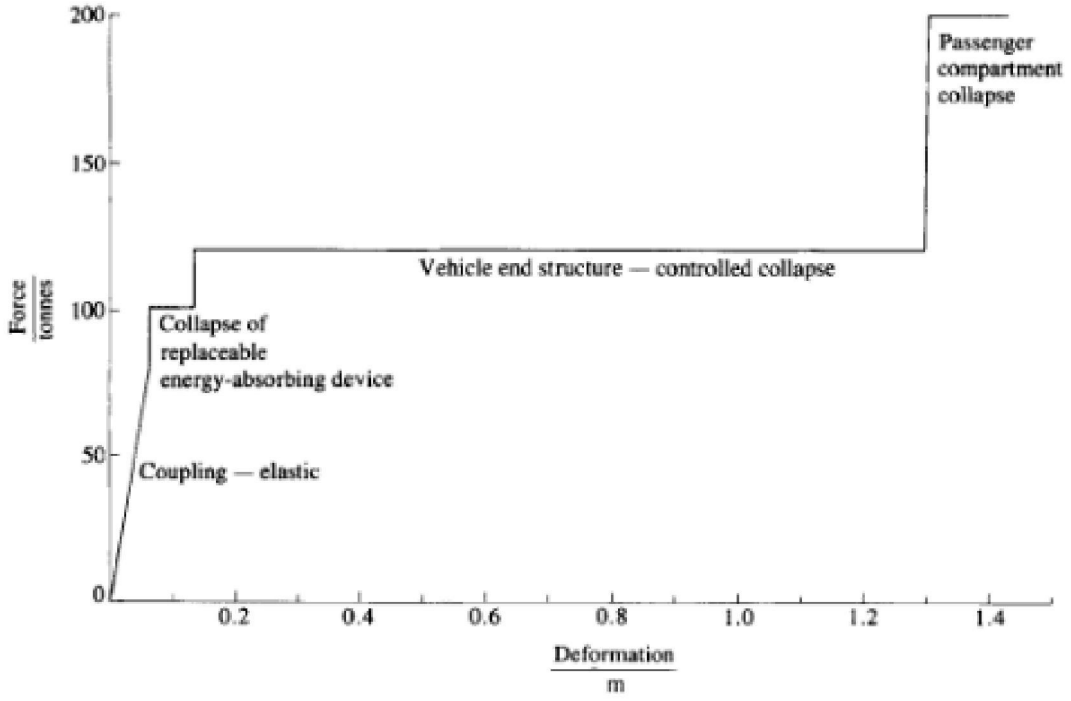

Figure 1: Ideal force-displacement diagram of vehicle end structure (Scholes, 1987)

Therefore, specialist energy absorber providers need to integrate into their products a number of challenging, and often contradicting, requirements. As shown above, the energy to dissipate can be very large. However, the energy absorber is to exhibit a maximum load, limited by the structural integrity of the vehicle the energy absorber is protecting. Longer strokes are then required, which may clash with the space limitations imposed by the railway vehicle manufacturers. Therefore, large force efficiencies are sought, which are often at odds with the stroke efficiency the energy absorber may exhibit, as will be shown in section 2.1.

As it will be shown in chapter 2, there are available a large number of different commercial energy absorbers, based on different energy absorption technologies. The industry has not been able to identify a design concept which clearly outperforms all other energy absorber

designs. There is no agreement about which underlying energy absorption mechanism is the best suited to railway crash conditions. Thus, there is scope to identify a novel concept or a modified existing concept capable of fulfilling the standard requirements in an improved manner.

1.2 Objectives of This Research

The final objective of this project is to provide the sponsor company, Oleo International, with an innovative energy absorbing mechanism concept which improves the performance over existing designs. Proof of this improvement must be provided by means of physical testing. In addition, as required by the standard BS EN 15227 (British Standards, 2010b), simulation techniques must be developed and a numerical model must be calibrated, capable of accurately predicting the behaviour and performance of the proposed concept.

In order to achieve these objectives, a series of intermediate objectives were identified.

- Identification of a potential improved energy absorber concept by means of a rigorous theoretical assessment
- Physical testing of the potential improved concept
- Comparison of the performance
- Development of the a numerical model of the improved energy absorber concept, calibrated against the result of the physical testing

1.3 Portfolio and Structure of This Report

This chapter has discussed the motivation for this Engineering Doctorate. Chapter 2 discusses the state of the art of the available commercial railway energy absorbers and the scientific literature of the underlying energy absorbing mechanism. Chapter 4 states the methodology used to achieve the proposed objectives. Chapters 5 and 6 detail the experimental and simulation activity respectively. Chapter 7 discusses the main outcomes of the experimental and simulation work carried out. Chapter 8 outlines the main conclusions of the project, including suggestions for further work. Table 3 lists the portfolio submissions completed during this EngD. The table states where in this Innovation Report the portfolio submissions are covered.

N°	PORTFOLIO SUBMISSION TITLE	REPORT SECTION
1	Railway vehicle energy absorber requirements; energy absorption mechanisms and existing applications to railway industry	2
2	Selection Process of Suitable Energy Absorption Mechanism for Railway Vehicle Crashworthiness Applications	2
3	Axial Splitting of Metal Tubes: Static and Dynamic Testing and Simulation Correlation	3
4	Determination of the Fracture Behaviour of Axial Splitting Tubes and the Numerical Prediction of Their Energy Absorption Capabilities (paper published in the International Journal of Crashworthiness)	4, 5, 6 & 7
5	Radial Expansion of Metal Tubes: Static and Dynamic Testing and Simulation Correlation	4, 5, 6 & 7
6	Hybrid Expansion/Splitting Tubes: Static and Dynamic Testing and Simulation Validation	4, 5, 6 & 7
7	Quasi-Static and Dynamic Testing of Splitting, Expansion and Hybrid Tubes under Oblique Loading Conditions, and Results Comparison	4, 5, 6 & 7
8	Quasi-static Testing of Full-scale Demonstrator of the Hybrid Tubes at Oleo International	7

Table 3: Details of the portfolio submissions and correlation with the chapters in this document

2 Literature Review: Performance Assessment Criteria and Commercial Energy Absorbers used in the Railway Industry

The standard requirements for railway vehicles energy absorbers were introduced in section 1.1. It is worth stressing that, in order to protect the railway vehicle and passengers, BS EN 12663 (British Standards, 2010a) limits the maximum load transferred by the energy absorber to the vehicle during the collision. For these specific requirements, the most suitable assessment parameters have been identified.

2.1 Energy Absorbers Assessment Criteria (Submission 1)

Force and displacement are the main parameters that determine the performance of an energy absorber. The objective is to achieve the ideal force-displacement response shown in the diagram of Figure 1. The assessment metric which best captures this is the force efficiency, i.e. the ratio of mean force to peak force. In addition, in response to the standard overriding prevention requirements, a method to assess overriding performance must be found. An additional requirement is the necessity for compactness, as demanded by railway vehicle manufacturers. In this case, the most appropriate assessment metric is the stroke efficiency. The stroke efficiency is the ratio of stroke to total length of the device.

2.1.1 Force Efficiency

The area under the force-displacement curve shows the energy absorbed by the device. In order to maximise the energy absorbed, it is desirable to design the energy absorber to exhibit a constant mean force over the crushing length. The mean force can be calculated as $F_{mean} = E / s$, where *E* is the total energy absorbed and *s* is the stroke. The force efficiency ratio, defined as $\eta_F = F_{mean} / F_{peak}$. Due to the maximum force limitation imposed by the Standard, the magnitude of the mean resistive force in an energy absorber must be as close as possible to the magnitude of the peak load. Figure 2 shows a schematic representation of the force-displacement of an energy absorber. The energy absorbed by an energy absorption device, the area under the load curve, can be compared to the potential maximum energy absorption, delimited by the peak load curve.

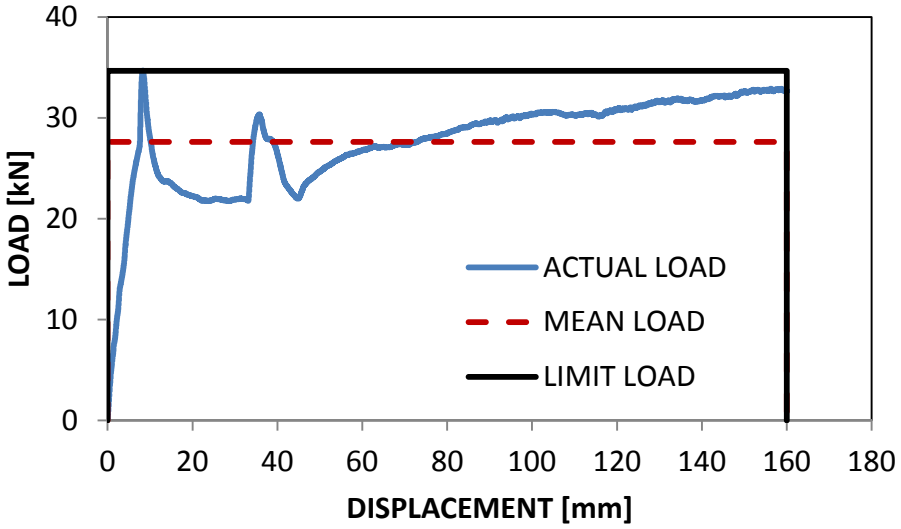

Figure 2: Comparison of energy absorbed by a device (area under the mean force curve) with the potential maximum energy absorption (area under the limit load curve, delimited by the peak load)

2.1.2 Stroke Efficiency

A device could crush over most of its length or require a design length several times longer than the actual stroke. Stroke efficiency is defined as $\eta_S = s/L$, where *s* is the stroke and *L*, the total length of the energy absorber. Ideally, an energy absorber would utilise as much of its length as practicable. However, 100% efficiency may not be feasible due to the residual material packed by the deformation force. Figure 3 shows typical stroke efficiency values for different energy absorbers.

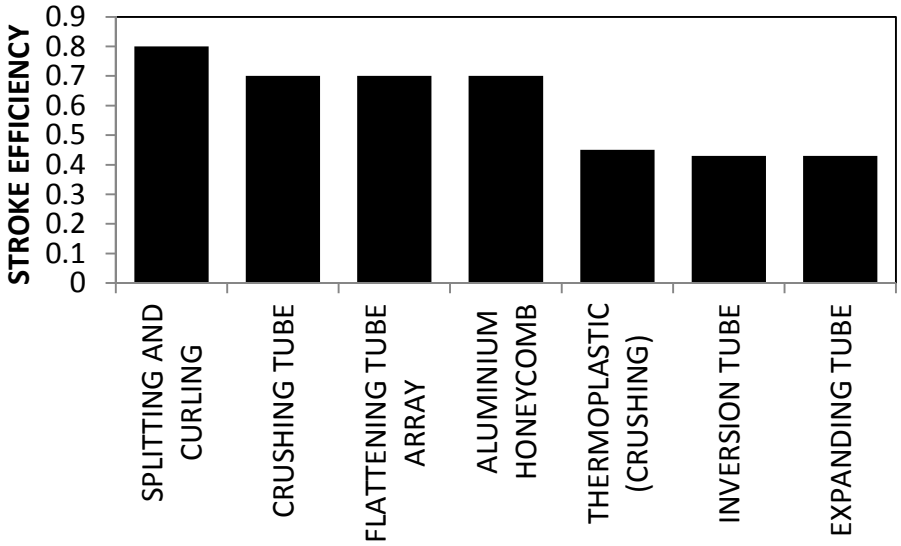

Figure 3: Stroke efficiency values for some energy absorbers (Jones, 1997)

2.1.3 Overriding Prevention Assessment Criteria

Standard BS EN 15227 establishes that the acceptance criterion for the overriding limitation is that the validation simulation demonstrates that, with an initial vertical offset of 40 mm at the point of impact (with the standing train unit at a lower level than the moving train unit) the criteria for deceleration and survival space are achieved.

The behaviour of energy absorbers subjected to oblique or off-axis loading differs for different energy absorbing mechanisms. (Huss, 2005) and (Nagel and Thambiratnam, 2006) confirmed that crumple columns, which exhibit 'steeply falling' force-displacement curves (Calladine and English, 1984), tend to reduce their mean resistive force and energy absorption as they are subjected to off-axis or oblique loading. However, 'flat-topped' energy absorbers, (Calladine and English, 1984), behave in a different manner to crumple columns.

The automotive industry pioneered the oblique loading testing of thin-walled crumple columns. As opposed to railway vehicles, cars can be hit at an angle. Crumple columns are used as energy absorbers at the front of cars and, therefore, the behaviour of crumple columns under transverse loading has been the subject of extended research. (Han and Park, 1999) stated that oblique load conditions were usually implemented in numerical models by impacting columns against an inclined rigid wall without friction. The outcome of these studies was to ascertain the decrease of the mean load when subjected to an increasing inclined rigid wall. This methodology allowed finding the critical angle at which a column collapse mode changes from progressive axial mode to global buckling collapse. Figure 4 shows typical deformation shapes of a crumple column subjected to progressive axial buckling (left) and subjected to oblique loading (right). The crumple column, crushed by the inclined, plate shows catastrophic global buckling collapse mode of the column.

(Nagel and Thambiratnam, 2006) used a test rig configuration which allowed the application of oblique loading to the energy absorber. The sample, a crumple column, was attached to the testing machine through a special rig designed to achieve the required inclined angle. The cross head lowered the sample onto the anvil or load-bearing surface to recreate the impact. Figure 5 shows this arrangement.

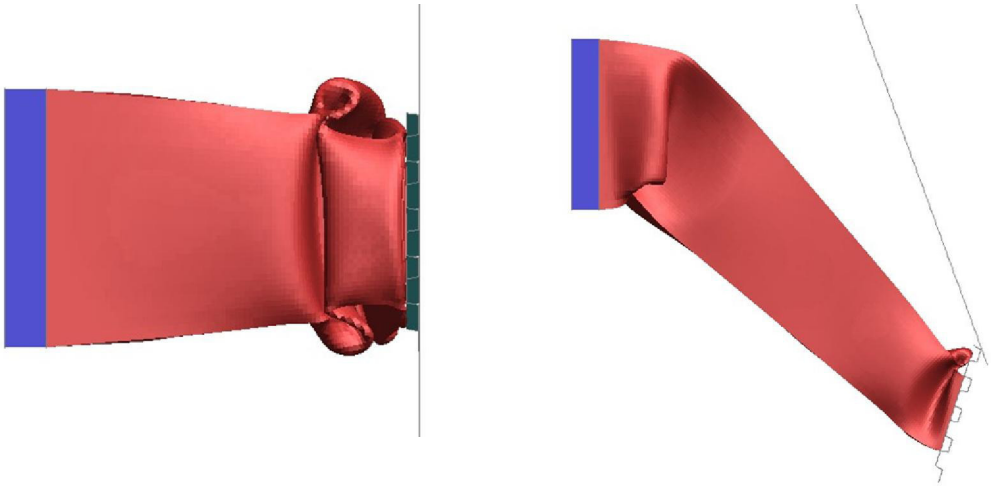

Figure 4: Progressive axial collapse (left) and catastrophic global buckling collapse (right) modes on a square tapered crash column

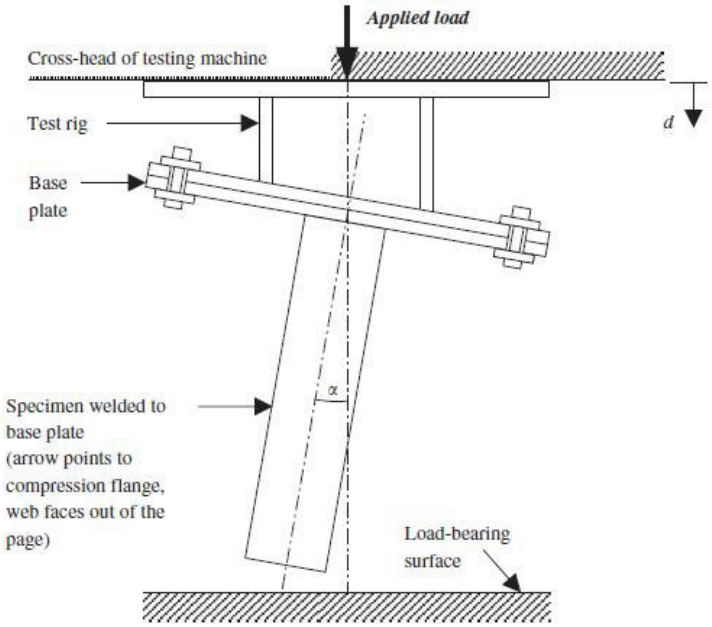

Figure 5: Inclined test rig and attached sample arrangement (Nagel and Thambiratnam, 2006)

(Børvik et al., 2003) devised a similar method to induce oblique loading onto crumple columns. The samples were clamped at the lower end, while the compression load was applied vertically downwards by a hydraulic actuator. The lower end was clamped to a semi-circular cradle capable of rotating to recreate any impact angle. Figure 6 shows this arrangement.

The issues regarding the overriding prevention assessment criteria and testing methodology will be further explored in chapter 4.

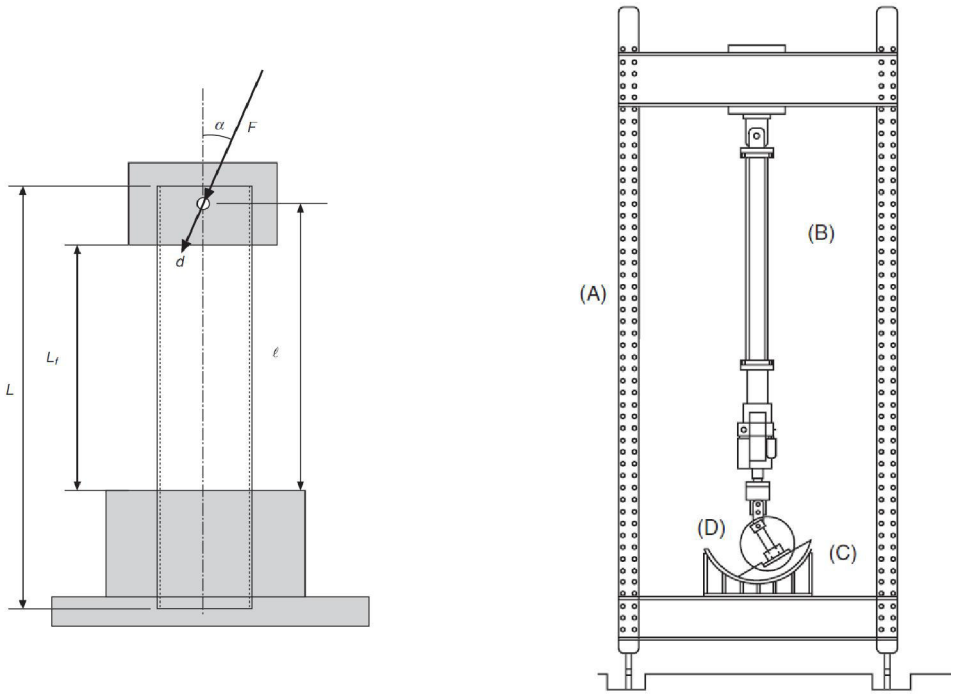

Figure 6: Clamped sample column detail (left) and test arrangement overview (right) of quasi-static testing of crumple columns subjected to oblique loading (Børvik et al., 2003)

2.2 State of the Art of Energy Absorbers in the Railway Industry (Submission 1)

(Calladine and English, 1984) identified two generic types of energy absorption structures, termed type I and type II. Type I, 'flat topped' energy absorbers exhibit constant force-displacement curve. Instead, type II energy absorbers exhibit an oscillating force-displacement curve, caused by the progressive buckling nature of the devices based on this energy absorption mechanism. Figure 7 shows the force-displacement characteristics of the two types. Due to the maximum admissible force limitation, type I energy absorbers are widely employed in the railway industry, as they maximise the dissipated energy per unit of stroke. However, the railway industry also utilises type II energy absorbers, such as crumple columns, as will be shown below.

This section reviews different energy absorption mechanisms and corresponding commercial application. There is a number of books that treat crashworthiness and energy absorption systems, (Johnson and Mamalis, 1978), (Jones, 1997) and (Lu and Yu, 2003). There is also a number of review papers on the subject, (Alghamdi, 2001) or (Olabi et al., 2007). The following is a review of the most relevant energy absorption mechanisms and applications.

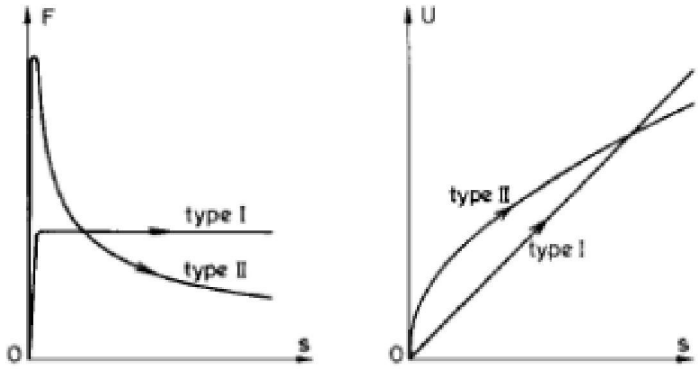

Figure 7: Force-displacement (left) and energy-displacement (right) for idealised type I and type II structures (Calladine and English, 1984)

2.2.1 Axial Crushing of Thin-walled Structures

Thin-walled tubes undergoing progressive buckling are among the most common collapsible energy absorbers (Alghamdi, 2001). Tubular crumple columns tend to exhibit force-displacement curves with an oscillating force, typical of the type II energy absorber shown in Figure 7 (Calladine and English, 1984). (Alexander, 1960), (Mamalis and Johnson, 1983), (Wierzbicki and Abramowicz, 1983) and (Abramowicz and Jones, 1997), among others, have extensively researched the behaviour of crumple columns.

Crumple columns are favoured by the automotive industry. Metallic tubes are easily manufactured. In addition, crumple columns are inherently lightweight, as they do not require heavy dies to crush them. For these reasons, crumple columns are universally accepted as the most suitable energy absorbers

However, crumple columns exhibit low force efficiency. Figure 8 shows a typical force-displacement response of a square tube subjected to axial loading. Periodic fluctuations, corresponding to fold formation, follow the initial high peak, forming the typical peak-and-trough curve. As explained in section 2.1.1, this property, coupled with the load limitation imposed to railway vehicles, leads to low force efficiency. For this reason, they are not so widely used by the railway industry. An example of railway application of this energy absorption mechanism is a design from Oleo International, shown in Figure 9.

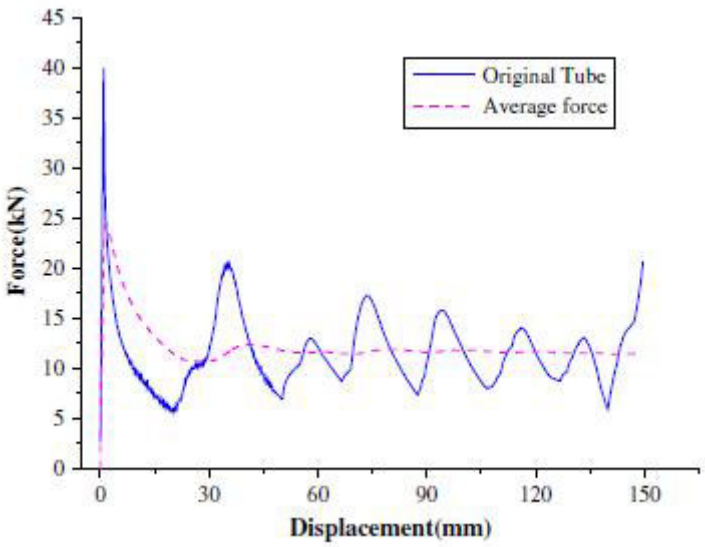

Figure 8: Typical square tube force-displacement properties (Zhang et al., 2009)

Figure 9: Oleo International crumple column design

2.2.2 Tube Inversion

Circular tubes are inverted by turning circular tubes inside out against a die, in order to absorb energy. Tube inversion can also be realised without a die, in which case the process is called free inversion. (Reid, 1993) studied the three collapse mechanisms for circular tubes, progressive buckling, inversion and splitting (which will be introduced below). The research confirmed that these tubes are energy absorbers of type I. Figure 10 shows inversion tubes at different stages of stroke (Reid, 1993). It can be noted that the stroke efficiency of inversion tubes is poor due to the non-collapsible nature of the stroked section of the tube.

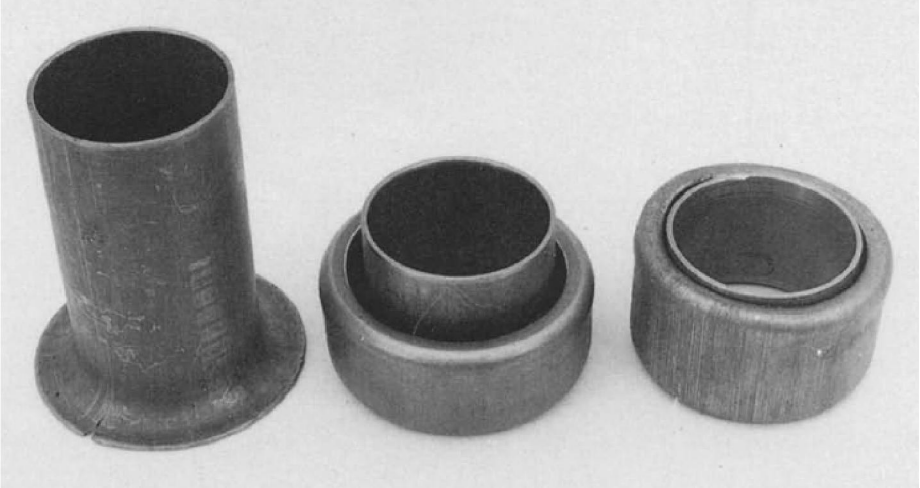

Figure 10: Inversion tubes at different stages of the inversion process (Reid, 1993)

2.2.3 Cellular Structures

Most common cellular materials are honeycombs and foams. Honeycombs and metallic foams are among the most widely used energy absorbers. Honeycombs display near regular force-displacement curve, once past the initial peak load.

Figure 11 shows the force-displacement curve for HexWeb honeycomb aluminium core (HEXCEL, 2012). An example of the application of this energy absorber in the railway industry is Dellner's D-BOX design, shown in Figure 12.

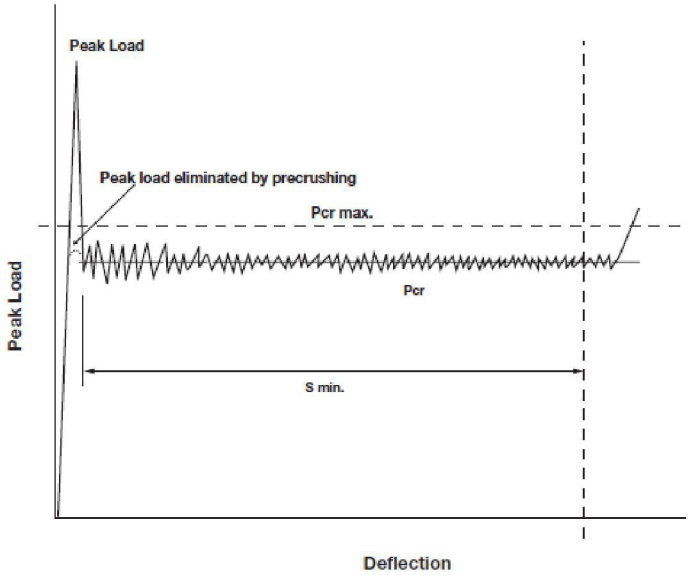

Figure 11: HEXCEL HexWeb honeycomb core force-displacement curve (HEXCEL, 2012)

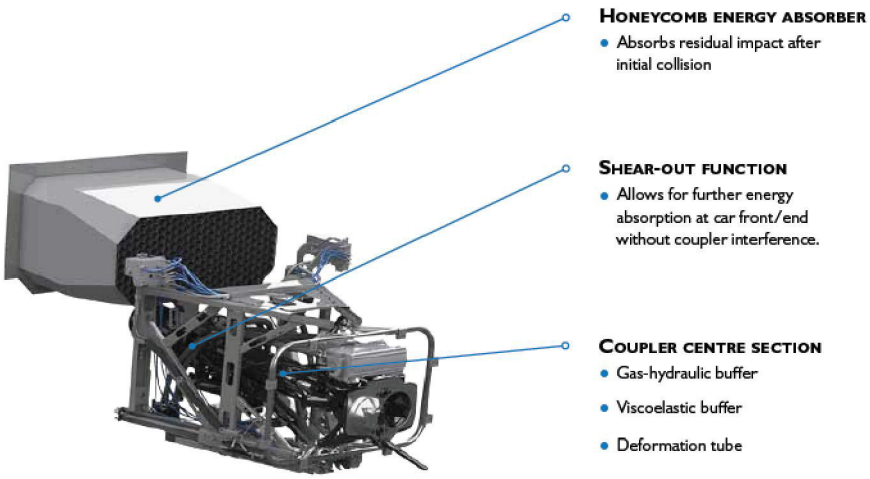

Figure 12: Dellner D-BOX crash energy absorbing concept

2.2.4 Struts

Strut systems are based on load carrying core elements embedded within a sleeve support. Figure 13 shows a schematic view of an energy absorber concept based on the strut technology (Mayville, 2001). This mechanism can be classified as type II energy absorber.

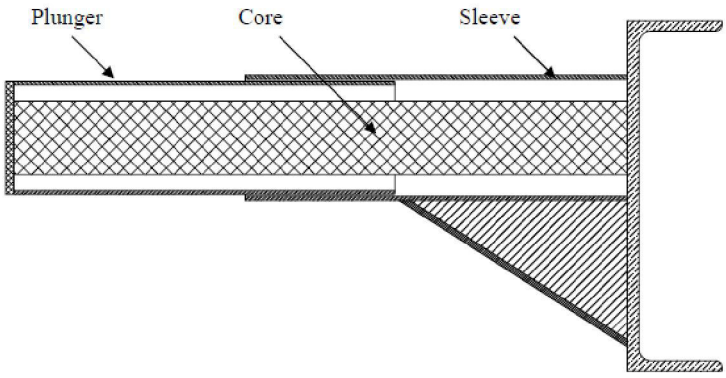

Figure 13: Schematic view of the strut energy concept (Mayville, 2001)

2.2.5 Cutting/Chipping

Energy can be absorbed by means of cutting or chipping metal. AXTONE Group provides an example of this technology applied to the railway industry, Figure 14. In this particular example, the energy is absorbed by cutting the exterior of telescoping metal tubes. These tubes do not collapse under the application of the impact load and, therefore, suffer from low stroke-efficiency ratios.

Figure 14: AXTONE Group AX-ZKL1 crash buffer (AXTONE)

2.2.6 Tube Splitting

The splitting of cylindrical or square tubes has been extensively researched, (Stronge et al., 1983) (Reddy and Reid, 1986) (Huang et al., 2002b, Huang et al., 2002c, Huang et al., 2002a, Cheng and Altenhof, 2005) (Yi Jin et al., 2006) (Jin et al., 2010) (Chung Kim Yuen et al., 2013). Splitting tubes are available as commercial railway energy absorbers Figure 15.

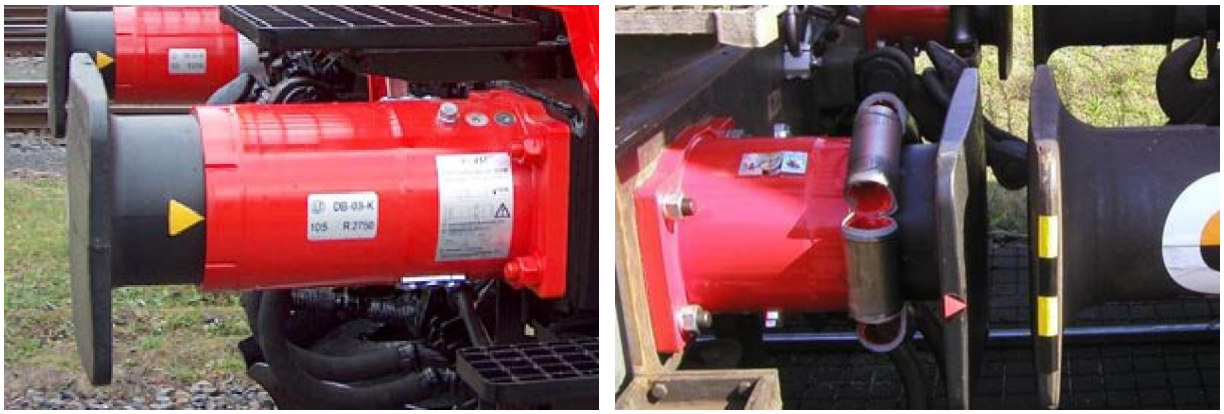

Figure 15: EST splitting crashbuffer (Schneider, 2002)

The resistive force offered by a splitting tube mainly depends on the flaring radius of the punching die. The radius can be reduced to increase the force. However, there is a limit of how much the radius can be reduced. When a critical flaring radius is reached, the process becomes unstable or tube inversion could occur instead.

Friction plays a significant part in the energy absorption mechanism of splitting tubes. However, the scientific literature does not agree on the value of the friction coefficient present in the die against tube contact. Table 4 summarises the quasi-static coefficients of friction quoted in the literature. It can be seen that there is little agreement about which is

the most realistic value of the friction coefficient. The dry friction coefficient ranges from 0.2 to 0.56, and the lubricated friction coefficient from 0.1 to 0.2.

FRICTION COEFFICIENT	**(Stronge et al., 1983)**	**(Reddy and Reid, 1986)**	**(Huang et al., 2002b)**	**(Yi Jin et al., 2006)**	**(Jin et al., 2010)**	**(Chung Kim Yuen et al., 2013)**
TUBE MATERIALS	Aluminium	Aluminium and Steel	Aluminium and steel	Aluminium	Aluminium	Aluminium
DRY	0.56	0.5	0.2	0.3	-	0.3
LUBRICATED	0.18	0.2	-	-	0.1	-

Table 4: Coefficients of friction present in the axial splitting of tubes as quoted in the literature

The literature is also sparse on the tube fracture prediction. The main research has been directed to finding the crack propagation energy (Cotterell and Reddel, 1977), (Mai and Cotterell, 1984), (Lu et al., 1994), (Lu et al., 1998). The crack propagation energy is useful in order to ascertain the proportion of energy which is dissipated by inhomogeneous plastic deformation around the splitting crack area. However, in order to predict the splitting tube performance through the use of numerical methods, such as FEA, the fracture strain of the material under the splitting conditions needs to be ascertained. (Ko et al., 2007) states that splitting tubes experience ductile fracture under plane stress conditions. This fracture mode has been the object of intense research (Rice and Tracey, 1969), (Johnson and Cook, 1985), (Wierzbicki et al., 2005), (Bao and Wierzbicki, 2004), (Xue, 2007). Fracture ductility is understood as the ability of a material to undergo large deformation without fracture. Ductile fracture of crack-free bodies is mainly dependent on the current values of components of the stress and strain tensors and their histories, (Wierzbicki et al., 2005). The fracture locus is represented as the fracture strain (dependent variable) versus a value representative of the stress state (independent variable). Figure 16 shows the shape of a typical fracture locus. Note that the independent variable in this case is the triaxiality (η), a widely used parameter used to describe the stress or strain state. It is measured as the ratio of hydrostatic (σ_m) and Von Misses equivalent stress ($\bar{\sigma}$). The ratio of the principal strains $\alpha = \varepsilon_2/\varepsilon_1$ can also be used to represent the stress state.

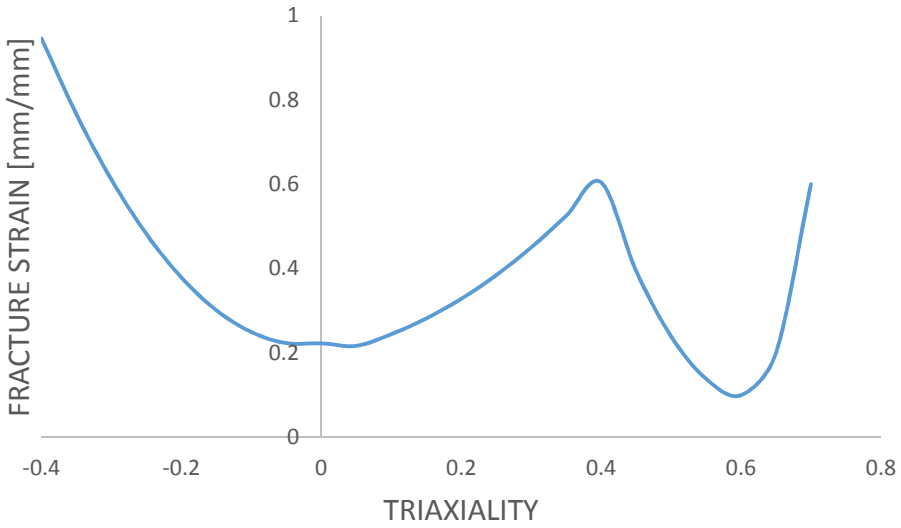

Figure 16: Typical fracture locus (Wierzbicki et al., 2005)

Both, the friction conditions between the punching die; and the stress state conditions (and associated fracture) around the splitting crack area must be found in order to produce an accurate numerical model of the splitting tube.

2.2.7 Radial Expansion

Radial expansion tubes are widely used energy absorbers in the railway industry. Owing to their non-collapsible nature, energy absorbers based on tube radial expansion are thought to be particularly well suited to resist any oblique loading while dissipating energy. However, for the same reason, the stroke-efficiency of the element is limited to a maximum of 50%, since there is a need for a die of length comparable to that of the tube, Figure 17 shows a commercial example of the application of expansion tubes.

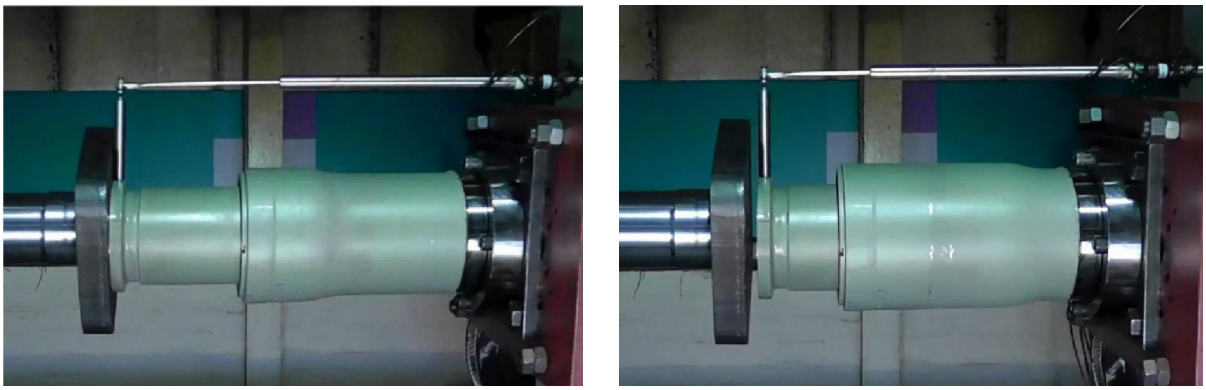

Figure 17: Oleo International deformation tube: un-deformed (left) and deformed (right) state

The literature coverage of expansion tubes is sparse (Lu, 2004), (Almeida et al., 2006), (Fischer et al., 2006), (Shakeri et al., 2007), (Ahn et al., 2008), (Karrech and Seibi, 2010), (Yang et al., 2010). Expansion tubes dissipate energy by means of plastic deformation and friction. Table 5 shows a summary of the quasi-static coefficients of friction quoted in the literature. Unlike splitting tubes, the scientific literature appears to agree that the coefficient of friction for lubricates tubes is small, of the order of $\mu = 0.05$.

	(Lu, 2004)	(Almeida et al., 2006)	(Shakeri et al., 2007)	(Ahn et al., 2008)	(Karrech and Seibi, 2010)	(Yang et al., 2010)
TUBE MATERIAL	Steel	Aluminium	Steel	-	-	Aluminium
COEFFICIENT OF FRICTION	0.20	0.02 (lubricated) 0.20 (dry)	0.05 (coated) 0.10 (dry) 0.25 (blasted)	0.05	0.05-0.35	0.05

Table 5: Friction coefficients quoted in the literature

2.2.8 Combined Radial Expansion-Splitting Tubes

(Ko et al., 2011) suggested a novel concept of a tearing tube based on expansion and splitting energy absorption mechanisms. Figure 18 shows a test conducted on the suggested tearing tube and die. The authors claimed that the resistive load increased by 30%, in comparison to the mean load of the expansion only stage of the energy absorber concept.

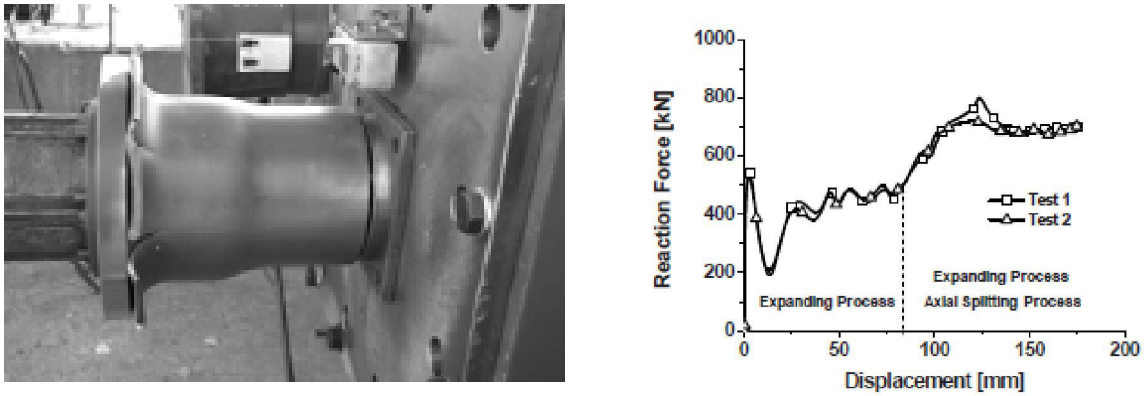

Figure 18: Crushed tearing specimen (left) and load-displacement response (right), (Ko et al., 2011)

2.3 Conclusion from the Review (Submission 1)

The literature showed that the most suitable assessment criteria for railway vehicles energy absorbers are force efficiency, stroke efficiency and overriding prevention performance.

However, there is no standard or agreement about the most suitable overriding prevention criteria to assess the energy absorbers. This will be explored in chapter 4.

The review of energy absorbers for railway vehicles showed that this is a dynamic subject and the design has not yet reached maturity. None of the existing energy absorption designs exhibit excellent performance in terms of the assessment criteria stated above. This suggests that there is scope for improving the existing designs or creating new concepts.

The literature review also highlighted that several characteristics of the underlying energy absorption mechanisms are not fully understood yet, particularly in the case of splitting tubes. There is a lack of information in the literature about two critical parameters which are necessary to predict accurately the behaviour of splitting tubes:

- Static and dynamic friction coefficients between the splitting tube and the die
- Fracture strain magnitude of the material as it splits under the loading of the die

It also would be sensible to confirm whether the friction coefficient quoted in the literature for radial expansion tubes is accurate.

3 Selection Methodology of the Most Suitable Energy Absorber (Submission 2)

A methodology is needed to assist the search for an improved concept of energy absorber for railway vehicles. (Rowell et al., 1999) and (Mullur et al., 2003) identified decision matrices as a particularly suitable methodology to perform this task. Another methodology, Total Design (Pugh, 1990), was found to be simpler to apply. This method does not use weights to accomplish concept comparison. Instead, it highlights the understanding of the requirements before the concepts are generated. (Woolley et al., 2000) included the use of the Total Design method in the development of a medical device. (Thakker et al., 2009) applied the method to the conceptual design of an impulse turbine for power generation from wave energy.

3.1 Application of the Total Design Method

The Total Design method comprises sequential activities: the market needs, the product design specification, the conceptual design, the detail design, manufacture and marketing. The scope of the project is not a finalised commercial product, but the demonstration of a different energy absorption mechanism with improved capabilities. Therefore, the following explanation will be constrained to the conceptual design selection.

The conceptual design phase comprises two stages: the generation of solutions and the evaluation of these solutions. The two stages are applied initially to the existing energy absorption mechanism. After the initial evaluation has been performed, the process is repeated. The most suitable design concept, selected after the initial evaluation, can be improved by trying to overcome its weaknesses. The strong features of the other designs might be incorporated into the selected design and improve its characteristics. The evaluation of proposed solutions will be accomplished by using the data available in the literature. There is no available data about the overriding prevention performance of most of the initially proposed concepts. For this reason, the comparison between the proposed conceptual solutions was carried out with the aid of finite element analysis.

The existing energy absorption mechanisms such as axial crumpling, inversion, splitting and radial expansion were used as the initial concepts. Since axial crumpling elements are

known to be unreliable under transverse solicitations, a modification of this energy absorption mechanism was included. A collapsible guiding mechanism was incorporated to the crumpling element.

The evaluation was aided with the construction of a selection matrix, shown in Table 6. The comparison was carried out on a 'better than' (+), 'worse than' (-) or 'same' (S) basis. The requirements related to the energy absorber performance were assigned double the score, (++), (--) and (SS). Table 6 shows the results of the evaluation. The number of (+), (-) and (S) were counted and it was found that the expansion tubes are equally suitable to the crumple columns. Splitting tubes were found to be the third most promising mechanism.

After the initial evaluation had been performed, the process was repeated where the advantageous features of the initial concepts were combined. Two concepts were conceived following this method: an expansion-splitting design concept and an expansion, splitting and crumpling design concept. The evaluation was performed again, using the expansion energy absorber as the datum, as shown in Table 7.

CONCEPTS CRITERIA	CRUMPLE	INVERSION	SPLITTING	EXPANSION	CRASH COLUMN + COLLAPSING GUIDING
FORCE EFFICIENCY	datum	++	++	++	SS
STROKE EFFICIENCY		--	SS	--	--
SPECIFIC ENERGY ABSORPTION		SS	--	SS	--
ANTICLIMBING BEHAVIOUR		SS	++	++	++
NUMBER OF PARTS		-	-	-	-
COST		-	-	-	-
STAND ALONE		S	S	S	S
EASE OF MANUFACTURING		-	-	-	-
MAINTENANCE		S	S	S	S
AESTHETICS		S	S	+	+
LIFE IN SERVICE		S	-	S	S
Σ +		2	4	5	3
Σ -		5	6	5	7
Σ S		8	5	5	5

Table 6: Initial Concepts Decision Matrix

CONCEPTS **CRITERIA**	EXPANSION	EXPANSION+ SPLITTING	EXPANSION+ SPLITTING+ CRUMPLING
FORCE EFFICIENCY	datum	SS	--
STROKE EFFICIENCY		++	++
SPECIFIC ENERGY ABSORPTION		++	++
ANTICLIMBING BEHAVIOUR		--	--
NUMBER OF PARTS		S	-
COST		+	-
STAND ALONE		S	S
EASE OF MANUFACTURING		-	-
MAINTENANCE		S	S
AESTHETICS		-	S
LIFE IN SERVICE		-	-
Σ +		5	4
Σ -		5	8
Σ S		5	3

Table 7: Enhanced Concepts Decision Matrix

The result of the second evaluation was that the datum (expansion tubes) and the expansion-splitting tubes were equally suitable.

3.2 Results of the Selection Method

There are not yet any commercial products based on the expansion-splitting technology. They have not been researched in any detail, and their performance is still largely unknown. Therefore, the expansion-splitting energy absorbing mechanism stands out as a potentially innovative energy absorber. These novel energy absorbers could be capable of fulfilling the standard requirements in a more efficient manner than the existing solutions. Therefore, the expansion-splitting tubes will be the research object of this project. The expansion-splitting tubes may be referred to as *hybrid* tubes in the text, for reasons of economy of space.

4 Experimental and Simulation Methodology

Chapter 2 highlighted the hybrid (expansion-splitting) tubes as a potentially improved energy absorber for railway vehicles. In addition, the lack of information about the friction regime between the die and the tube in tubes subjected to splitting was identified. The fracture strain and stress state around the splitting crack are also unknown. It is therefore necessary to research these particular areas of the splitting tubes performance. In addition, it may be necessary to confirm the information about the friction regime between the die and tube in tubes subjected to expansion.

In order to find these unknowns, splitting tubes were tested quasi-statically and dynamically. Finite Element Analysis (FEA) numerical models, representative of the testing, were built and the friction coefficient was inferred from the correlation between test and simulation results. A new methodology was necessary to infer the fracture strain and stress state at the tip of the splitting crack. A similar activity was performed using expansion tubes.

Hybrid tubes were tested quasi-statically and dynamically. The acquired knowledge was then included into the numerical models of the hybrid tubes to validate the previous results.

The test results could also be used to compare the performance of splitting, expansion and hybrid tubes in terms of force efficiency. The stroke efficiency can be inferred from the geometry of the tubes alone. Additional testing was identified necessary to assess the splitting, expansion and hybrid tubes performance under oblique loading.

In this chapter the test material, test equipment, analysis and simulation methods will be described.

4.1 Specimens

4.1.1 Splitting Test Specimens (Submissions 3 and 4)

Cold drawn tubes, made of mild steel E355 as per BS EN 10305-4:2011 (British Standards, 2011), were used as specimens for the axial splitting test. The specimens were cut to a length of 200 mm and 150 mm, for the quasi-static and dynamic testing respectively; and the end faces machined. The specimens used for the oblique loading testing were 150 mm long in all instances. The tubes were tested in their as-received condition, i.e. no further heat treatment was performed. The dimensions of the tubes were 30 mm outer diameter

and 2 mm wall thickness. The size of the tested tubes was scaled to accommodate the applied loads to the 100 kN limit of the Instron 5800R 100 kN test machine. A Buehler precision saw was used to cut notches onto the specimen, which are perpendicular to the tube length, Figure 19, in order to ease the splitting of the tube. The notches were 0.7 mm wide and approximately 1.5 mm long. Notches were approximately equally spaced around the rim of the tube. The nominal masses of the tubes were 271 g and 203 g, for the 200 mm and 150 mm long tubes respectively.

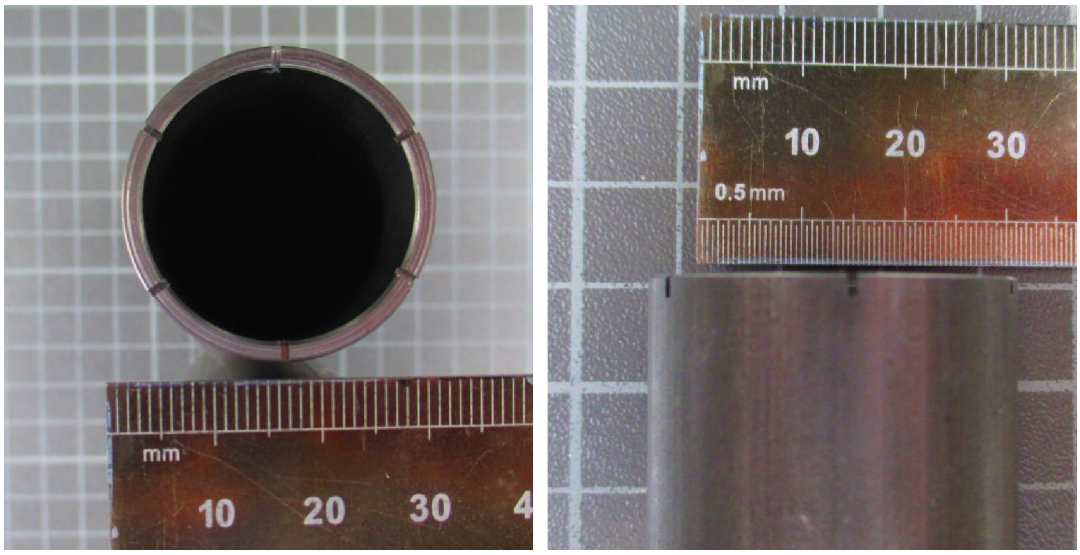

Figure 19: Specimen with six notches cut on the flat top surface

The flaring die was made of tool steel EN24. The die was hardened by oil quenching. The die's radius of flare was 8 mm and its mass 390 g. Figure 20 shows the dimensions of the die. A diamond pyramid hardness (DPH) indentation test was performed on the die. The splitting die had an average hardness Hv = 385 kgf/mm^2. According to the formula YS = -90.7 + 2.876 * Hv, specified by (Pavlina and Van Tyne, 2008), the corresponding yield strength was σ_y = 1016 MPa.

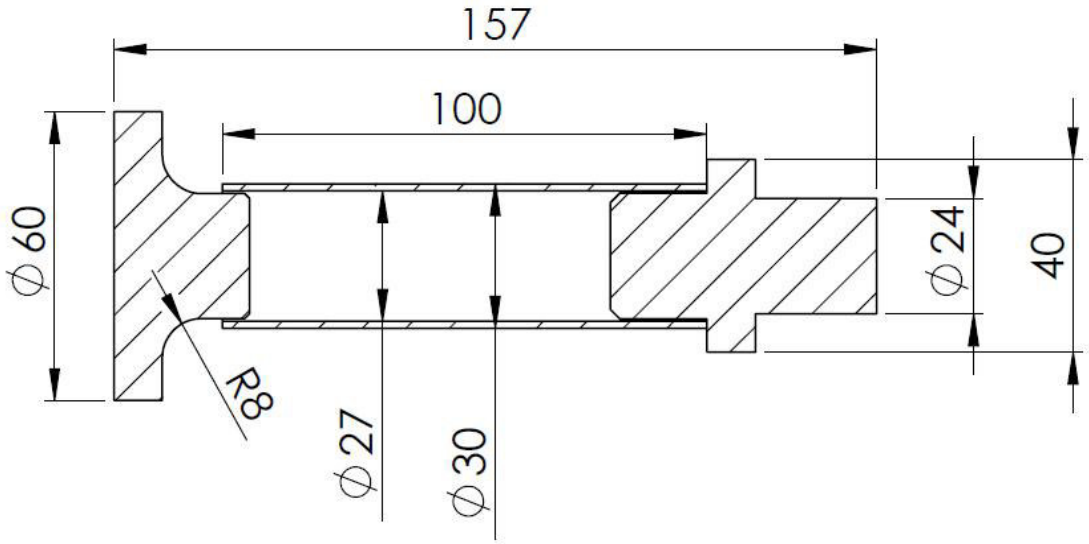

Figure 20: Dimensions of the flaring die

4.1.2 Expansion Test Specimens (Submission 5)

The tubes employed in the expansion test were similar to those employed in the splitting test, with the exception of the tube length of the quasi-static test tubes, which was reduced to 150 mm. The reason for this shortening can be found in that the resistive load, once the steady-state is reached, is practically constant. The nominal mass of the tubes was 204 g.

The conical dies were made of tool steel EN24. The dies were hardened by oil quenching. There were two dies with expansion ratio R = 1.10 and two dies with expansion ratio R = 1.25, with cone semi-angle A = 15° and A = 30° in each case. The indentation test showed that the R110A15 and R110A30 specimens had an average hardness Hv = 190 kgf/mm^2, whereas the R125A15 and R125A30 specimens had an average hardness Hv = 385 kgf/mm^2, with corresponding yield strengths σ_y = 455 MPa and σ_y = 1016 MPa, for the R = 1.10 and R = 1.25 dies respectively. The dimensions of the dies are shown in Figure 21.

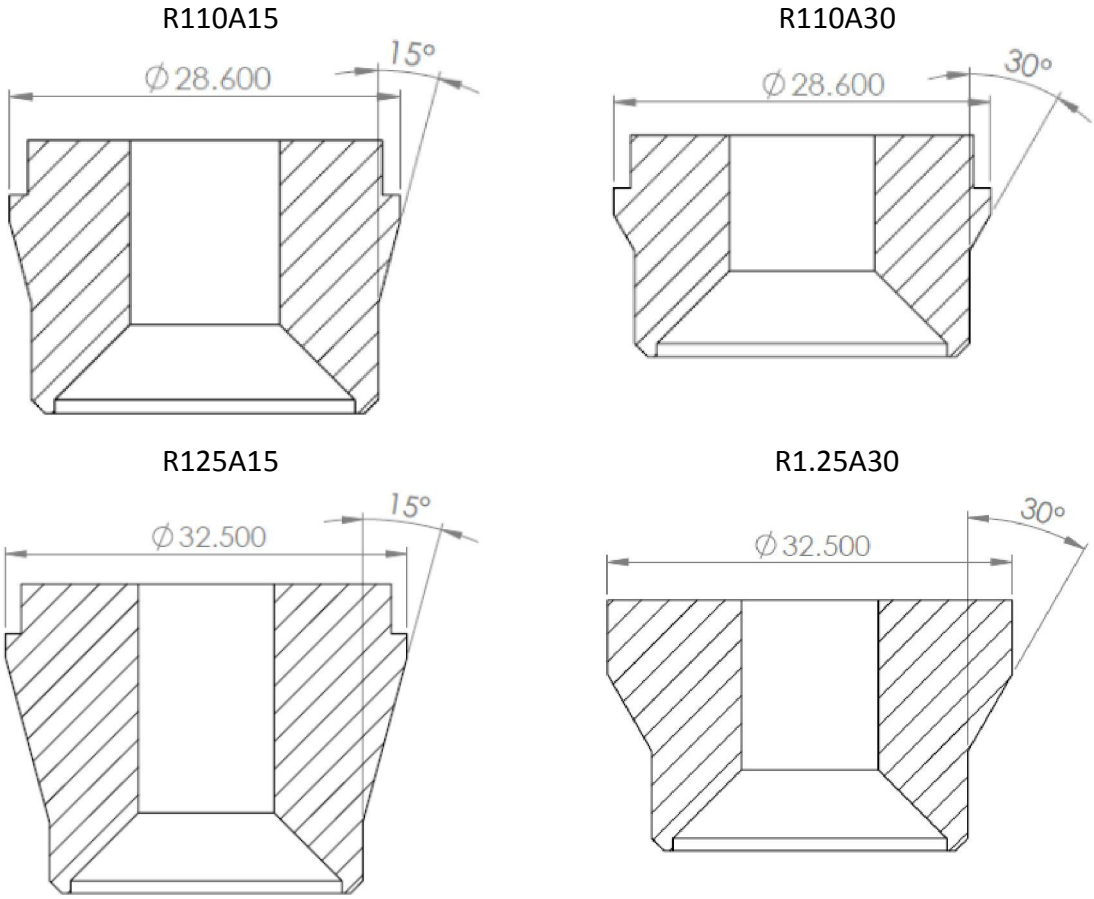

Figure 21: Dimensions of the conical dies

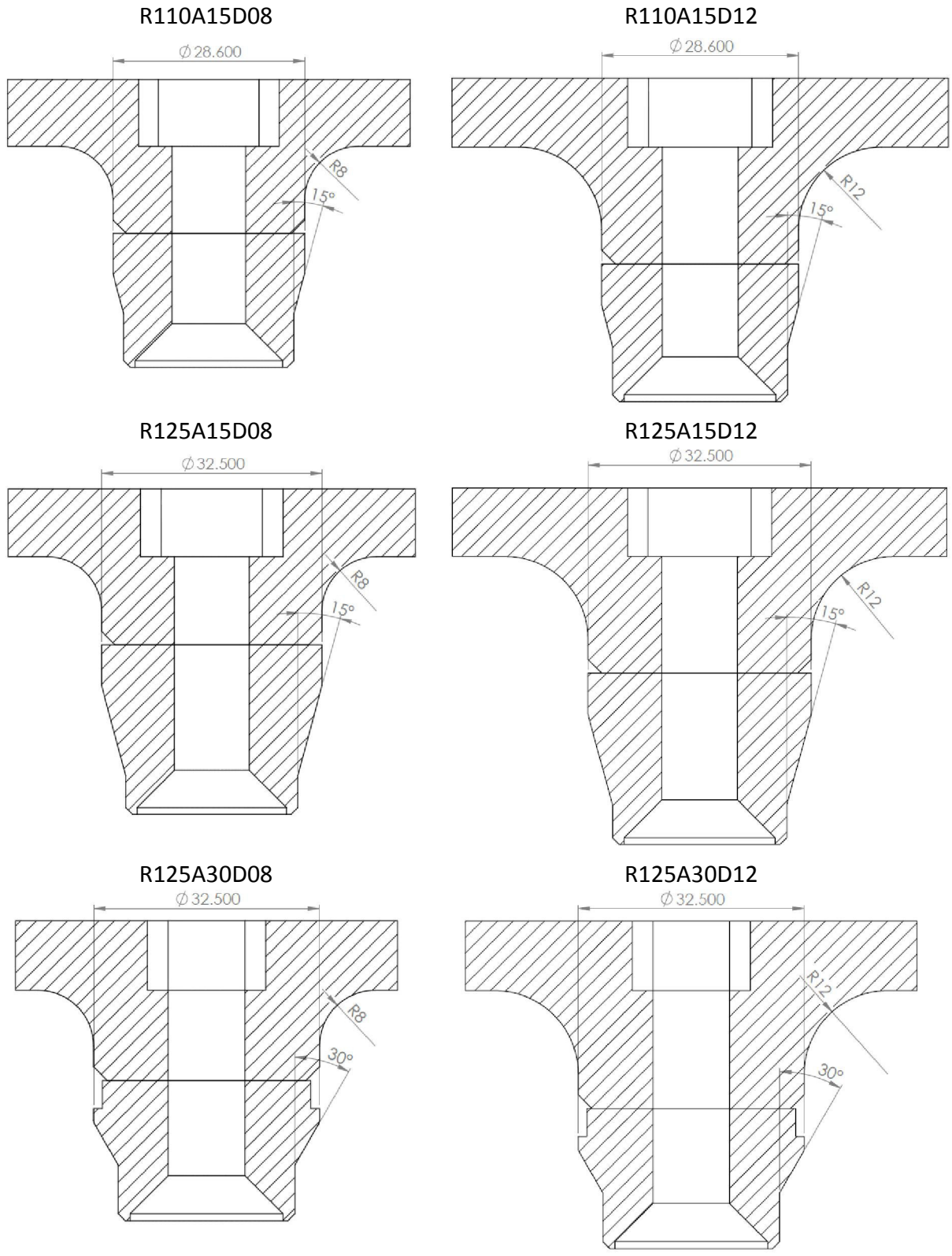

Figure 22: Dimensions of the hybrid dies

4.1.3 Hybrid Test Specimens (Submission 6)

The tubes employed in the hybrid test were identical to those employed previously. The combined conical and splitting dies were made of tool steel EN24. The dies were hardened

by oil quenching. There were two dies with expansion ratio R = 1.10 and cone semi-angle A = 15°, featuring flaring dies of radius 8 mm and 12 mm respectively. There were also two dies with expansion ratio R = 1.25 and cone semi-angle A = 15°, featuring flaring dies of radius D = 8 mm and D = 12 mm respectively. Additionally, there were two dies with expansion ratio R = 1.25 and cone semi-angle A = 30°, featuring flaring dies of radius 8 mm and 12 mm respectively. The dimensions of the dies are shown in Figure 22.

4.1.4 Nomenclature of the Specimens

To save space the tubes were assigned a compact nomenclature. The name of the expansion and hybrid tubes follows this convention (the third part within the brackets only applies to the hybrid tubes):

R _ _ _ A _ _ (D _ _)

The first part of the name refers to the expansion ratio of the conical die. If the die features an expansion ratio of R = 1.25, the first part of the specimen starts with R125. If the die features an expansion ratio of R = 1.10, then the first part of the specimen starts with R110. The second part of the name refers to the conical semi-angle of the die. Thus, the second part of the name could be A15 or A30, depending on the die having a conical semi-angle of A = 15° or A = 30°, respectively. The third part of the name applies to the hybrid tubes only. Two different splitting dies with flaring radii D = 8 mm and D = 12 mm were attached to the expansion dies to conform the hybrid die. The hybrid dies with flaring radius D = 8 mm included D08 to their name, whereas the ones with flaring radius D = 12 included D12 to their name. For example, a hybrid die with expansion ratio R = 1.25, conical semi-angle A = 15° and flaring radius D = 12 mm would be referred to as R125A15D12.

For the rest of this document the splitting tubes shall be referred to as splitting tubes.

Table 8 shows the complete list of specimens and nomenclature.

SPECIMEN	EXPANSION RATIO	CONICAL SEMI-ANGLE (°)	FLARING RADIUS (mm)	NOMENCLATURE
SPLITTING	-	-	8	SPLITTING
EXPANSION	1.10	15	-	R110A15
	1.10	30	-	R110A30
	1.25	15	-	R125A15
	1.25	30	-	R125A30
HYBRID	1.10	15	8	R110A15D08
	1.10	15	12	R110A15D12
	1.25	15	8	R125A15D08
	1.25	15	12	R125A15D12
	1.25	30	8	R125A30D08
	1.25	30	12	R125A30D12

Table 8: Nomenclature of the splitting, expansion and hybrid tubes

4.2 Materials (Submissions 4, 5, 6 and 7)

The material properties of the tubes were determined through tensile test using a contact extensometer. The test pieces dimensions and test procedure were as per BS EN 6892-1:2009 (British Standards, 2009). Figure 23 shows the stress-strain curve of a representative coupon cut from the E355 steel tubes. A power curve relation of the form $\sigma = K\varepsilon^n$ has been fitted to the data, with parameters K = 389.7 MPa and n = 0.1395. Five tensile specimens cut from the tube in the axial direction were used to determine the stress-strain properties.

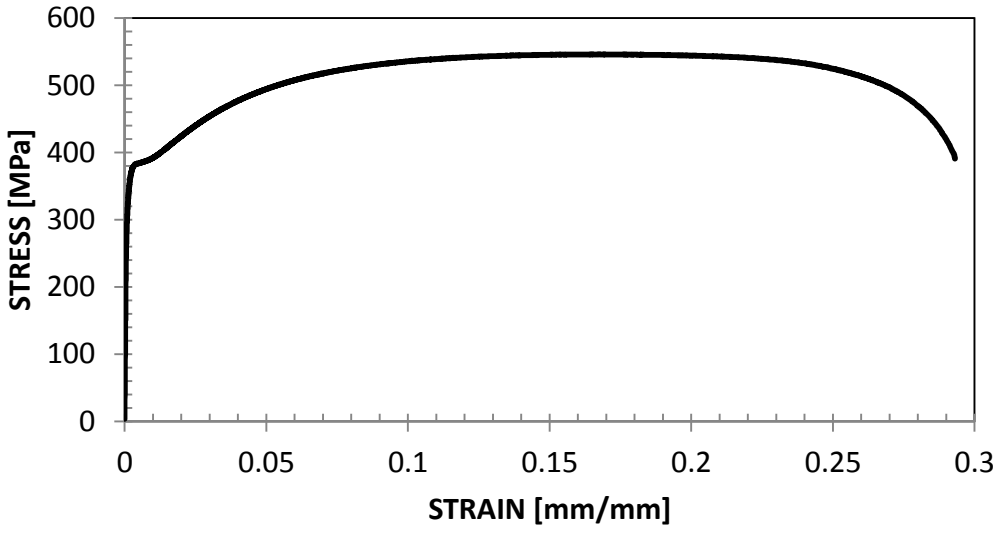

Figure 23: Engineering stress-strain curve of E355 steel

4.3 Axial Quasi-static Testing (Submissions 3, 4, 5 and 6)

A screw-driven Instron 5800R 100kN Universal Test Machine (UTM) was used to crush the specimens. Three repeats of each specimen were tested. The load cell in the machine was

rated to 100 kN and it read to an accuracy of ± 25 N (Instron, 2005). Figure 24 shows the test assembly arrangement. Copper grease was applied on the die radius surface and around the tube bore. The machine crosshead was located under the assembly support. It compressed the tube against the die and platen at a constant rate of 16 mm/min. A pre-load of 200 N was applied on each specimen prior to the test. The applied load and the crosshead displacement were recorded.

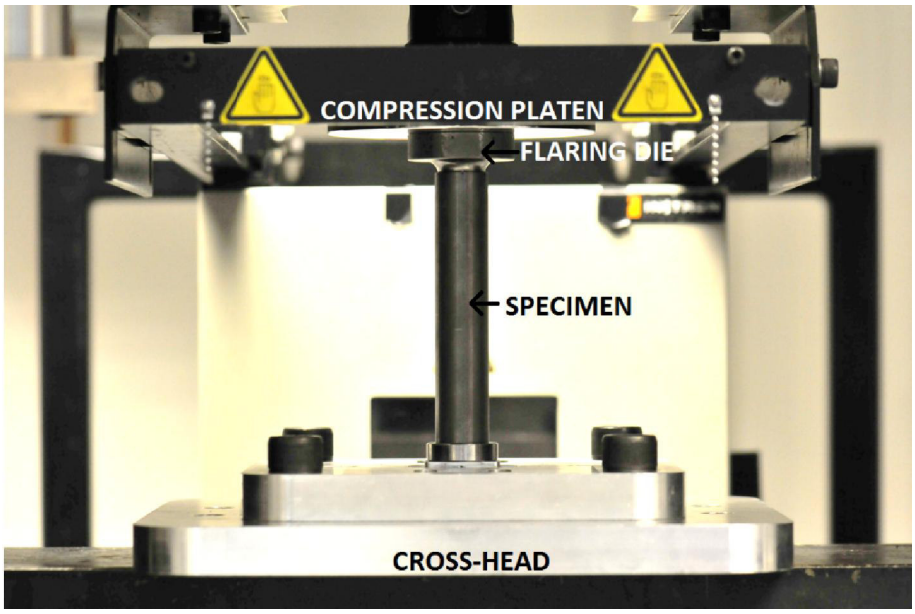

Figure 24: Splitting tube specimen mounted on the test rig

4.4 Axial Dynamic Testing (Submissions 3, 4, 5 and 6)

The test equipment used to perform the dynamic analysis was an Instron 10 kJ drop tower. It consists of a vertically oriented impact test machine. The spring assisted machine uses spring elastic energy and gravitational potential energy from the carriage mass to achieve impact energy of up to 10 kJ. The maximum speed that can be achieved is 17 m/s. The variable mass of the carriage assembly is 73.5 kg without any additional mass, such as that of the impact plate. The machine includes a velocity sensor. The standard Instron velocity sensor, consisting of a flag and optical sensor, measures the speed of the carriage shortly before the impact. In addition, a laser sensor measures the displacement of the falling mass or carriage. A 500 kN load cell is located on the mounting block, as shown in Figure 25. The actual arrangement of the dynamic test of splitting tubes includes the specimens attached to the mounting block, rather than the falling mass or carriage.

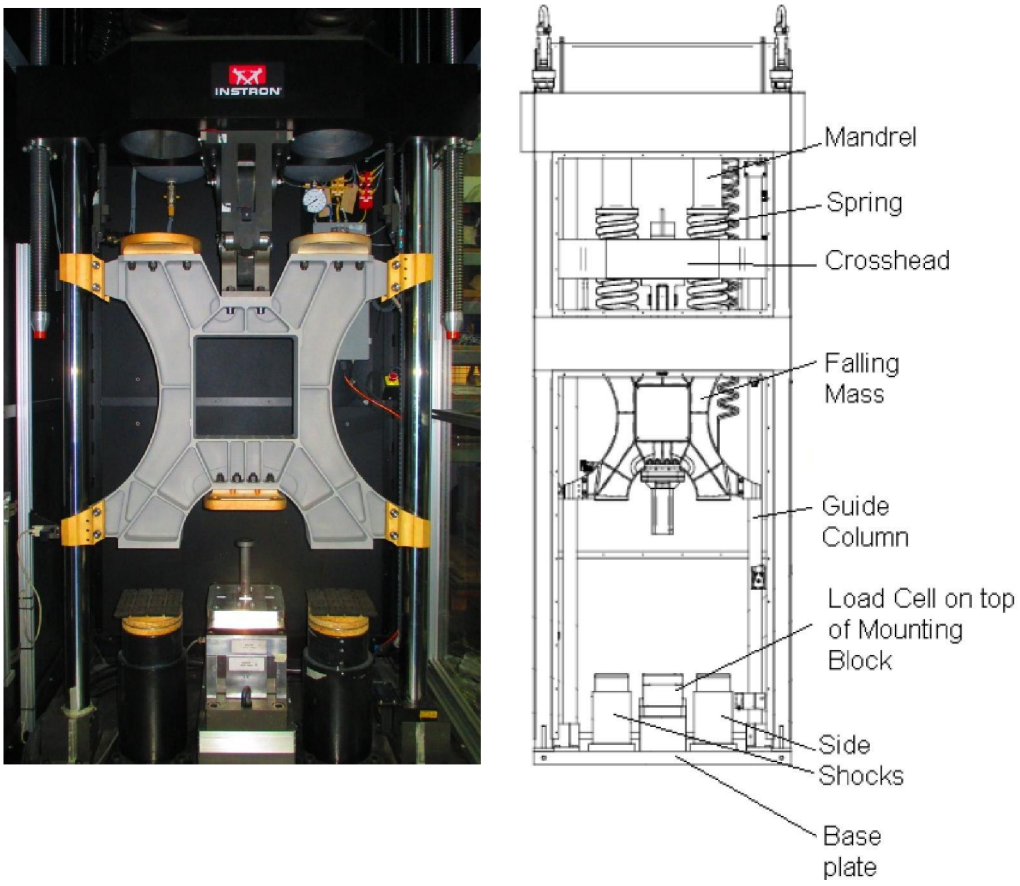

Figure 25: Schematic representation of the 10 kJ Instron drop tower (right) and actual arrangement (left) with tube shown on the mounting block

It was noticed that the load-displacement curves of all dynamically tested tubes exhibited a noisy profile, which was not noticeable for the static test machine. The frequency of the load vibration was found to be similar in all specimens, as shown in Figure 26. It is believed that the peaks and troughs were artificially induced by the drop tower equipment during dynamic testing. Therefore, filtering of the curve was deemed to be acceptable and applied to all data acquired by the drop tower.

Three repeats of each specimen were tested. All the specimens were quasi-statically pre-crushed, in order to ensure crash stability and prevent any damage to the drop tower. The length of the pre-crush was selected to reach the steady-state load of the specimen observed during the quasi-static testing. The crush energy induced to the specimen by the drop tower was selected in order to exhaust the specimens as far as practicable. Table 9 shows the pre-crush stroke, impact speed and nominal energy induced onto the specimens. Note that the actual energy absorbed by the specimens is marginally larger, due to the potential energy difference between the height of the impact point and the height of the

mass rest point. The actual energy absorbed by the specimens will be described in chapter 5.

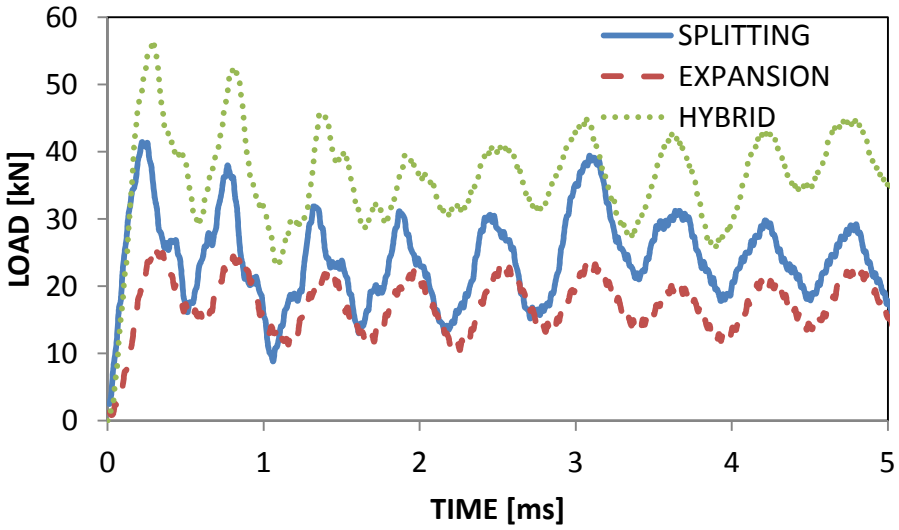

Figure 26: Load-displacement properties of splitting, expansion and hybrid specimens, from dynamic test, without filtering

		PRE-CRUSH STROKE (mm)	IMPACT SPEED (m/s)	NOMINAL ENERGY (J)
SPLITTING		15	7.2	1900
EXPANSION	**R110A15**	35	4.90	883
	R110A30	35	5.00	919
	R125A15	45	5.30	1032
	R125A30	60	5.29	1027
HYBRID	**R110A15D08**	40	10.72	4225
	R110A15D12	40	10.00	3676
	R125A15D08	50	8.29	2666
	R125A15D12	50	10.60	4130
	R125A30D12	60	8.38	2724

Table 9: Pre-crush length, impact speed and nominal energy induced onto the specimens, tested dynamically

4.5 Oblique Loading Testing (Submission 7)

Oblique quasi-static and dynamic tests were performed on a selection of splitting, expansion and hybrid tubes. The difference between the axial and oblique tests consisted on the inclusion of an inclined crushing platen. Two crushing platens, featuring 5° and 10° angle from the horizontal, were used to perform the tests, Figure 27. Table 10 shows the number of repeats of each of the selected specimens intended to be tested.

Figure 27: View of the 5° inclined plate, lowered onto a pre-crushed splitting specimen

SPECIMEN-DIE	5° PLATE ANGLE	10° PLATE ANGLE
SPLITTING	3	3
EXPANSION-R110A15	3	3
EXPANSION-R125A15	3	3
HYBRID-R110A15D08	3	3
HYBRID-R125A15D08	3	0

Table 10: Number of tubes intended to be tested for each type of energy absorber

SPECIMEN	DIE	PLATE ANGLE (°)	PRE-CRUSH STROKE (mm)	IMPACT SPEED (m/s)	NOMINAL ENERGY (J)
SPLITTING		5	50	5.1	1040
SPLITTING		10	50	5.1	1073
EXPANSION	**R110A15**	5	50	4.3	740
	R110A30	10	50	4.4	799
	R125A15	5	50	6.9	1904
	R125A30	10	50	-	-
HYBRID	**R110A15D12**	5	50	6.3	1588
	R110A15D08	10	50	6.8	1907
	R125A15D12	5	50	7.3	2132
	R125A15D08	10	50	-	-

Table 11: Plate angle, pre-crush length, impact speed and nominal energy induced to the specimens, tested dynamically under oblique loading conditions

In the case of the dynamic testing, the mass of the carriage assembly was 80 kg and 83 kg respectively due to the inclusion of the 5° and 10° inclined plates. Table 11 shows the plate angle, pre-crush stroke, impact speed and nominal energy induced to the specimens.

It was shown in section 2.1.3 that the Standard requires simulation of the railway vehicles with an initial vertical offset of 40 mm at the point of impact. If the energy absorber, which would act as the point of impact, has a length of L = 1000 mm, the angle related to such offset would be α = 2.3°, as shown in Figure 28. Therefore, it was assumed that the selected angles of 5° and 10° presented a more severe case and would cover the Standard requirements.

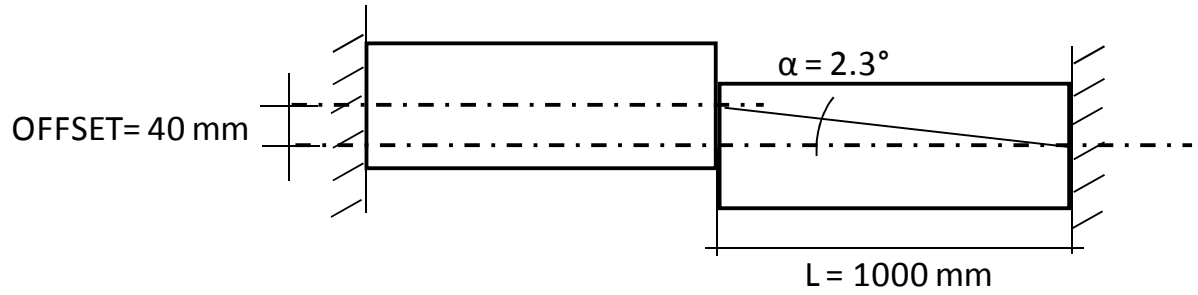

Figure 28: Schematic view of colliding energy absorbers, offset by 40 mm, and its related force inclined angle, α = 2.3°, given n energy absorber length of L = 1000 mm

4.6 Methodology of the Oblique Loading Performance Assessment of Type I Energy Absorbers (Submission 7)

Energy absorbers based on different energy absorbing mechanisms react differently to oblique loading. Crumple columns (type II energy absorbers) exhibit a reduction of their axial load as the transverse load increases. When a critical transverse loading is reached, there is transition from progressive to global buckling, at which point the energy absorber collapses catastrophically (Børvik et al., 2003). Type I energy absorbers utilising a die to deform the tube, such as splitting or expansion tubes, increase their axial load as the transverse load increases, as shown in Figure 29. This may be a consequence of the general bending of the tube under the transverse loading. The bending, and the plastic deformation and energy absorption, increases with the magnitude of the transverse load. The transverse loading depends directly on the axial force and the platen inclination angle, as shown in Figure 30, where F_A and F_T are the axial and transverse loads, α is the platen inclined angle and L is the length of the tube. Therefore, the axial mean load increase observed on the tubes tested under oblique loading conditions should be independent of the type of energy absorbing mechanism employed, whether splitting, expansion or hybrid. However, this contradicts the test results, as will be shown in section 5.4.

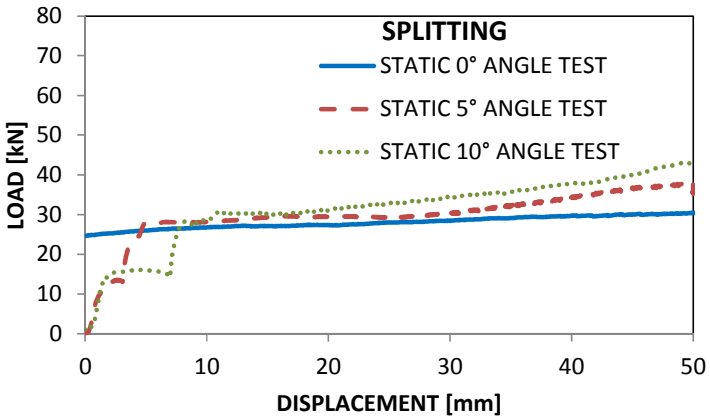

Figure 29: Load-displacement properties of a splitting tube, tested under 0°, 5° and 10° inclined plates

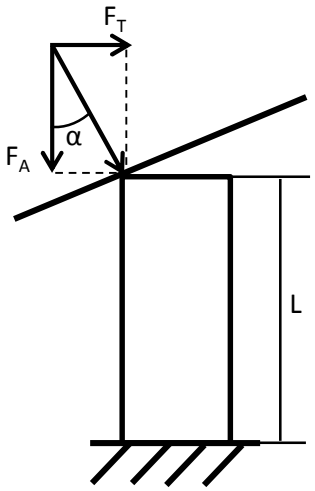

Figure 30: Schematic representation of the loading transmitted to the tube crushed against an inclined plate

Due to the lack of data about type I energy absorbers under oblique loading conditions in the literature, a new methodology to assess the oblique loading performance is proposed here. The mean load under oblique conditions (5° and 10° inclined plates) was plotted against the mean load under axial conditions (0° plate). An example is shown in Figure 31, with the data for the expansion tubes (R110A15 and R125A15) crushed by the 5° inclined plate. Note that, as expected, both specimens exhibit a larger mean load under oblique conditions than under axial conditions. However, the R125A15 specimen exhibits a larger increase. Ideally, an energy absorber would exhibit no increase of the mean load under oblique conditions. Each data point would lie on the ideal behaviour trace (similar mean

load under oblique and axial conditions). The more the data deviates from the ideal behaviour, the more sensitive is the energy absorber to the transverse loading.

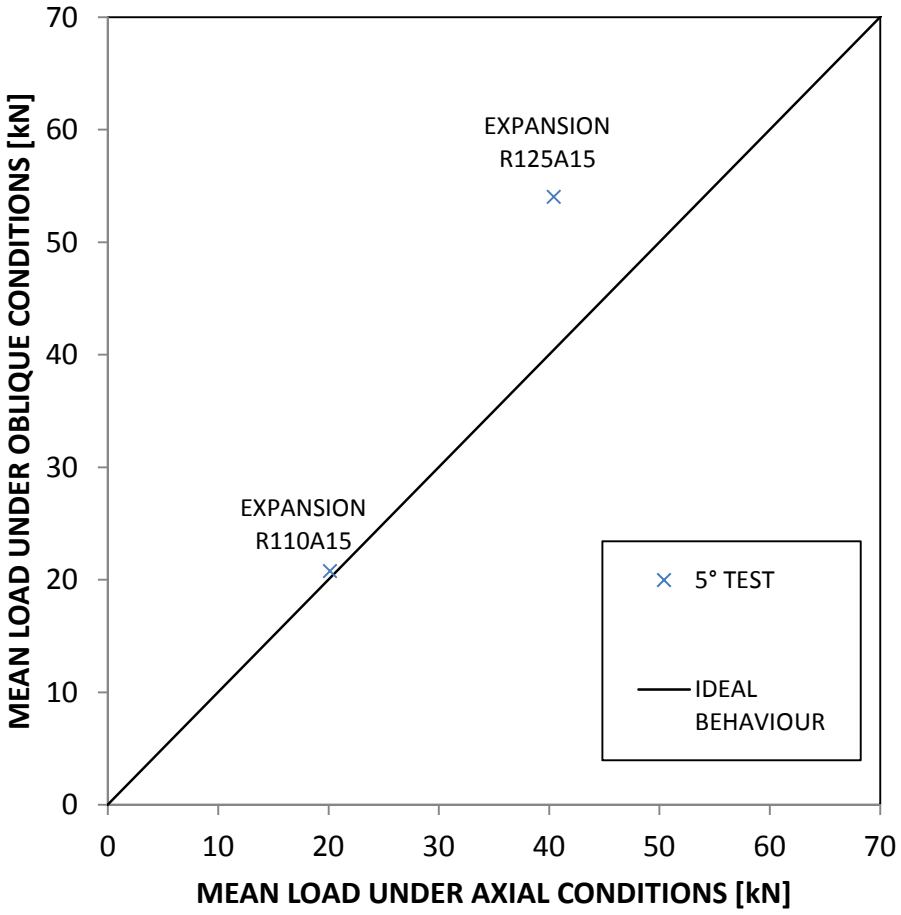

Figure 31: Mean load under oblique conditions vs. mean load under axial conditions of the expansion specimens with different expansion ratio (R = 1.10 and R = 1.25), crushed by the 5° inclined plate

4.7 Fracture Strain and Stress State Measurement Methodology (Submissions 3 and 4)

The GOM Aramis 3D commercial software (GOM, 2013) was used to measure the splitting tube displacement and strain at the tip of the crack along the length of the tearing tube (Moreno et al., 2015). The specimens must exhibit a stochastic pattern, i.e. random spots of contrasting black and white colours, within each facet (software discretised section areas) for the image processing to determine the strain. For featureless specimens, such as the splitting tubes, a coating made of two layers of spray is required. The substrate layer is a

solid coat of black paint and the upper layer is a random speckled pattern of white paint, sprayed using an airbrush.

Although 2D digital image correlation (DIC) techniques, featuring a single camera, are appropriate for a flat surface, here a curved surface is presented. Therefore a 3D set-up, featuring two cameras, is preferred. For a 3D set-up, a sensor with two cameras needs to be calibrated prior to measurement, as shown in Figure 32. The configuration used was 5M system (2448x2050 megapixels) with a Titanar A 75 mm focal length lenses. This configuration allowed for a measuring volume of dimensions 65 x 65 x 55 mm^3. The calibration object used was a CQ/CP20 55x44, under the GOM nomenclature. The measuring distance was 730 mm, the slider distance 284 mm and the camera angle 25° (refer to Figure 32). Figure 33 shows the actual set-up on the tensile machine. Each of the facets was set to contain 15 x 15 pixels. For this case, the resulting facet length was 0.44 mm.

The axial location of the tip of the tearing crack was determined by visual inspection in each of the images. The crack tip can be pinpointed and the software outputs its axial coordinate. Figure 34 shows a splitting sequence of a tube with six notches and von Mises strain mapping, measured by the GOM Aramis 3D software.

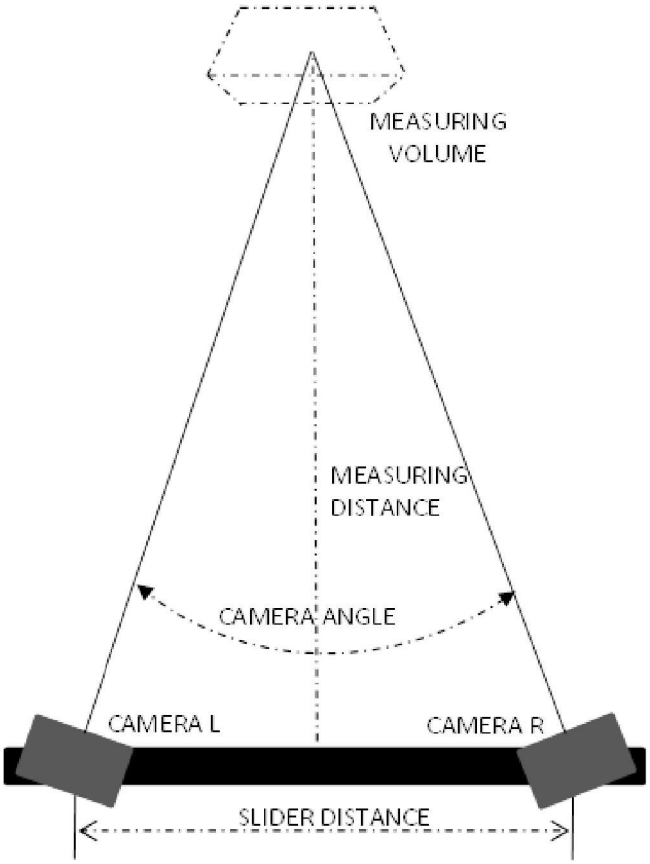

Figure 32: GOM Aramis 3D hardware configuration

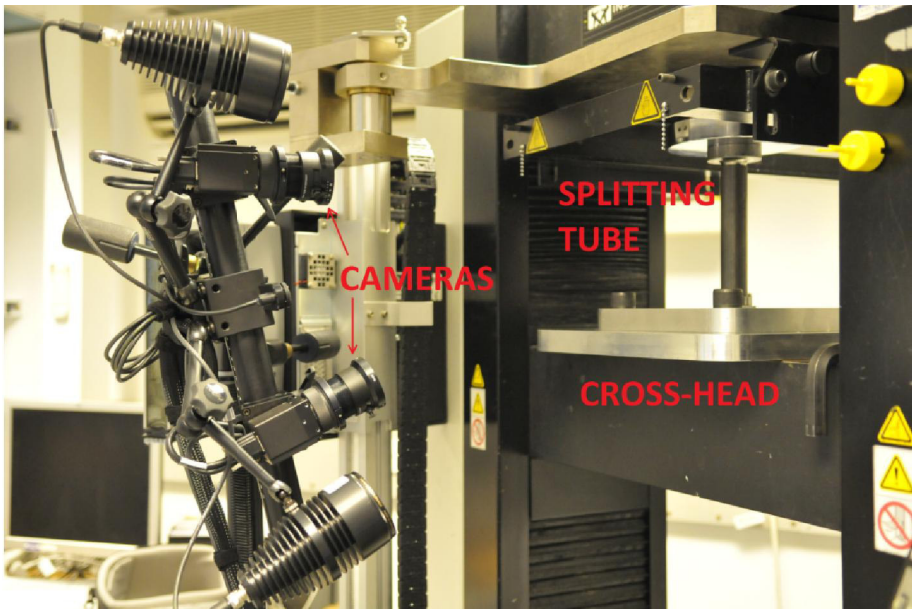

Figure 33: Cameras, light and tensile machine set-up

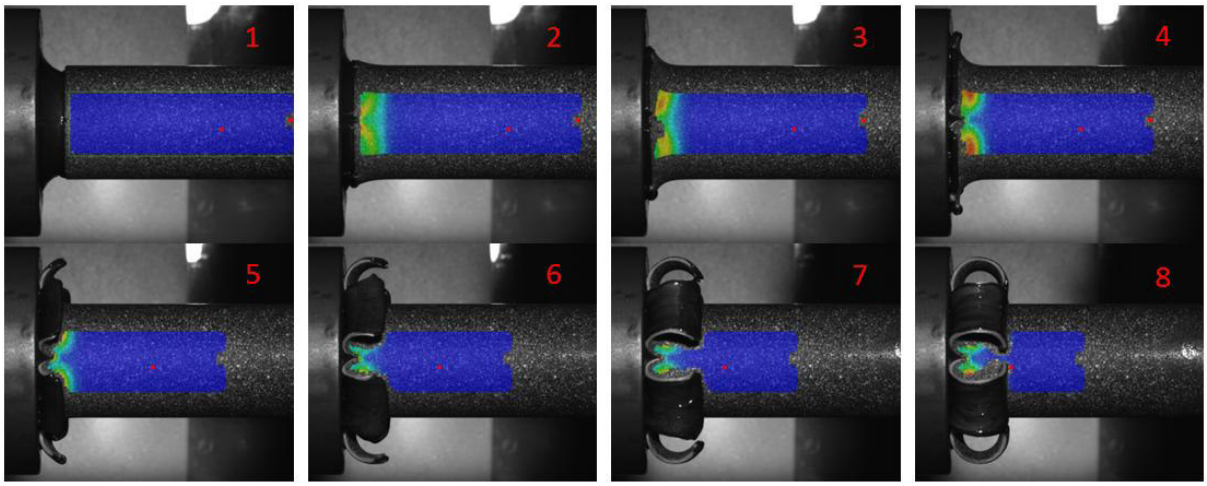

Figure 34: Sequence of splitting for a tube with six notches and von Mises strain mapping, measured by GOM Aramis 3D

The DIC technique suffers from a major inconvenience: the software is unable to interpret the speckle pattern up to the edge. As a consequence, strain facets created by the GOM software disappear at a certain distance from the tip of the crack, typically less than the length of a facet, as shown in Figure 35. A new methodology was developed to extrapolate to the tip of the crack the value of the strain data measured by the DIC system.

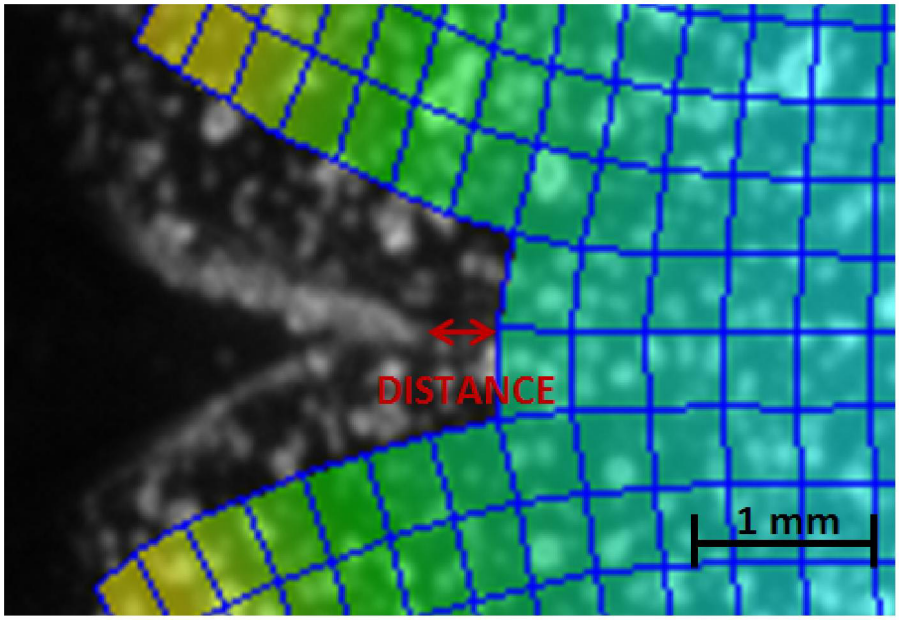

Figure 35: Distance between the facet field and the crack tip

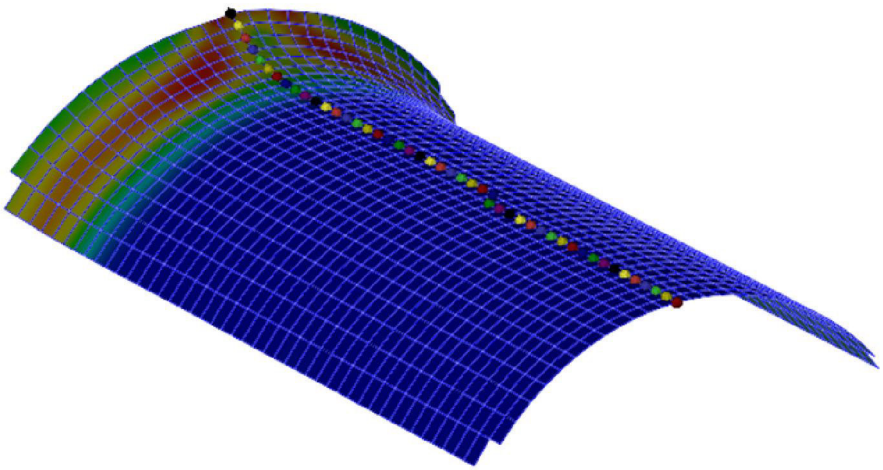

Figure 36: von Mises strain facet field and data nodes alongside the path of the crack

Figure 36 shows the data nodes alongside the path of the advancing crack. The strain history of each of these nodes was measured. Figure 37 shows the von Mises strain history vs. the axial distance to the crack tip of one of these nodes. It can be observed that the distance of the last data point from the crack tip, which corresponds to the moment when the facet disappears, is approximately 0.25 mm, about half the length of a facet. A second order polynomial was fitted to the data and the fracture strain was inferred by extrapolation. The fracture strain value, extrapolated in that manner, allows us to estimate the von Mises strain at which the tube tears.

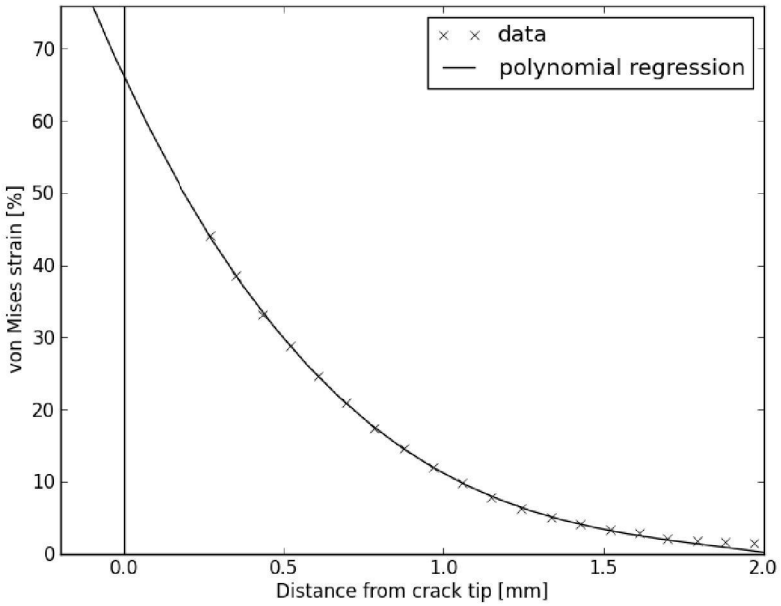

Figure 37: von Mises strain vs. axial distance to the tip of the crack, for one data node alongside the path of the crack

The stress state was also estimated from the measurements. The stress state is typically represented by the stress triaxiality. However, it is also commonly represented in terms of the strain components: the ratio of principal strains $\alpha = \varepsilon_2/\varepsilon_1$. This data is readily available from the GOM system. Figure 38 shows the directions of the major principal strain and the minor principal strain, respectively. The major principal strain corresponds to hoop strain, whereas the minor principal strain corresponds to axial strain.

Figure 39 shows the strain ratio for the same data node used in Figure 37, for a specimen with six notches. From the strain ratio development, it can be observed that compression (axial strain) is initially predominant, but the strain ratio rapidly settles to a constant value. The strain ratio at the crack tip was inferred by linearly extrapolating, similarly to the von Mises strain.

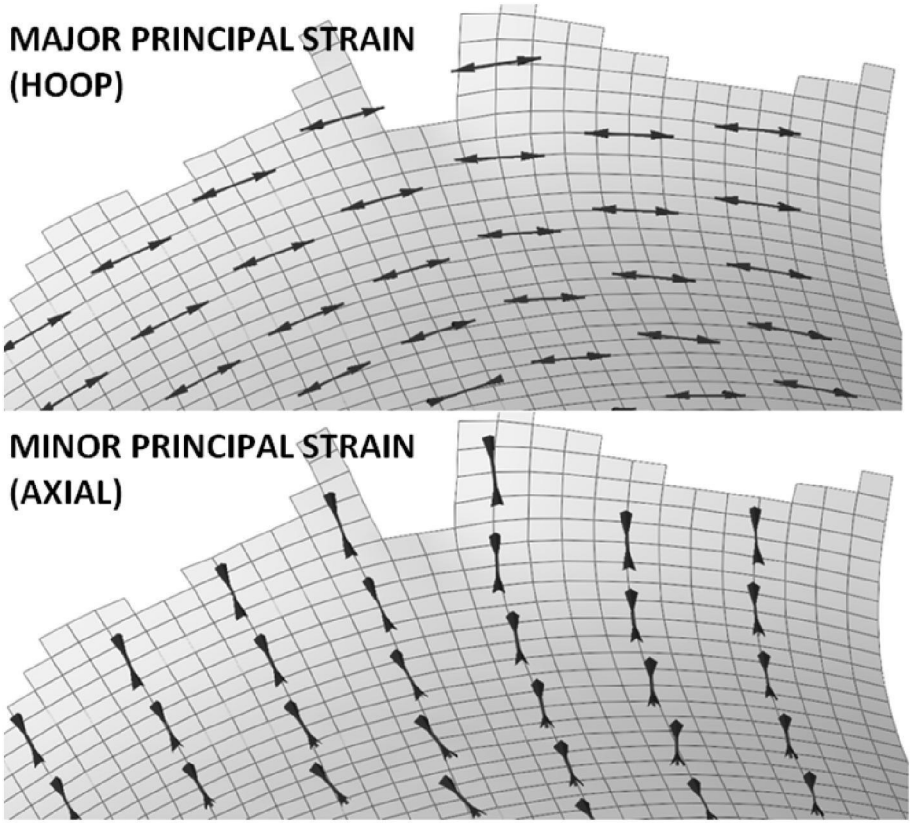

Figure 38: Direction of major (above) and minor (below) principal strains, measured by DIC

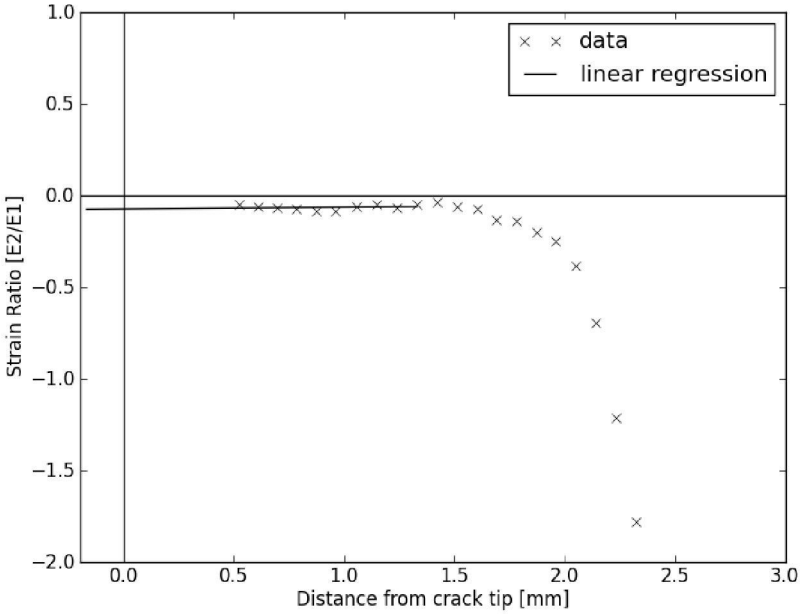

Figure 39: Strain ratio (minor strain over major strain) vs. axial distance to the tip of the crack, for one data node alongside the path of the crack

4.8 Finite Element Analysis Methods (Submissions 3, 4, 5, 6 and 7)

Finite Element Analysis (FEA) is the conventional method used to predict the performance of crash structures. The standard BS EN 15227 (British Standards, 2010b) requires a calibrated numerical model of the energy absorbers. In this project, the explicit FEA commercial code LS-DYNA was used to perform the simulation of the energy absorbers.

4.8.1 Model Set-up

The quasi-static numerical model of the splitting tube comprised four parts: the rigid die, the deformable tube, the sections of deformable tube alongside fracture path and the rigid tube support, as shown in Figure 40. The numerical model of the hybrid tube was built using the same methodology. The numerical model of the expansion tubes omitted the fracture line part, as no fracture is observed during the tests. The die was modelled as a rigid part due to computational time considerations. The fracture line part included a deletion element capability as it will be stated in section 4.8.3, whereas the deformable tube part did not include any deletion element capability. The fracture strain, determined following the methodology stated in section 4.7, was included in the material card as a constant fracture strain criteria. It was deemed necessary to separate the deformable tube into two groups to

prevent deletion of elements where no element deletion was observed, such as areas of tube to die contact areas. The resulting large strain, due to high contact pressure between the rigid die and the deformable tube, predicted early deletion of the elements in contact, as shown in Figure 41. As a result, the reaction load of the splitting tube was under-estimated. The inclusion of the fracture line part corrected this issue.

An automatic penalty-based contact formulation was selected for the two contact areas: between the die and the deformable tube (*CONTACT_AUTOMATIC_SURFACE_TO_SURFACE) and tube self-contact between the curled strips and the un-deformed section of the tube (*CONTACT_AUTOMATIC_SINGLE_SURFACE). The choice of the friction coefficient will be discussed in the next section.

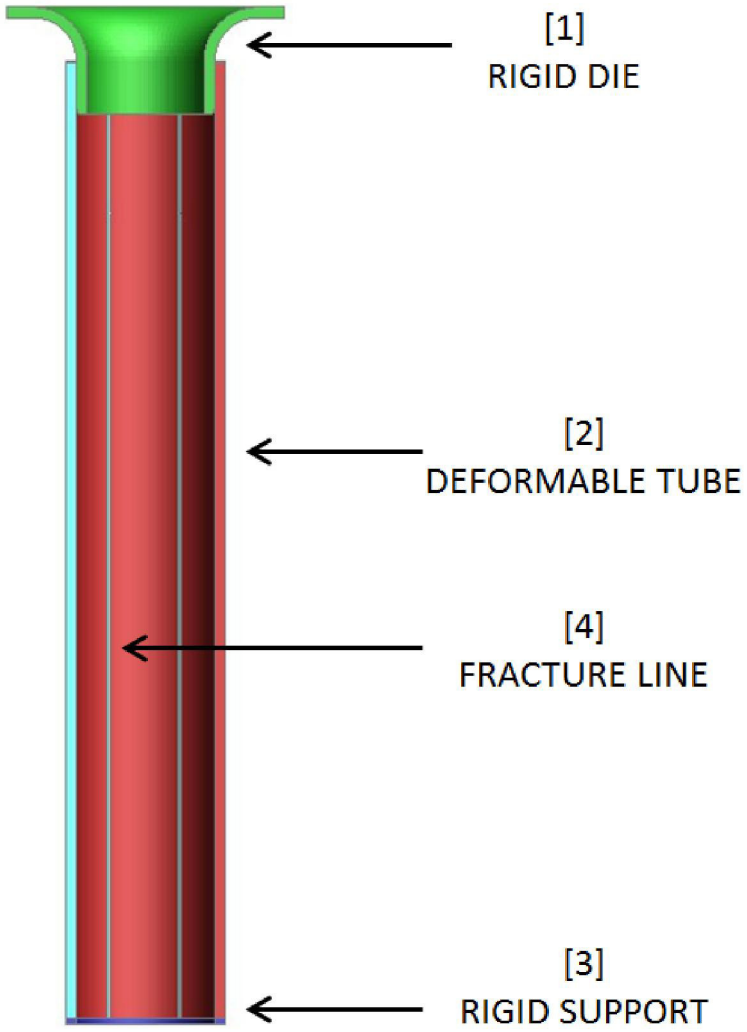

Figure 40: Section of the hybrid tube model showing four parts: rigid die [1], deformable tube [2], rigid support [3] and fracture line [4]

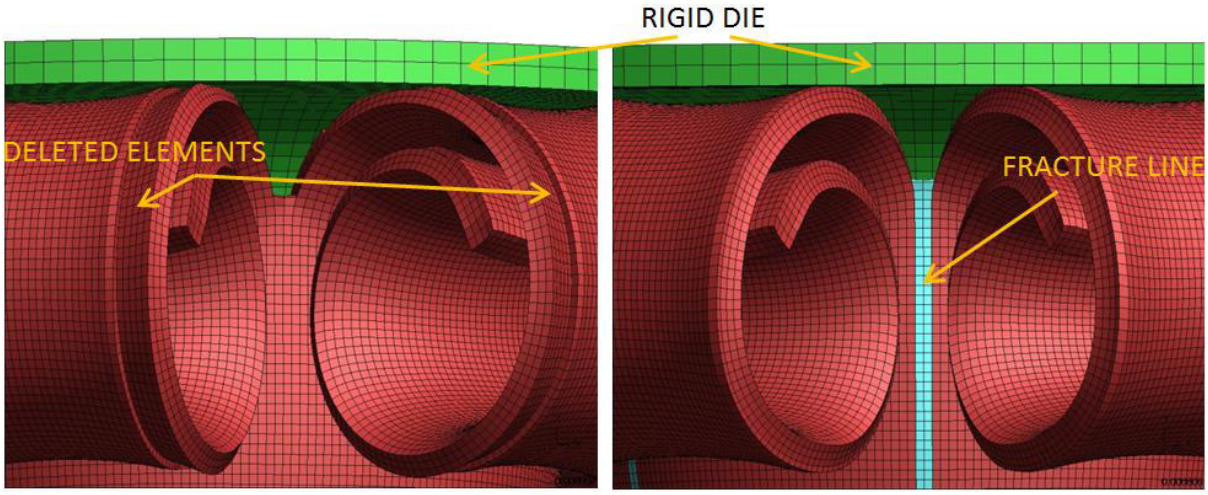

Figure 41: Model without additional part for fracture line (left) and with additional part (right)

The dynamic numerical model included an additional part, Figure 42, to represent the drop tower carriage. In this case, an initial velocity, rather than constant speed, was imposed to the rigid carriage part.

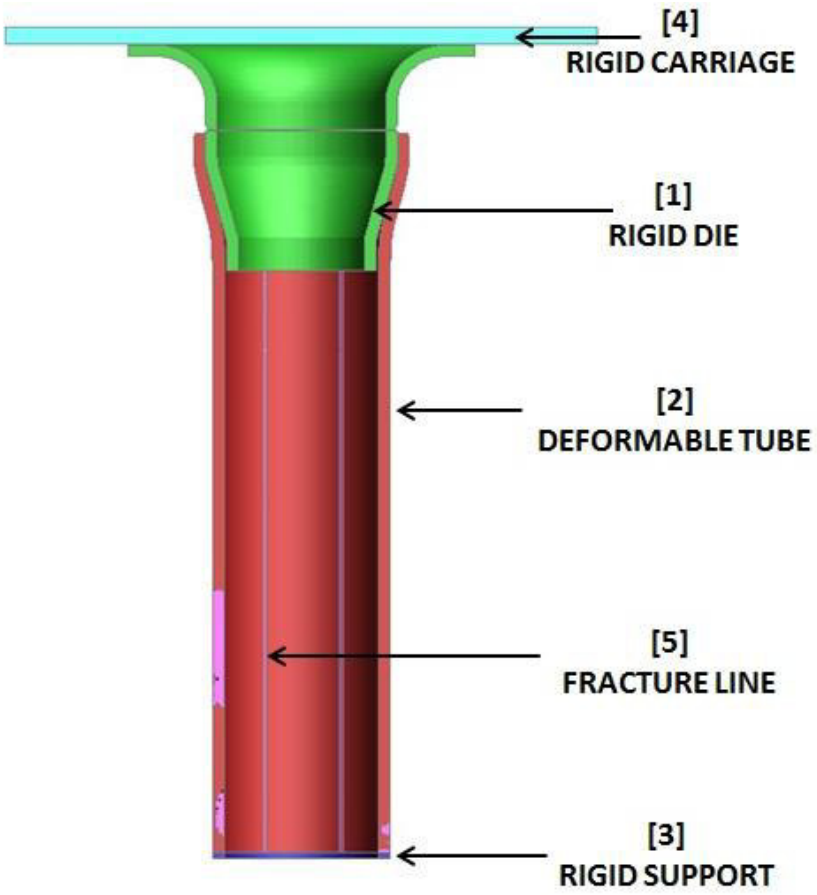

Figure 42: Section of the hybrid tube showing four parts: rigid die [1], deformable tube [2], rigid support [3], rigid carriage [4] and fracture line [5]

4.8.2 Element Type

The simulation elements were fully integrated hexahedral solids. Shell elements have a plane stress assumption (Hallquist, 2006), only valid for sufficiently thin materials. In order to keep an appropriate length to thickness ratio, shell elements would have to be unacceptably large. Solid elements give accurate results as they correctly model the stress in all three directions. However, they need to keep a cubic shape to avoid numerical instabilities. To assess the sensitivity of the results due to the mesh size, three different models with 2, 4 and 8 elements through thickness were created. The models took 10 minutes, 50 minutes and 10 hours to complete respectively, for a crush length of 160 mm. Figure 43 shows the load-displacement for numerical models with 2, 4 and 8 elements through thickness. The model with 2 elements through thickness overestimated the energy absorption by 44% with respect to the model with 4 elements. The model with 8 elements through thickness underestimated the energy absorption by 7% with respect to the model with 4 elements. The decision to choose the model with four elements through thickness for subsequent modelling was based on the necessity to keep the model running time within acceptable limits. Fully integrated elements were selected to avoid hourglassing (Hallquist, 2006).

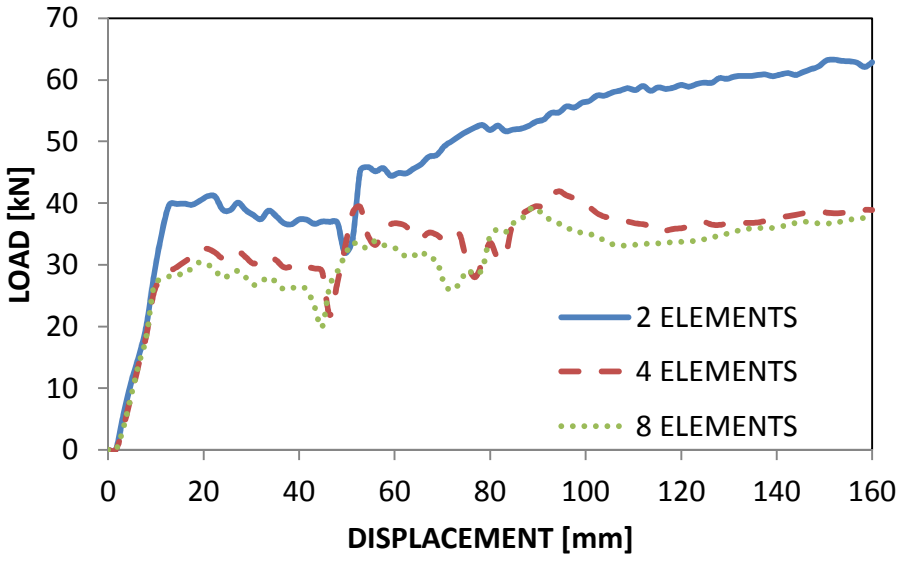

Figure 43: Load-displacement properties of numerical model with 2, 4 and 8 elements through thickness

4.8.3 Material

The material used, E355 steel, is assumed to be isotropic. For isotropic materials, the LS-DYNA material model, *MAT_PIECEWISE_LINEAR_PLASTICITY can be used. This material models plasticity by introducing a monotonically increasing curve. The curve in Figure 23 was converted into true stress-true strain curve and imported into the FEA material card. Failure can be simulated with this model. Elements are deleted when the strain reaches a critical value.

4.8.4 Control

The speed of the physical quasi-static testing was 16 mm/min. The test lasted 10 minutes to achieve 160 mm of stroke. This length of simulation time is not feasible with timesteps of the order of 10^{-8} s. In order to reduce the simulation run time, time scaling can be used. This simply consists of an artificial increase of the die speed until the run time is within practical limits. There are two requirements to use time scaling. The material needs to be strain rate insensitive and the kinetic energy of the system needs to remain lower than 5% of the internal energy (Prior, 1994) and (Choi et al., 2002). A numerical model was run at different die constant speeds: 50 m/s, 25 m/s, 12.5 m/s and 6.25 m/s, to assess the impact of time scaling in this particular model. Figure 44 shows the load-displacement characteristics of these models. The models run at 12.5 m/s and 6.25 m/s converge to a similar load-displacement curve. Table 12 shows the percentage of kinetic energy with respect to the total energy dissipated in the models run at 50 m/s, 25 m/s, 12.5 m/s and 6.25 m/s die speed. It can be noted that, although the percentage of kinetic energy over total energy of the model run at 25 m/s is under the 5% limit for acceptability, this speed did not match the experimental quasi-static test results. Subsequently, all static simulations were run at 12.5 m/s of rigid die speed.

DIE SPEED [m/s]	50.00	25.00	12.50	6.25
KINETIC ENERGY [%]	10.3	2.9	0.8	0.2

Table 12: Percentage of kinetic energy with respect to the total energy present in the models run at 50 m/s, 25 m/s, 12.5 m/s and 6.25 m/s die speed

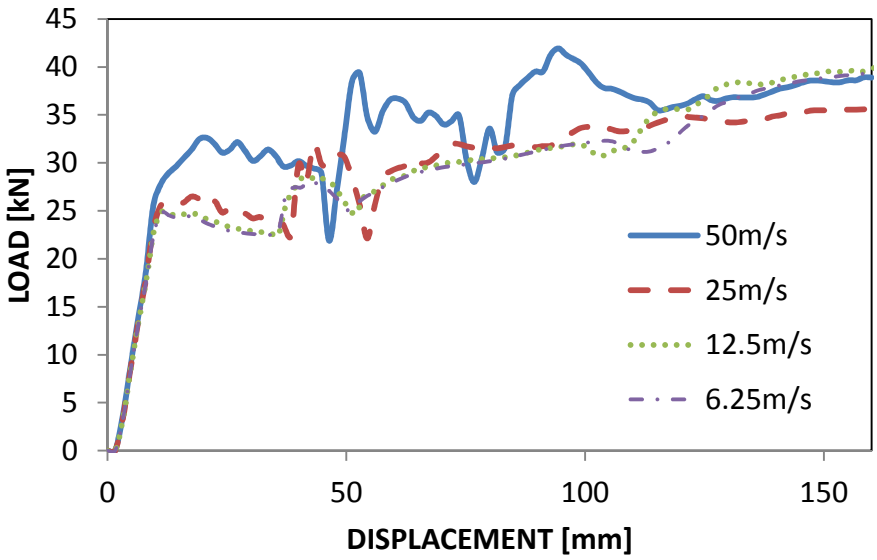

Figure 44: Load-displacement properties of a numerical model run at 50 m/s, 25 m/s, 12.5 m/s and 6.25 m/s die speed

4.8.5 Calibration and Validation of the Numerical Models

The calibration of the numerical models was performed by adjusting the friction coefficient of the numerical model (including the fracture strain found following the methodology stated in section 4.7) until the load-displacement properties of the test specimens and their energy absorption capabilities matched. This methodology of assessing the friction coefficients was adopted due to the difficulty to perform specific friction testing methods which capture the friction regime present between the deforming tube and the die. (Almeida et al., 2006) found that the ring compression test, used to assess the friction coefficient present between specimens undergoing large plastic deformation was not adequate in the case of expansion tubes.

The numerical models of the hybrid tubes were used to validate the parameters found during the calibration activity.

5 Experimental Assessment of the Axial and Oblique Loading under Quasi-static and Dynamic Conditions

This chapter details the results of the quasi-static and dynamic testing performed on the splitting, expansion and hybrid under axial and oblique loading conditions.

5.1 Axial Testing of Splitting Tubes (Submissions 4)

5.1.1 Quasi-static Testing

Three repeats of two types of splitting tubes, with four and six notches, were crushed quasi-statically between the die and the machine crosshead. In submission 3 and 4 it was shown that the results were very repeatable. Figure 45 show the comparison of the load-displacement curves of the splitting specimens with four and six notches. Note that the energy absorption of the specimen with four notches is significantly larger than the specimen with six notches.

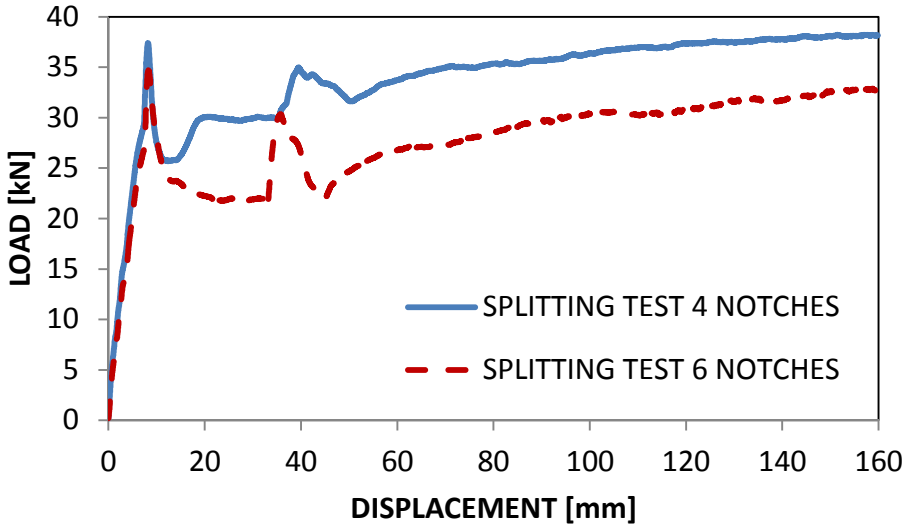

Figure 45: Load- displacement properties of splitting tubes with four and six notches

Table 13 shows the energy absorption, stroke, mean and peak load results of quasi-static testing of splitting tubes with four and six notches. Subsequently, all tubes which experience splitting, whether splitting or hybrid tubes, had six notches cut. The tubes with six notches dissipate less energy and are more stable.

TYPE	ENERGY (kJ)	STROKE (mm)	MEAN LOAD (kN)	PEAK LOAD (kN)
4 NOTCHES	5.394	160	33.7	38.2
6 NOTCHES	4.435	160	27.7	34.7

Table 13: Energy absorption, stroke, mean and peak load results of quasi-static testing of splitting tubes with four and six notches

5.1.2 Dynamic Testing

Three tubes of each type were tested and the results were repeatable. Figure 47 shows image series of the dynamic test of a splitting specimen with six notches. Figure 48 shows a comparison of the load-displacement properties of the two types of splitting specimens under quasi-static and dynamic conditions. In the case of the dynamic testing, the peak load could not be ascertained as its magnitude may have been concealed by the filtering applied to the raw data, see section 4.4. Table 14 shows the energy absorption, stroke, mean load and mean load variation between the quasi-static and dynamic results of dynamic testing of splitting tubes with four and six notches. Note that the quasi-static mean load in Table 14 was evaluated for the same section tested under dynamic conditions, to include the effect of the pre-crush. The quasi-static mean load is approximately similar to the dynamic mean load.

Figure 46: Scale of the deformed splitting tube

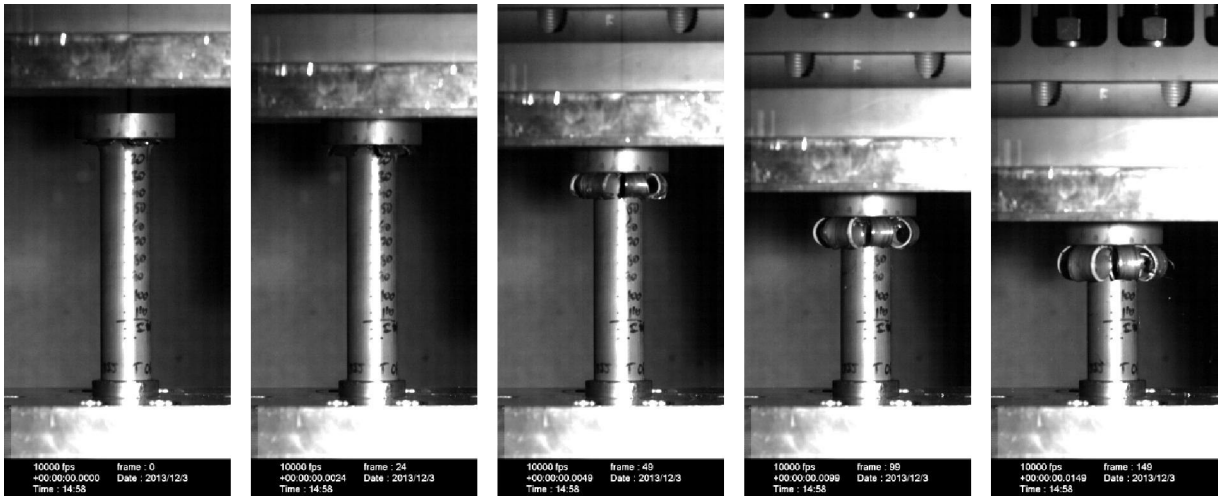

Figure 47: Sequence of the dynamic test of a splitting specimen with six notches

5.2 Axial Testing of Expansion Tubes (Submission 5)

5.2.1 Quasi-static Testing

Three repeats of each type of the four types of expansion tubes, R11A15, R110A30, R125A15, R125A30, were quasi-statically tested. The results were repeatable. Figure 49 shows the comparison of the load-displacement properties of the four types of specimens. The energy absorption increases as the expansion ratio increases from R = 1.10 to R = 1.25 and as the cone semi-angle increases from A = 15° to A = 30°. Table 15 shows the energy absorption, stroke, mean and peak load results of quasi-static testing of the expansion tubes.

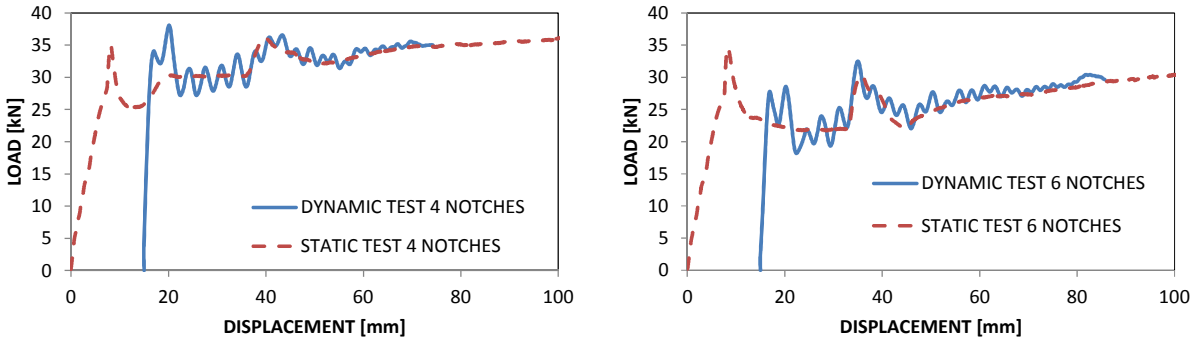

Figure 48: Load-displacement properties of the quasi-static and dynamic testing of the four (left) and six (right) notches specimens

TYPE	ENERGY (kJ)	STROKE (mm)	MEAN LOAD STATIC (kN)	MEAN LOAD DYNAMIC (kN)	Δ MEAN LOAD (%)
4 NOTCHES	1.932	59.23	32.3	32.6	0.9
6 NOTCHES	1.841	70.68	25.5	26.0	2.2

Table 14: Energy absorption, stroke, mean load and mean load variation between the quasi-static and dynamic tests of splitting tubes with four and six notches

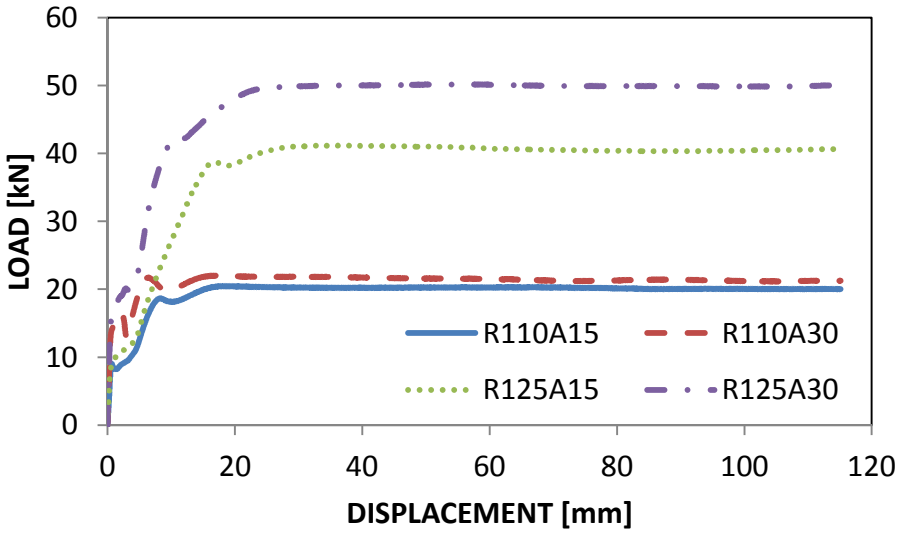

Figure 49: Load- displacement properties of expansion tubes R110A15, R110A30, R125A15 and R125A30

TYPE	ENERGY (kJ)	STROKE (mm)	MEAN LOAD (kN)	PEAK LOAD (kN)
R110A15	2.219	115	19.3	20.2
R110A15	2.401	115	20.9	21.6
R125A15	4.340	115	37.7	40.9
R125A30	5.444	115	47.3	50.2

Table 15: Energy absorption, stroke, mean and peak load results of quasi-static testing of expansion tubes R110A15, R110A30, R125A15 and R125A30

5.2.2 Dynamic Testing

Three repeats of each type of the expansion tubes were tested. Figure 51 shows image series of the dynamic test of an expansion specimen R110A15. Figure 52 shows the comparison of the load-displacement properties of the four types of specimens under dynamic conditions. Figure 53 shows the load-displacement properties of the quasi-static and dynamic testing of the four types of expansion tubes. It can be observed a general decrease of the mean load exhibited by the tubes tested under dynamic conditions. Table 16 confirms this observation: the mean loan decreased by 2.9% for the R125A30 specimen

to 13.2% for the R125A15 specimen. Note that the quasi-static mean load in Table 16 was evaluated for the same section tested under dynamic conditions, in order to ignore the effect of the pre-crush, specified previously in Table 9. Thus, the quasi-static mean load for the specimen R110A15 was calculated from displacement x = 35 mm to x = 90 mm, or, for specimen R125A15, from x = 45 mm to x = 75 mm.

It can be observed that the decrease is more noticeable on the specimens with smaller cone semi-angle, A = 15°.

Figure 50: Scale of the deformed R110A15 expansion tube

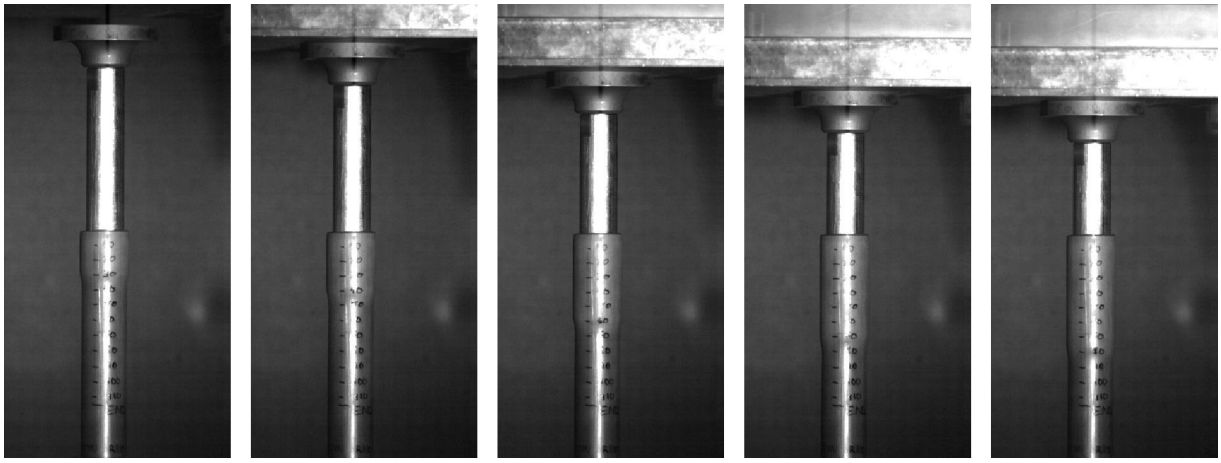

Figure 51: Sequence of the dynamic test of an expansion R110A15 specimen

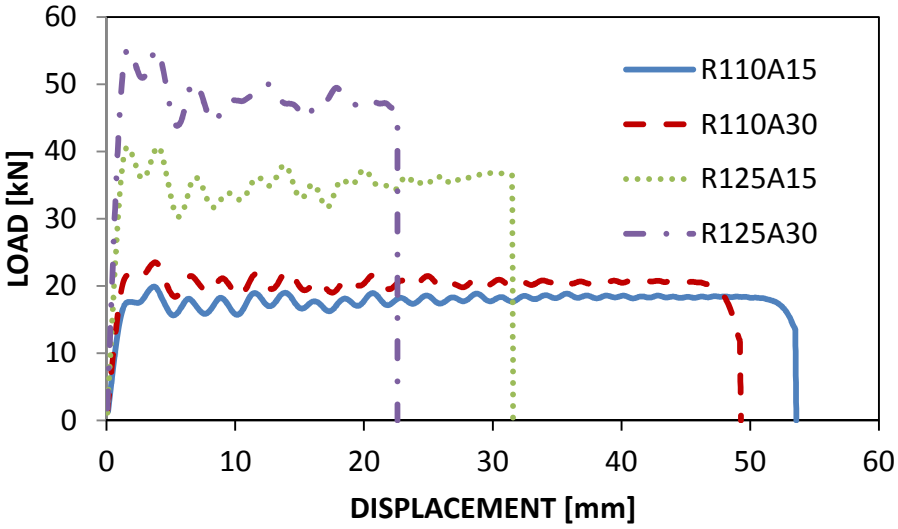

Figure 52: Load- displacement properties of expansion tubes R110A15, R110A30, R125A15 and R125A30 under dynamic conditions

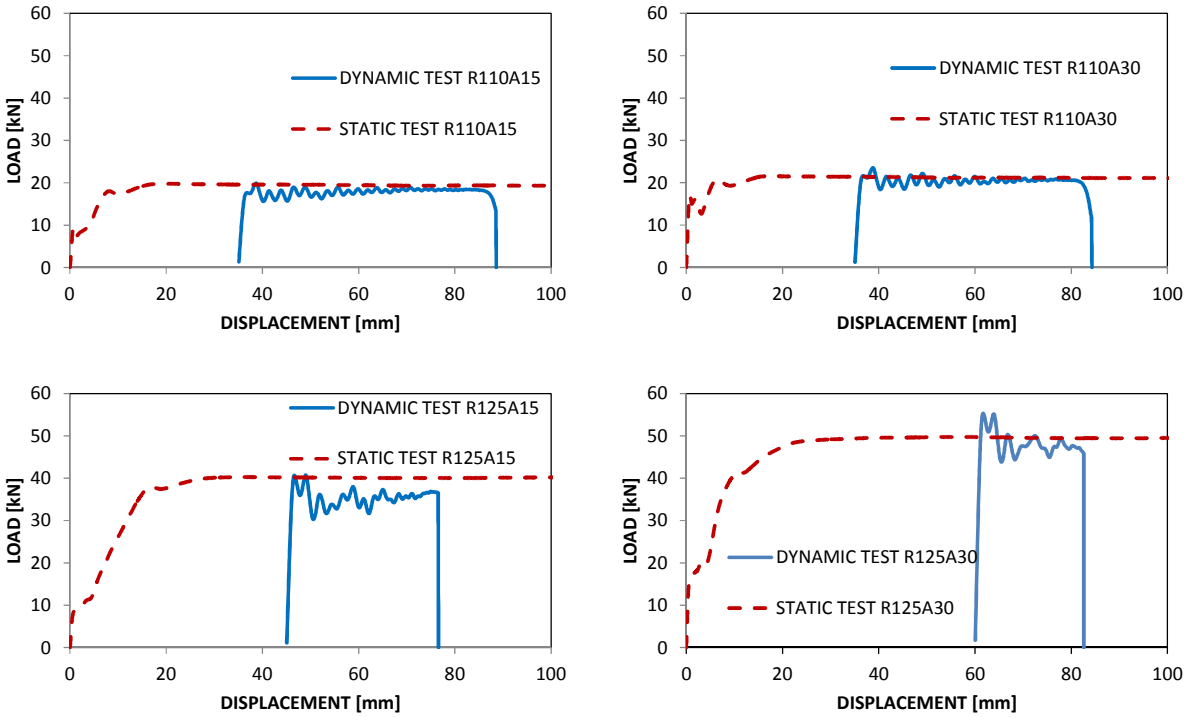

Figure 53: Load-displacement properties of the quasi-static and dynamic testing of the four types of expansion tubes

TYPE	ENERGY (kJ)	STROKE (mm)	MEAN LOAD STATIC (kN)	MEAN LOAD DYNAMIC (kN)	Δ MEAN LOAD (%)
R110A15	0.958	53.6	19.4	17.9	-7.9
R110A15	1.006	49.3	21.4	20.4	-4.7
R125A15	1.112	31.5	40.6	35.3	-13.2
R125A30	1.097	22.6	49.9	48.5	-2.9

Table 16: Energy absorption, stroke, quasi-static mean and dynamic mean loads and variation of the mean loads of the four types of expansion tubes

5.3 Axial Testing of Hybrid Tubes (Submission 6)

5.3.1 Quasi-static Testing

Three repeats of each type of the six types of hybrid tubes, R11A15D08, R110A15D12, R125A15D08, R125A15D12, R125A30D08 and R125A30D12; were quasi-statically tested. The results were repeatable, except specimens R125A30D08 and R125A30D12, which became unstable due to global buckling. Figure 54 shows the comparison of the load-displacement properties of the hybrid tubes R110A15D08, R110A15D12, R125A15D08 and R125A15D12. The energy absorption of the specimens with smaller splitting flaring radius was higher, as expected. Figure 55 shows the comparison of the load-displacement properties of the tubes R125A30D08 and R125A30D12. Both type of tubes experienced global buckling. It can be inferred that the critical global buckling load of tubes with this particular geometry is 70 kN. Table 17 shows the energy absorption, stroke, mean and peak load results of quasi-static testing of the hybrid tubes.

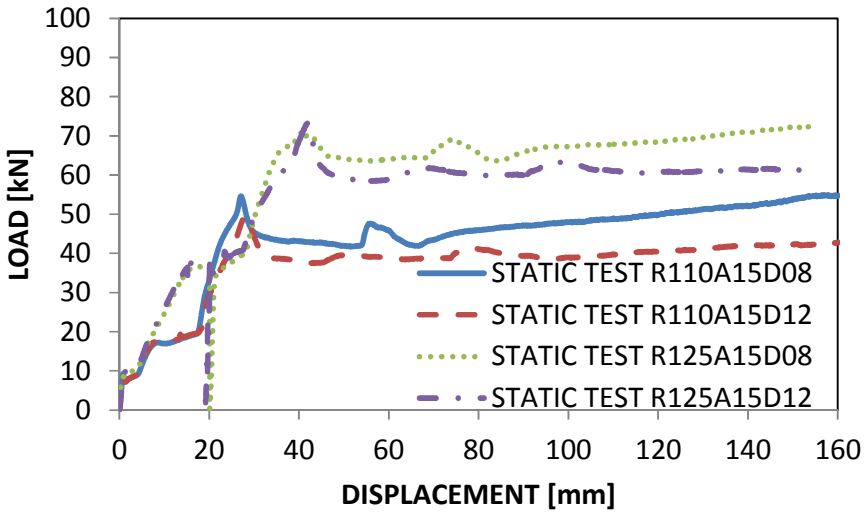

Figure 54: Load- displacement properties of hybrid tubes R110A15D08, R110A15D12, R125A15D08 and R125A15D12

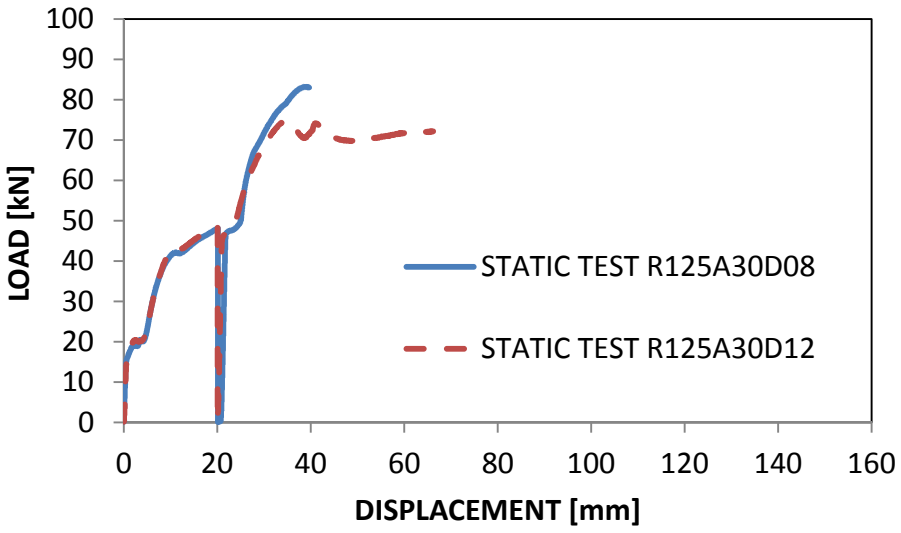

Figure 55: Load- displacement properties of hybrid tubes R125A30D08 and R125A30D12

TYPE	ENERGY (kJ)	STROKE (mm)	MEAN LOAD (kN)	PEAK LOAD (kN)
R110A15D08	7.012	160	43.8	52.1
R110A15D12	5.942	160	37.1	49.6
R125A15D08	9.253	160	59.7	70.1
R125A15D12	9.029	160	54.7	69.7

Table 17: Energy absorption, stroke, mean and peak load results of the quasi-static testing of hybrid tubes R110A15D08, R110A15D12, R125A15D08 and R125A15D12

5.3.2 Dynamic Testing

Three repeats of each type of the expansion tubes were tested and the results were very repeatable, as shown in submissions 6. Figure 57 shows image series of the dynamic test of an hybrid specimen R110A15D08. Figure 58 shows the load-displacement comparative properties of the quasi-static and dynamic testing of the hybrid specimens. Note that, under dynamic conditions the specimen R125A30D12 did not experience global buckling, exhibiting a mean load of 75 kN. Therefore, the critical global buckling load of tubes with this particular geometry under dynamic conditions must be over 75 kN. This behaviour appears to be consistent with (Karagiozova and Jones, 2008), who observed that crash columns were more stable at under higher strain rate loading.

Table 18 shows the energy absorption, stroke, quasi-static mean and dynamic mean loads and variation of the mean loads of the four types of the hybrid specimens.

Figure 56: Scale of the deformed R120A15D08 hybrid tube

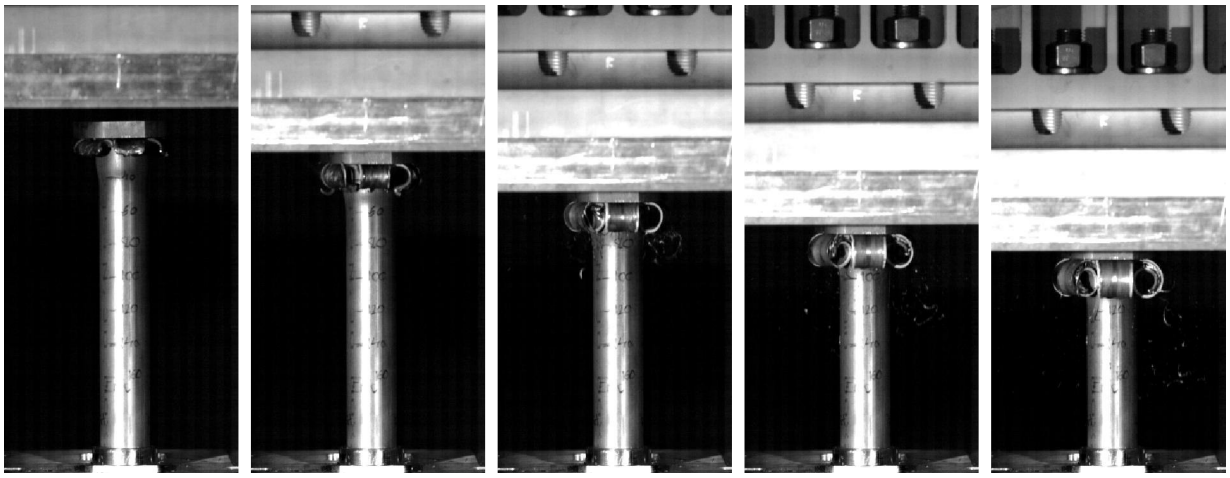

Figure 57: Sequence of the dynamic test of a hybrid R110A15D08 specimen

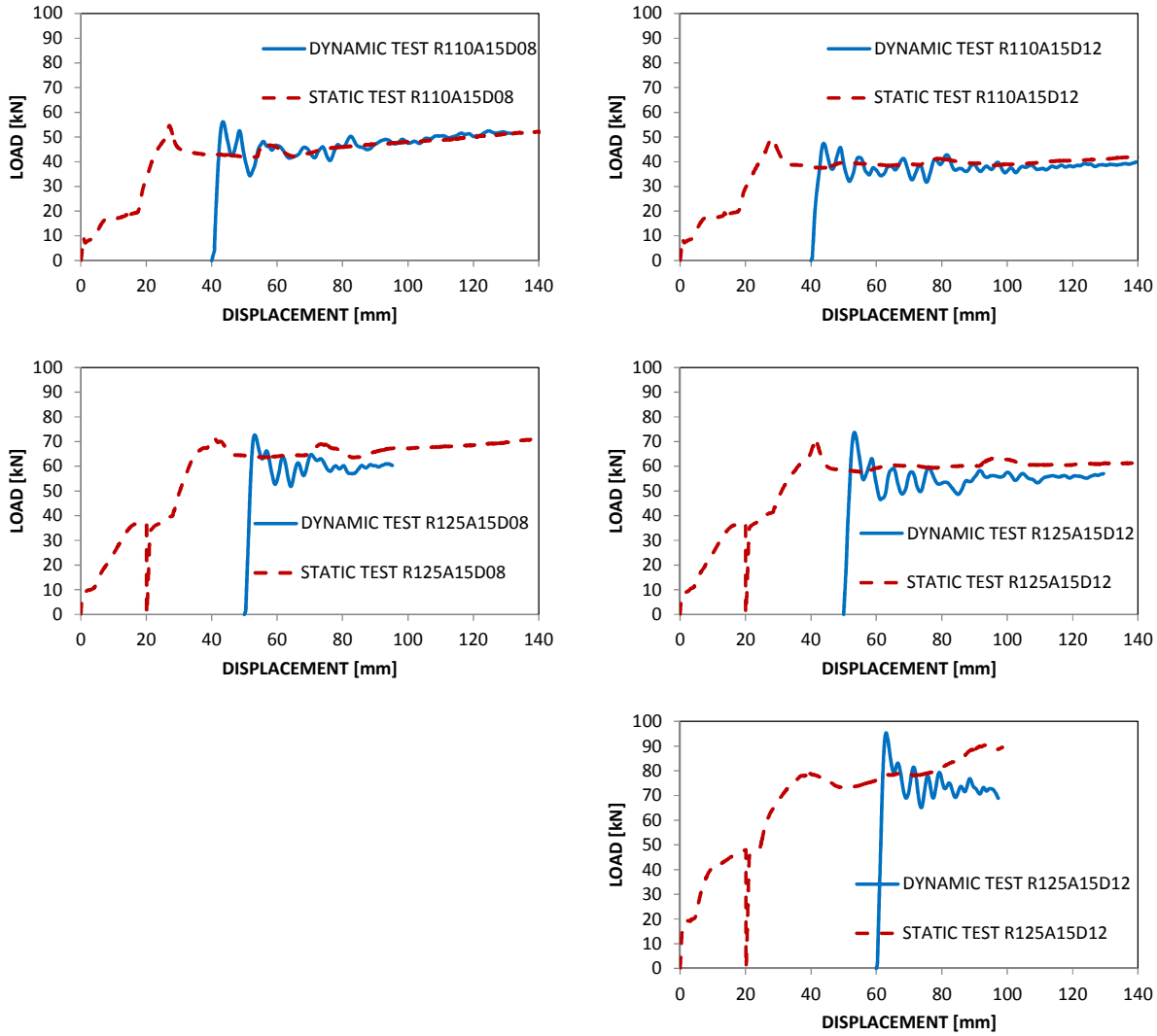

Figure 58: Load-displacement properties of the quasi-static and dynamic testing of the hybrid specimens R110A15D08, R110A15D12, R125A15D08, R125A15D12 and R125A30D12

TYPE	ENERGY (kJ)	STROKE (mm)	MEAN LOAD STATIC (kN)	MEAN LOAD DYNAMIC (kN)	Δ MEAN LOAD (%)
R110A15D08	3.723	89.8	47.2	46.8	-0.8
R110A15D12	4.271	98.1	39.6	37.8	-4.5
R125A15D08	4.317	45.2	65.3	59.2	-9.3
R125A15D12	2.682	79.7	60.3	54.2	-10.2
R125A15D12	2.742	37.2	82.4	74.8	-9.2

Table 18: Energy absorption, stroke, quasi-static mean and dynamic mean loads and variation of the mean loads of the four types of expansion tubes

5.4 Oblique Loading Testing (Submission 7)

5.4.1 Quasi-static Testing

Three repeats of the splitting, expansion (R110A15 and R125A15) and hybrid (R110A15D08 and R125A15D08) were tested under oblique loading conditions, using 5° and 10° inclined plates. Figure 59 to Figure 67 show the image series of these specimens. The specimen R125A15 could not be tested under the 10° inclined plate, as the die failed.

The expansion R125A15 specimen, unlike the expansion R110A15 specimen, exhibits a double curvature of the deformed tube. This is caused by the off-axis bending of the tube and the subsequent contact with the die, which has conformed to the angle of the crushing plate. Both specimens R110A15D08 and R125A15D08 experience global buckling under the 10° inclined plate compression, which indicates that the critical transverse global buckling load has been exceeded. The transverse loading induced to the tubes by the compression plates are a function of the axial loading and inclined angle, and therefore, independent of the type of tube. Table 19 shows the transverse loading induced to each specimen. It can be inferred that the critical transverse global buckling load for these particular tubes under quasi-static conditions is within the range of 5.7-8.0 kN.

			TRANSVERSE MEAN LOAD (kN)	
MECHANISM	**TYPE**	**AXIAL MEAN LOAD (kN)**	**5°**	**10°**
SPLITTING		28.5	2.5	5.0
EXPANSION	R110A15	20.2	1.8	3.6
	R125A15	40.4	3.5	7.1
HYBRID	R110A15D08	45.5	4.0	8.0
	R125A15D08	65.5	5.7	11.5

Table 19: Axial mean load and associated transverse load for load angles 5° and 10° of each type of tube

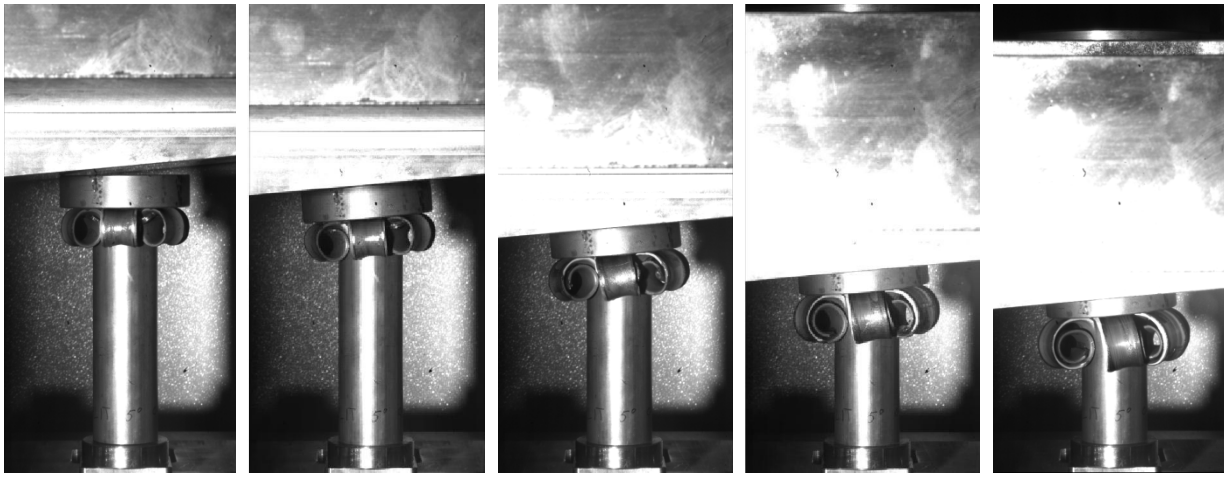

Figure 59: Sequence of the crushing of a splitting specimen by a 5° inclined plate

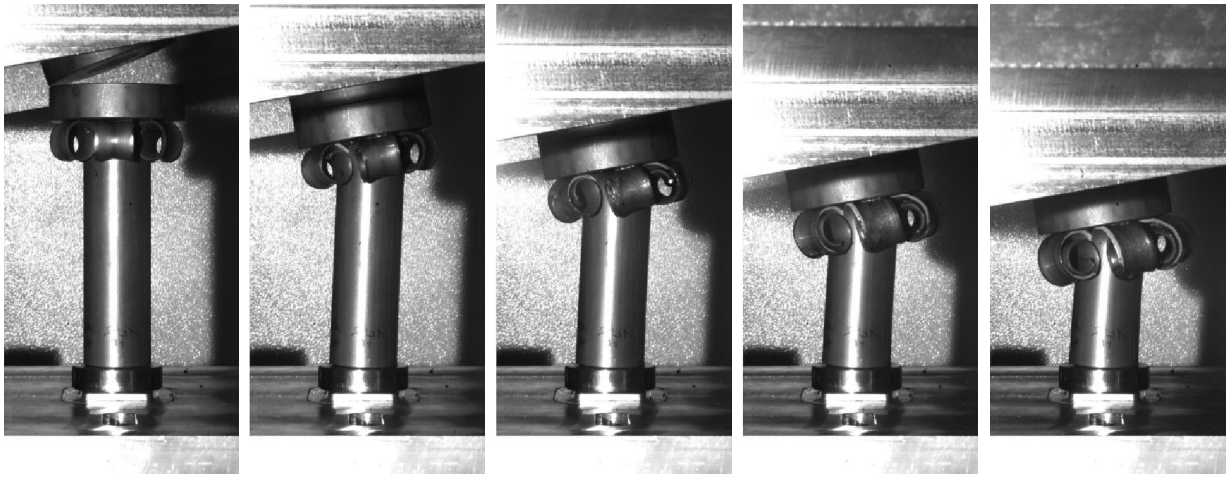

Figure 60: Sequence of the crushing of a splitting specimen by a 10° inclined plate

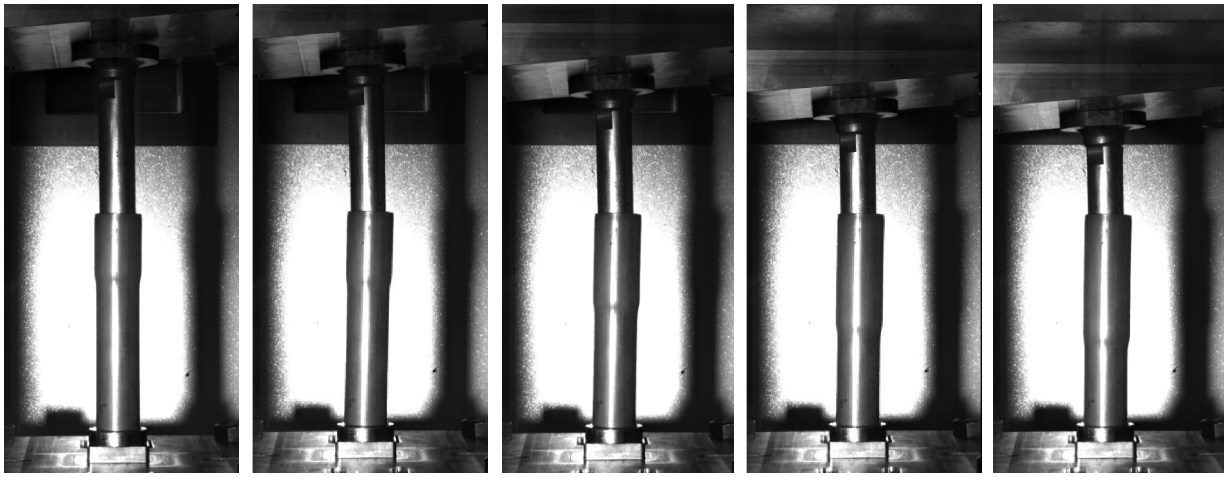

Figure 61: Sequence of the crushing of an expansion R110A15 specimen by a 5° inclined plate

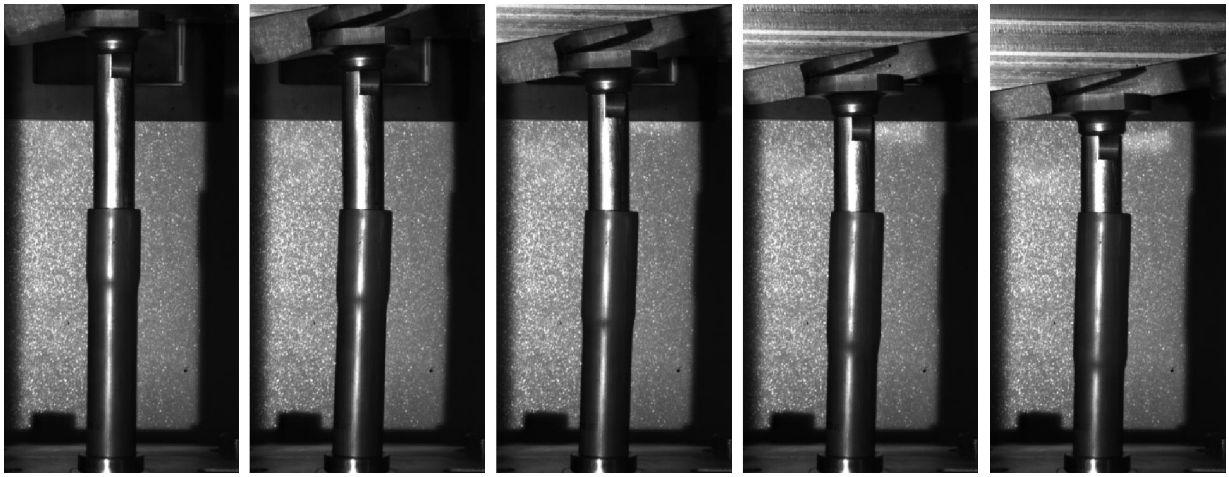

Figure 62: Sequence of the crushing of an expansion R110A15 specimen by a 10° inclined plate

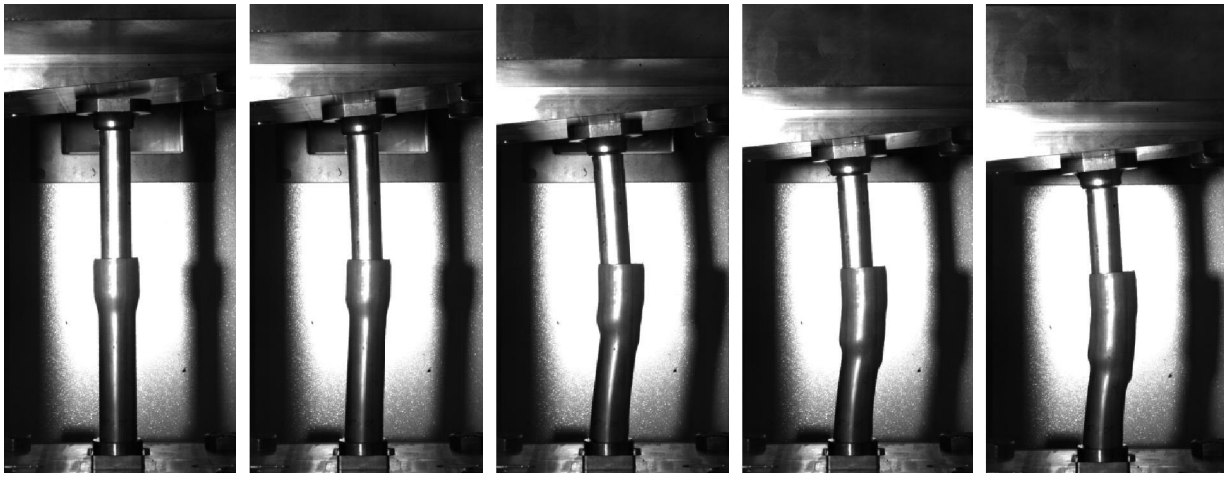

Figure 63: Sequence of the crushing of an expansion R125A15 specimen by a 5° inclined plate

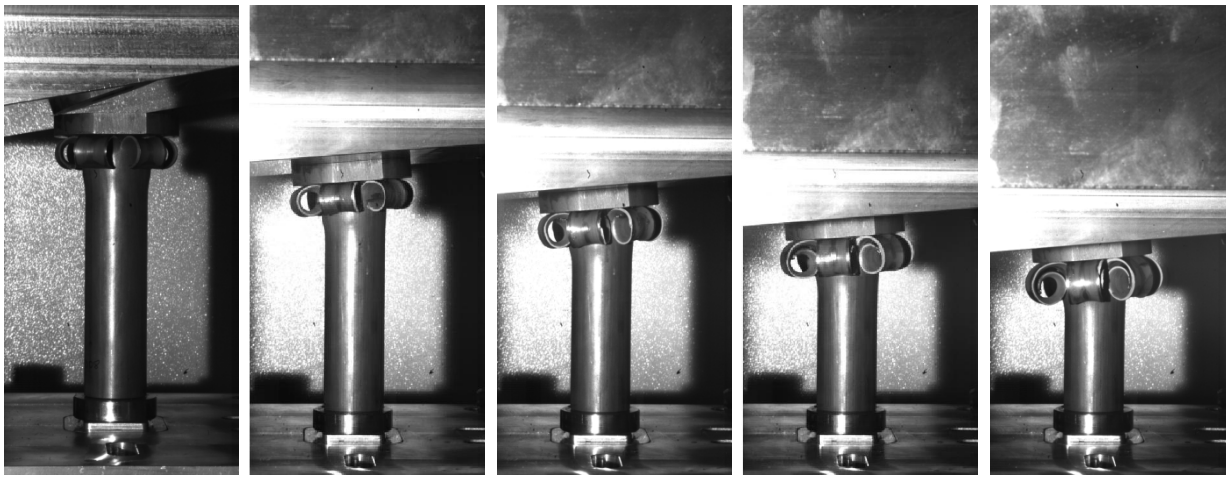

Figure 64: Sequence of the crushing of a hybrid R110A15D08 specimen by a 5° inclined plate

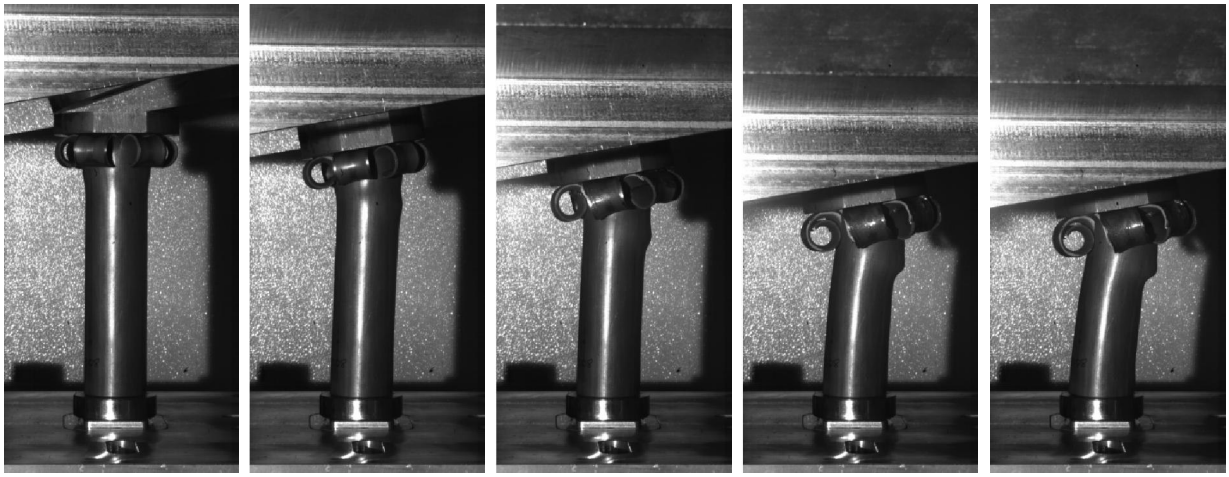

Figure 65: Sequence of the crushing of a hybrid R110A15D08 specimen by a 10° inclined plate

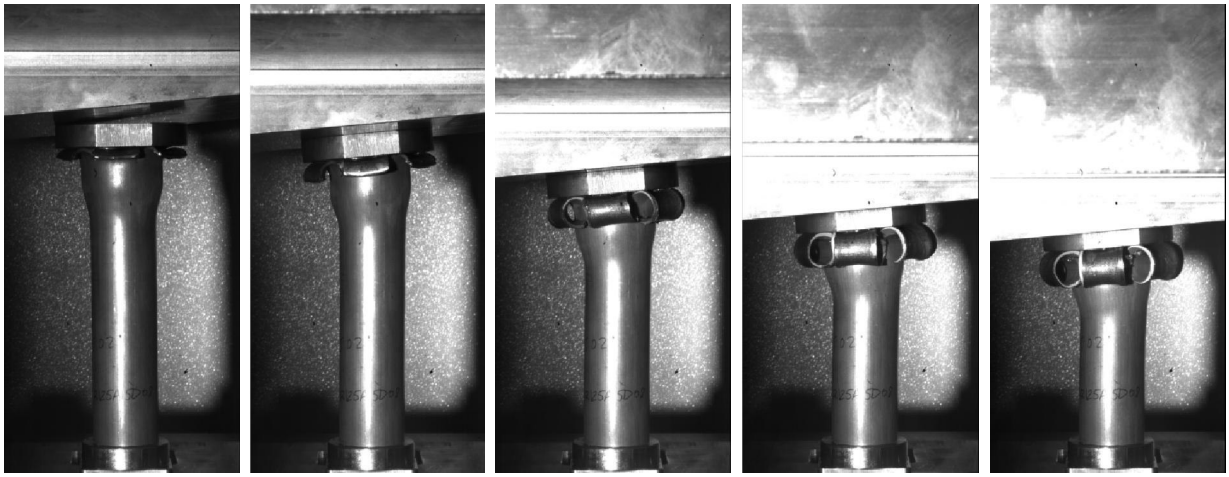

Figure 66: Sequence of the crushing of a hybrid R125A15D08 specimen by a 5° inclined plate

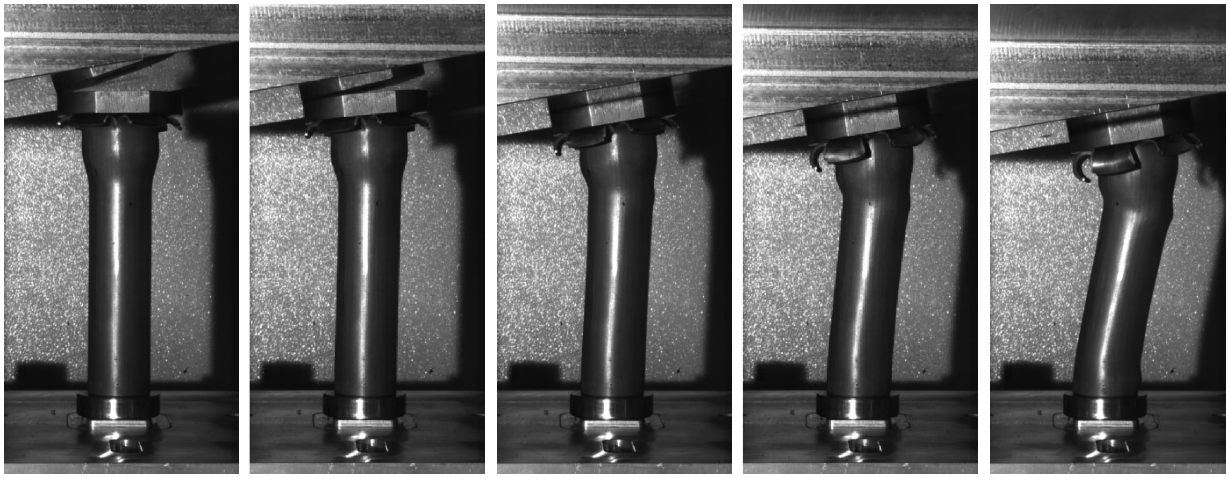

Figure 67: Sequence of the crushing of a hybrid R125A15D08 specimen by a 10° inclined plate

Three repeats of each type of specimens were tested and showed good repeatability. Figure 68 shows the load displacement properties of the splitting, expansion (R110A15 and R125A15) and hybrid (R110A15D08 and R125A15D08) specimens tested by 0°, 5° and 10° angle plates, under quasi-static conditions. Note that the general trend of the axial mean load is to increase as the plate angle (and the transverse load) increases. Table 20 quantifies this trend. Note that the increase is more obvious on the splitting specimens and, disproportionately, on the expansion R125A15 specimen. The increases exhibited by the expansion R110A15 and both hybrid specimens were consistently small.

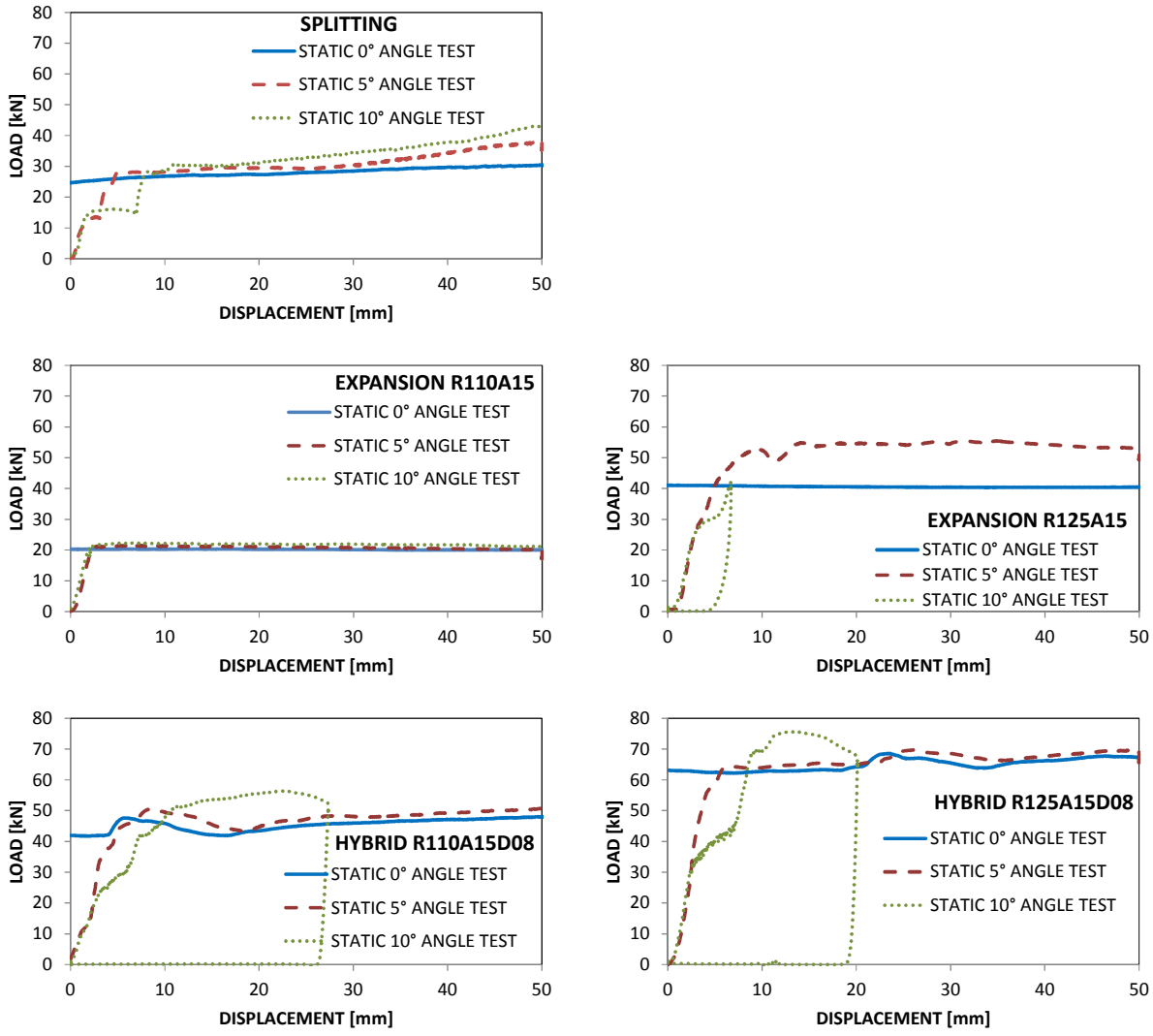

Figure 68: Load- displacement properties of the splitting, expansion (R110A15 and R125A15) and hybrid (R110A15D08 and R125A15D08) specimens tested by 0°, 5° and 10° angle plates, under quasi-static conditions

MECHANISM	TYPE	ANGLE (°)	ENERGY (kJ)	STROKE (mm)	AXIAL MEAN LOAD (kN)	INCREASE (%)
SPLITTING		0	1.14	40	28.5	0
		5	1.27	40	31.8	11.5
		10	1.40	40	34.9	22.3
EXPANSION	R110A15	0	0.81	40	20.2	0
		5	0.83	40	20.8	3.0
		10	0.87	40	21.8	7.9
	R125A15	0	1.62	40	40.4	0
		5	2.16	40	54.0	33.6
		10	-	-	-	-
HYBRID	R110A15D08	0	1.82	40	45.5	0
		5	1.92	40	47.9	5.2
		10	-	-	-	-
	R125A15D08	0	2.62	40	65.5	0
		5	2.69	40	67.2	2.6
		10	-	-	-	-

Table 20: Energy absorbed, axial mean load and mean load increase of the specimens subjected to 5° and 10° crushing plate

5.4.2 Dynamic Testing

Three repeats of each type of the expansion tubes were tested and the results were repeatable. Figure 69 shows that, under dynamic conditions, the specimen R110A15D08 could be successfully crushed by a 10° inclined plate.

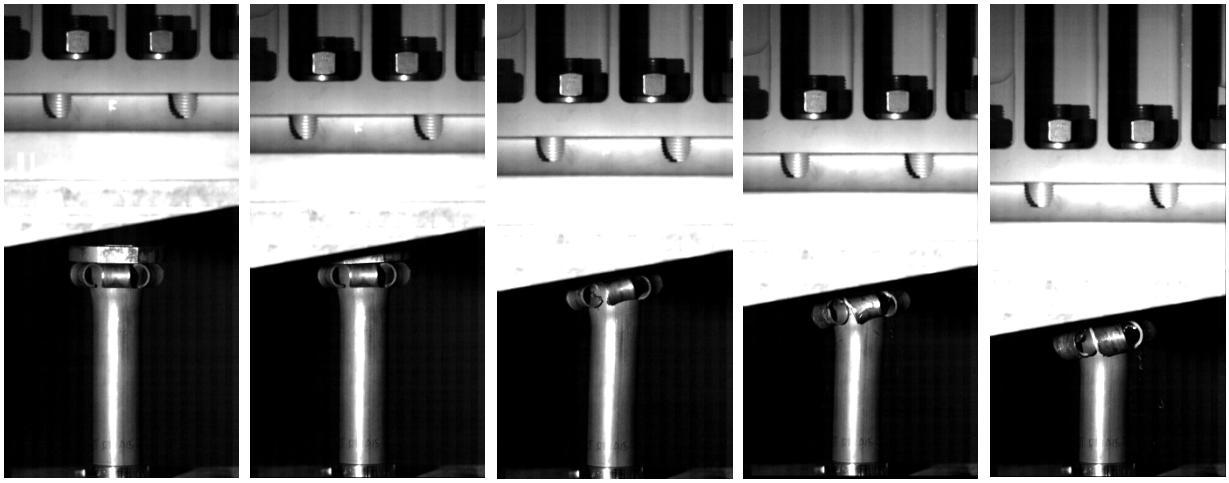

Figure 69: Sequence of the dynamic crushing of a hybrid R110A15D08 specimen by a 10° inclined plate

Figure 70 shows the load displacement properties of the splitting, expansion (R110A15) and hybrid (R110A15D08 and R125A15D08) specimens tested by 0°, 5° and 10° angle plates, under dynamic conditions. The specimen R125A15 could not be successfully tested. Figure

71 shows the sequence of the dynamic crushing of an expansion R125A15 specimen by a 5° inclined plate. The connection between the die rod and the die impact bearing surface failed, similarly as it happened to the quasi-static testing of the expansion R125A15 specimen under the 10° inclined plate.

The results, displayed in Table 21, present, with exceptions, a generally similar trend as that of the quasi-static results for the specimens crushed under the 5° incline plate, although the magnitude of the mean load increase is generally smaller.

The performance of the splitting and R110A15 expansion tubes tested under the 10° inclined plate show a lower mean load variation, contrary to the quasi-static results. The result of the R110A15D08 hybrid tube is consistent with the expected outcome.

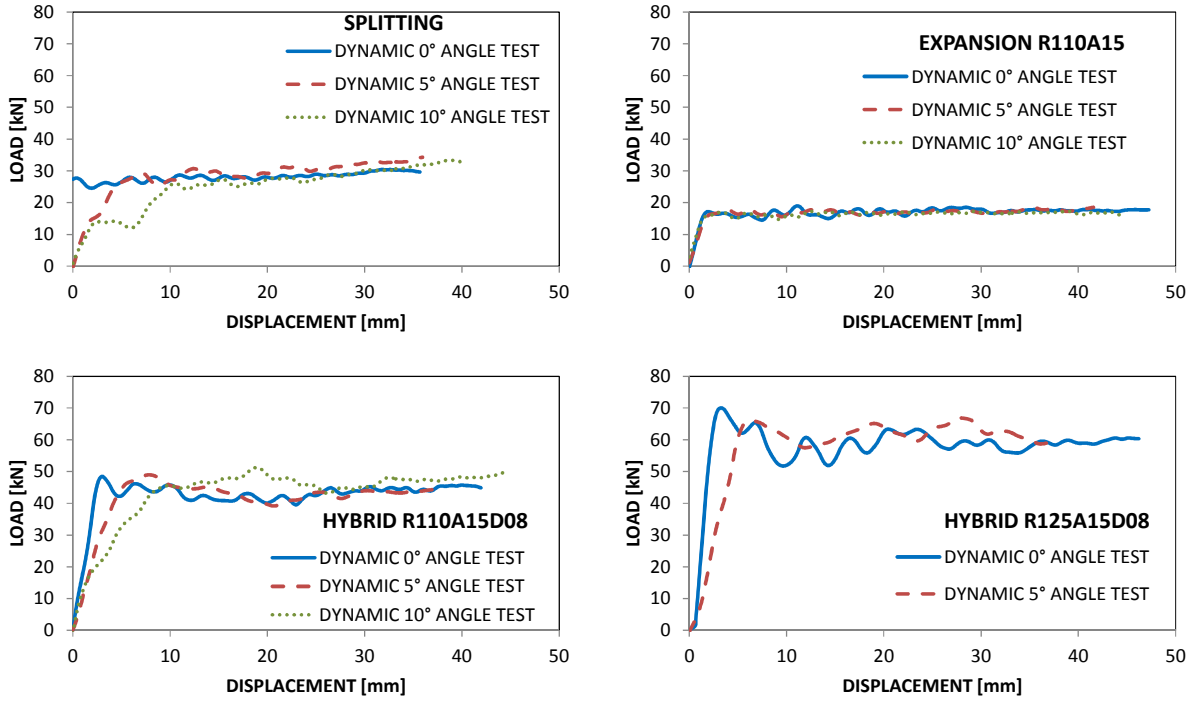

Figure 70: Load- displacement properties of the specimens splitting, expansion (R110A15 and R125A15) and hybrid (R110A15D08 and R125A15D08) tested by 0°, 5° and 10° angle plates, under dynamic conditions

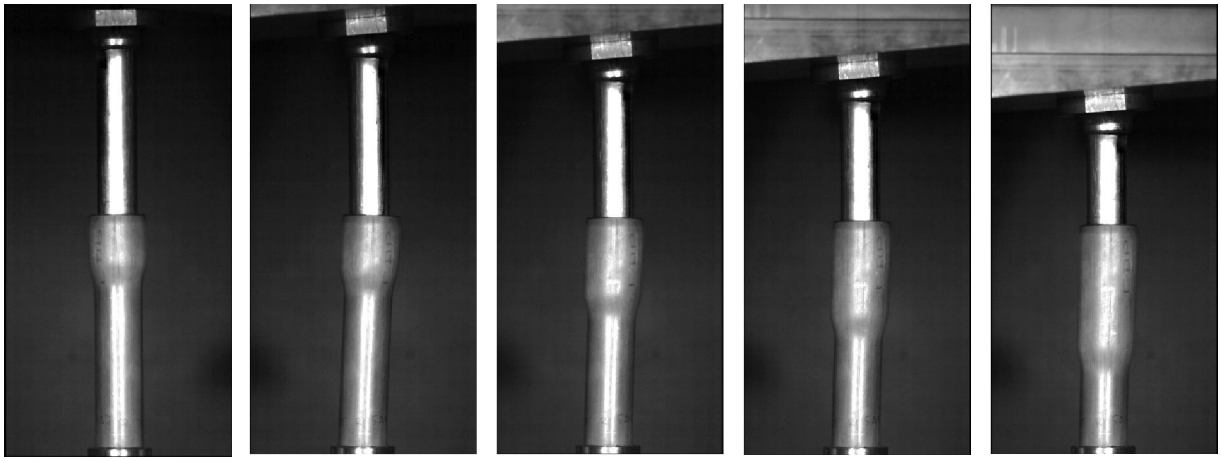

Figure 71: Sequence of the dynamic crushing of a hybrid R125A15 specimen by a 5° inclined plate

MECHANISM	TYPE	ANGLE (°)	ENERGY (kJ)	STROKE (mm)	AXIAL MEAN LOAD (kN)	INCREASE (%)
SPLITTING		0	1.000	35.7	28.0	0
		5	0.794	26.0	30.6	9.2
		10	0.863	30.3	28.5	1.6
EXPANSION	R110A15	0	0.646	37.3	17.3	0
		5	0.543	31.6	17.2	-0.8
		10	0.577	34.6	16.7	-3.8
	R125A15	0	0.743	21.6	34.4	0
		5	-	-	-	-
		10	-	-	-	-
HYBRID	R110A15D08	0	1.380	32.0	43.2	0
		5	1.241	27.8	44.6	3.4
		10	1.619	34.5	47.0	8.8
	R125A15D08	0	2.127	36.2	58.7	0
		5	1.692	27.4	61.9	5.3
		10	-	-	-	-

Table 21: Energy absorbed, axial mean load and mean load increase of the specimens subjected to 5° and 10° crushing plate

5.5 Fracture Strain Measurement Results (Submissions 4)

Three specimens of each, four-notched and six-notched splitting tubes, were tested and analysed with the DIC methodology stated in section 4.7. Table 22 shows a summary of the averaged values of the von Mises fracture strain, the axial distance between last data node and the tip of the crack and the strain ratio at the tip of the crack. The values of von Mises strain, and strain ratio are averaged from the number of data nodes used for each specimen. For von Mises strain and strain ratio the standard variation of each specimen is

tabulated in Table 22. It can be observed that the largest variation of von Mises strain corresponds to specimen 5, which exhibits a standard variation of 11.1% of strain.

SPECIMEN	1	2	3	AVERAGE 6 NOTCHES	4	5	6	AVERAGE 4 NOTCHES
NUMBER OF NOTCHES	6	6	6		4	4	4	
VON MISES STRAIN [%]	59.9±7.1	63.6±8.8	55.7±5.8	59.7	62.8±7.9	58.8±11.1	57.4±6.8	59.7
DISTANCE CRACK TIP-LAST DATA NODE [mm]	0.20	0.36	0.13	0.23	0.21	0.18	0.15	0.18
STRAIN RATIO α	-0.08±0.06	-0.16±0.06	-0.09±0.02	-0.11	-0.00±0.08	-0.03±0.06	-0.04±0.08	-0.03

Table 22: Fracture strain, crack-data node distance and strain ratio at the tip of the crack

Both types of specimens, six and four notches, exhibit similar von Mises fracture strain of $\varepsilon_f \approx 0.60$. This value is consistent with the fracture value of $\varepsilon_f \approx 0.61$, found by (Gruben et al., 2012) for a stronger steel, cold-rolled dual-phase steel Docol 600DL. The average axial distance between the last data node (before the facet disappears) and the tip of the crack is 0.23 mm and 0.18 mm for the six and four notches respectively. The distances are very similar in both cases and approximately half of the facet length, measured as 0.44 mm. The strain ratio α at the tip of the crack is $\alpha = -0.11$ and $\alpha = -0.03$ for the six and four notches specimens respectively.

6 Simulation Activity

The models shown in section 4.8.1 were used to predict the behaviour of the hybrid tubes. The models, as stated in section 4.8.5, required the knowledge of the friction coefficient and the fracture strain. *Calibration* of splitting and expansion models was performed, resulting in the finding of the appropriate coefficients of friction in each case. *Validation* was performed for the hybrid tubes by comparing the test results to the simulation results.

6.1 Fracture Strain Calibration (Submissions 3 and 4)

The value of the fracture strain at the tip of the crack in splitting tubes was found to be $\varepsilon_f \approx 0.60$ in section 5.5. This value was used in the numerical models of the splitting and hybrid tubes alike. Section 5.5 also suggests that the stress-state of the tip of the crack approximates plane strain conditions. Unfortunately, there is not enough information to build a fracture locus, similar to that in Figure 16, to include in the numerical model. A fracture locus was artificially constructed for steel E355 using the known value for plane strain and similarity with the fracture locus of a DP600 steel. The fracture locus was included in the numerical model of a hybrid R110A15D08 tube, without the additional part line described in section 4.8.1, and compared to a model using the additional part line methodology stated in section 4.8.1. Figure 72 shows the comparison of the load-displacement results for those two models. Note that the model which includes the fracture locus under-predicts the resistive load. This is caused by the contact instability created when elements away from the path of the crack get deleted, as shown in Figure 73. For this reason, all the numerical models featuring splitting were modelled using the methodology stated in section 4.8.1. This is true also for the numerical models of the oblique loading test specimens. Under oblique loading conditions it is reasonable to assume that the path of the crack is not straight, as modelled. However, section 6.5 will show that these models predict with reasonable accuracy the performance of tubes subjected to oblique loading.

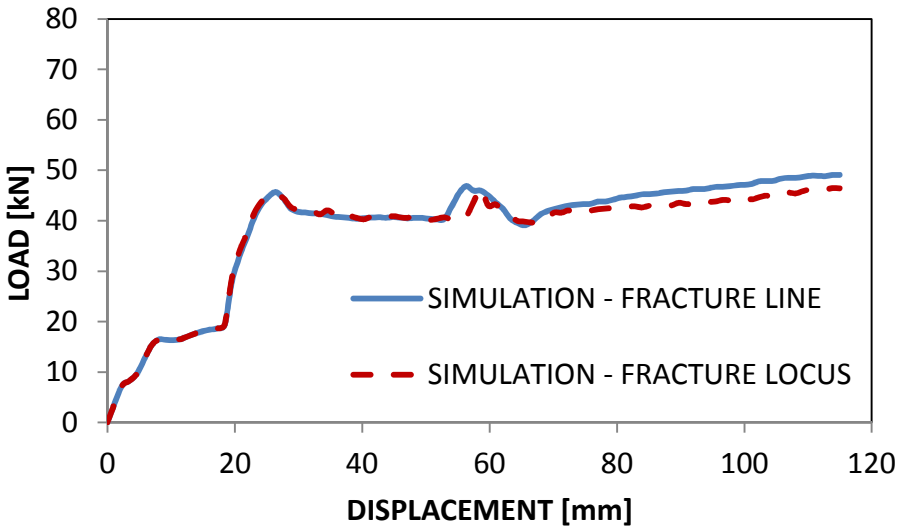

Figure 72: Load- displacement properties of the simulated hybrid tubes R110A15D08

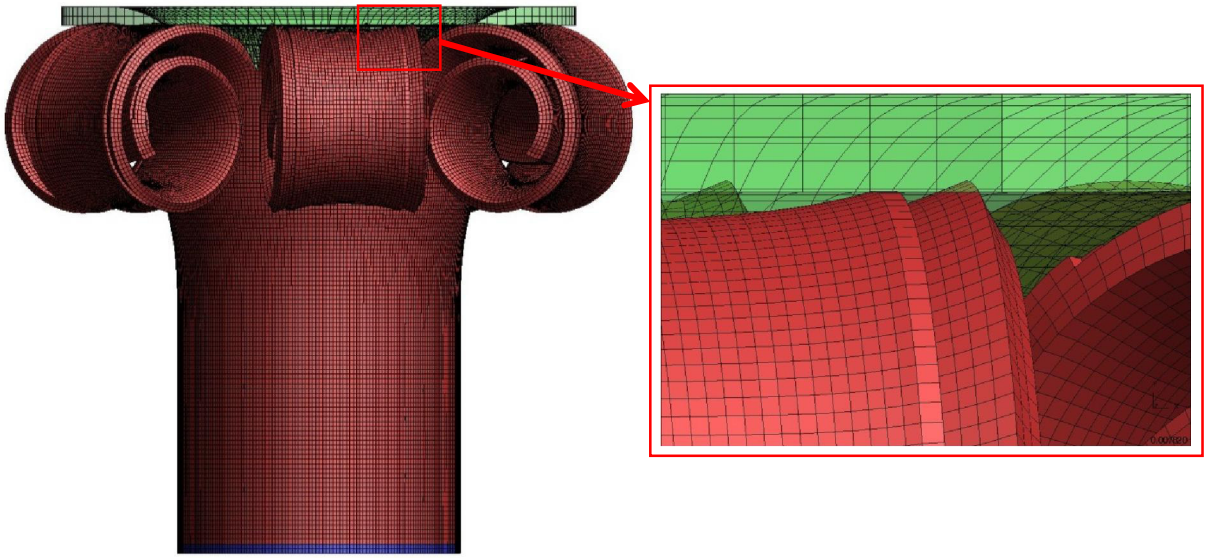

Figure 73: Detail of element penetration between the deformable tube and the rigid die, as a result of the spurious deletion of four rows of element on the inner surface of the deformable tube

6.2 Calibration of the Splitting Tubes Numerical Models under Quasi-static Conditions (Submissions 3 and 4)

In order to correlate the load-displacement properties from quasi-static test and finite element simulation, the coefficient of friction between the flaring die and the tube was adjusted. It was found that the friction coefficient $\mu = 0.07$ approximates the test data closely. Figure 74 shows a comparison of the load-displacement curves from test and the simulation activities, for the four (left) and six (right) notches specimens. The energy

absorption discrepancy between test and simulation is small, -1.04% and 0.16% for the specimens with four and six notches respectively. The simulation is thus able to predict accurately the load-displacement response of a splitting tube under static testing conditions. It can also be ascertained from the simulation that the proportion of energy dissipated by friction is 12% in both cases.

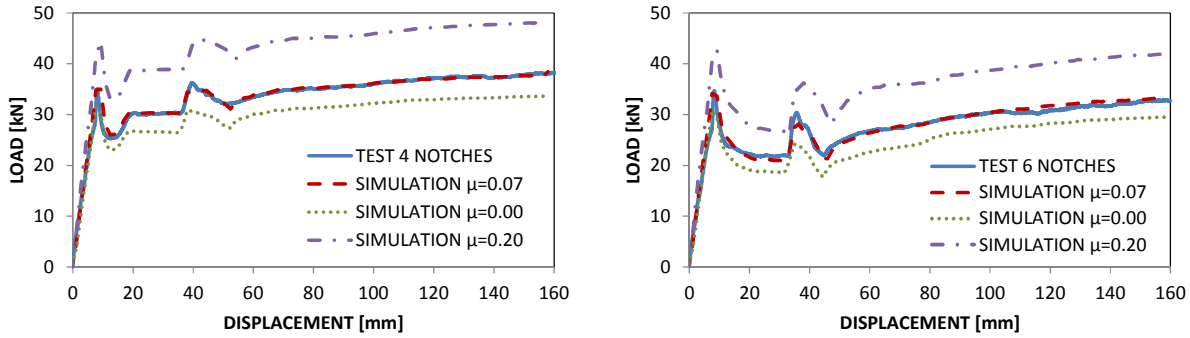

Figure 74: Comparison of load-displacement properties, for the quasi-static test specimen with four (left) and six (right) notches and FEA simulation results

6.3 Calibration of the Expansion Tubes Numerical Models under Quasi-static Conditions (Submission 5)

The simulation of the expansion tubes reproduced accurately their behaviour, as shown in Figure 75, except for the specimen with expansion ratio R = 1.10. Submission 5 showed that the R110A15 die deformed plastically during the event. The plastically deformed shape of the R110A15 die was modified in the numerical model until the deformation shape (the outer diameter) of the expanded tube from the simulation matched that measured from the test specimens. Table 23 shows the comparison (test vs. simulation) of the energy absorption of the expansion tubes. It also includes the static coefficients of friction between the die and deformation tube which match the test results. The range of the coefficients of friction is 0.07 to 0.11, which highlights the different friction conditions created by the different expansion ratios. It can also be ascertained from the simulation that the proportion of energy dissipated by friction is 23%, 28% and 14% for the R110A15, R125A15 and R125A30 expansion tubes respectively.

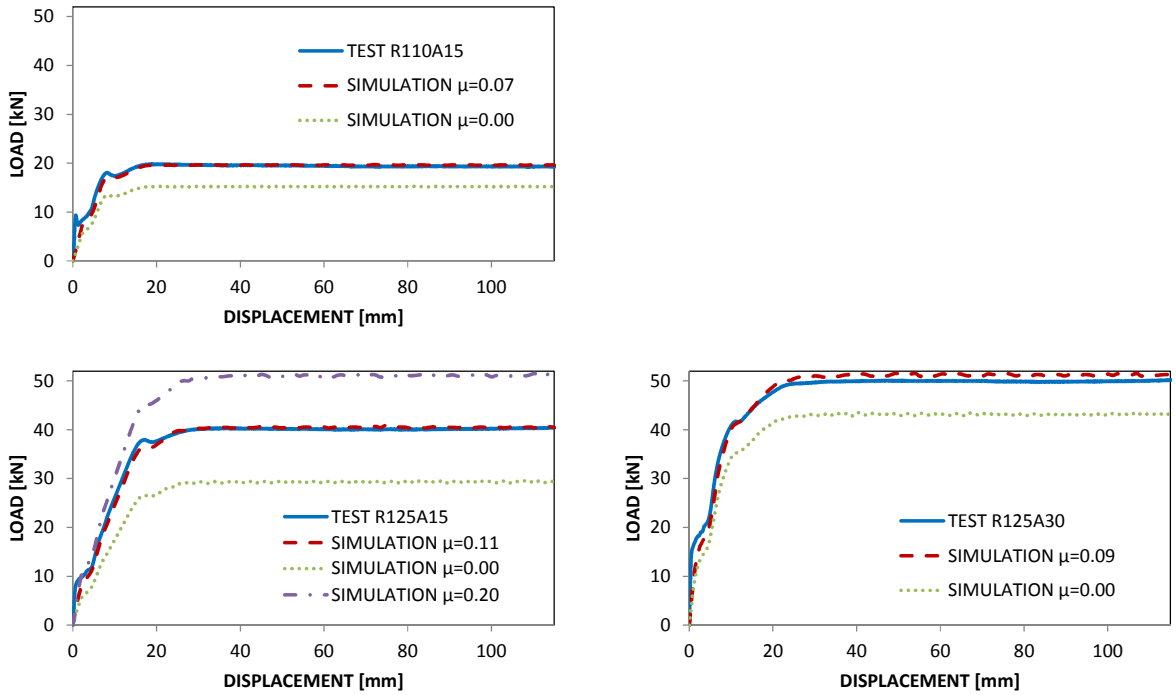

Figure 75: Comparison of load-displacement properties between the quasi-static test results of the R110A15, R125A15 and R125A30 specimens and FEA simulation results

		ENERGY (kJ)		
SPECIMEN	**μ**	**TEST**	**SIMULATION**	**Δ**
R110A15 (pre-modification)	0.07	2.166	2.302	6.28%
R125A15	0.11	4.340	4.391	1.18%
R125A30	0.09	5.444	5.529	1.56%

Table 23: Comparison (test vs. simulation) of the energy absorption of the expansion tubes; and static coefficients of friction between the die and deformation tube

6.4 Validation of the Numerical Models of the Hybrid Tubes under Quasi-Static Conditions (Submission 6)

The numerical models of the hybrid tubes included the values of fracture strain and friction coefficients found above. Figure 76 shows the load-displacement properties comparison of the hybrid tubes, between the quasi-static testing and simulation. Table 24 shows the variation of the mean load between the test and simulation. It is observed that the numerical models can predict the hybrid tubes behaviour accurately.

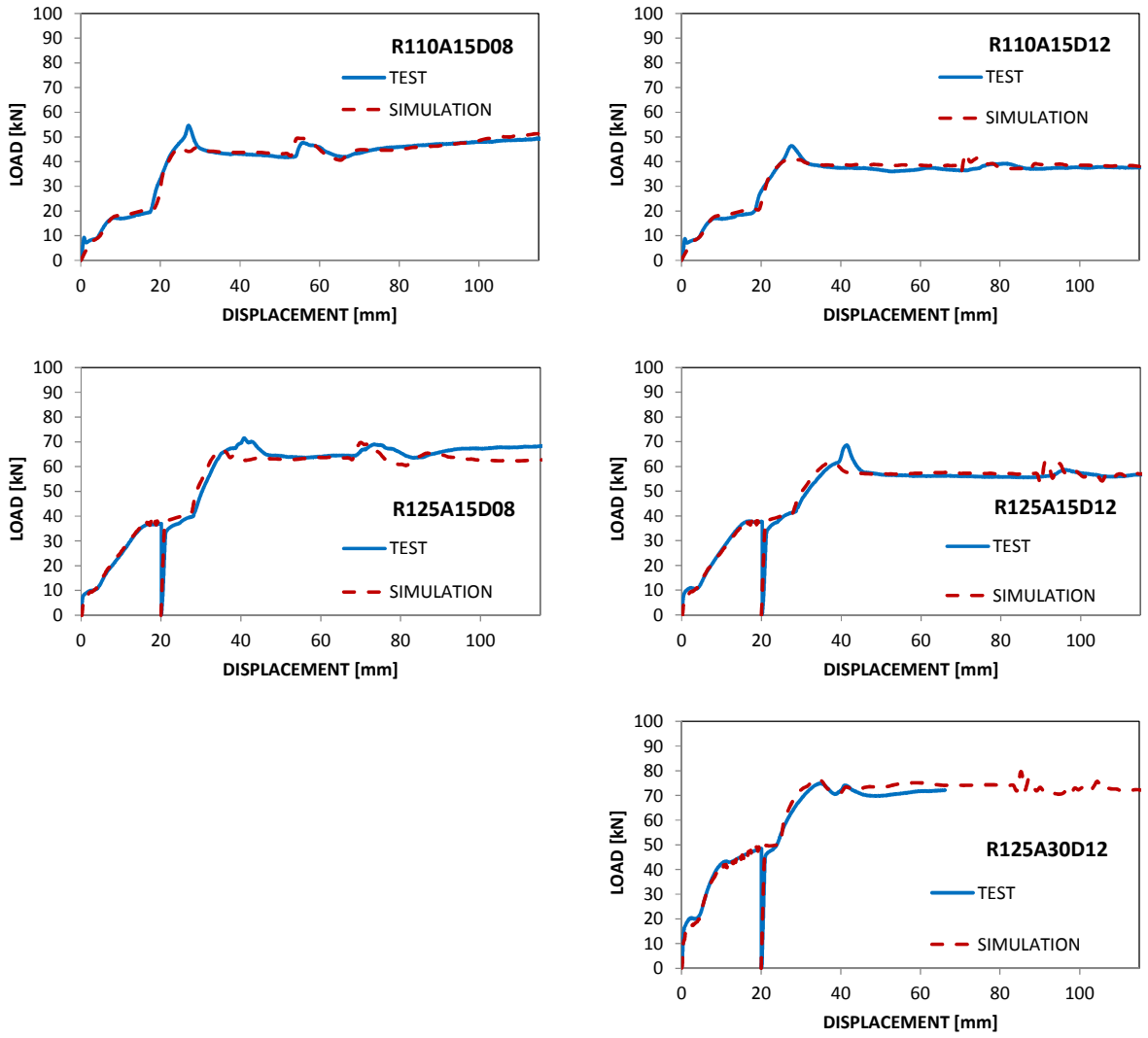

Figure 76: Load-displacement properties of the hybrid tubes from quasi-static testing and simulation

		ENERGY (kJ)		MEAN LOAD (kN)		
SPECIMEN	**STROKE (mm)**	**TEST**	**SIMULATION**	**TEST**	**SIMULATION**	**VARIATION MEAN LOAD (%)**
R110A15D08	115	4.63	4.64	40.3	40.3	0.13
R110A15D12	115	3.89	3.96	33.8	34.4	1.83
R125A15D08	115	6.37	6.28	55.3	54.6	-1.38
R125A15D12	115	5.69	5.74	49.5	49.9	0.88
R125A30D12	115	n/a	7.50	n/a	65.2	n/a

Table 24: Energy absorption properties of the specimens from quasi-static testing and simulation

6.5 Simulation of the Specimens Subjected to Oblique Loading (Submission 7)

Figure 77 shows the comparison of the load-displacement properties from quasi-static test and simulation of specimens subjected to oblique loading, 5° (left column) and 10° (right column) inclined plates. Table 25 shows the energy absorption comparison between the tubes tested under the 5° and 10° inclined plates and the numerical models.

The simulation offers a reasonably accurate prediction of the oblique loading events, except for the expansion tubes and the hybrid tubes under the 10° inclined plates. The simulation of the expansion R110A15 tubes exhibits a decreased energy absorption for which a reasonable explanation could not be found. The numerical model of specimen R125A15 predicts global buckling, which is not observed during testing. The numerical model of the hybrid R125A15D08 specimen under the 10° inclined plate predicts catastrophic tearing of the tube, rather than the global buckling observed during test.

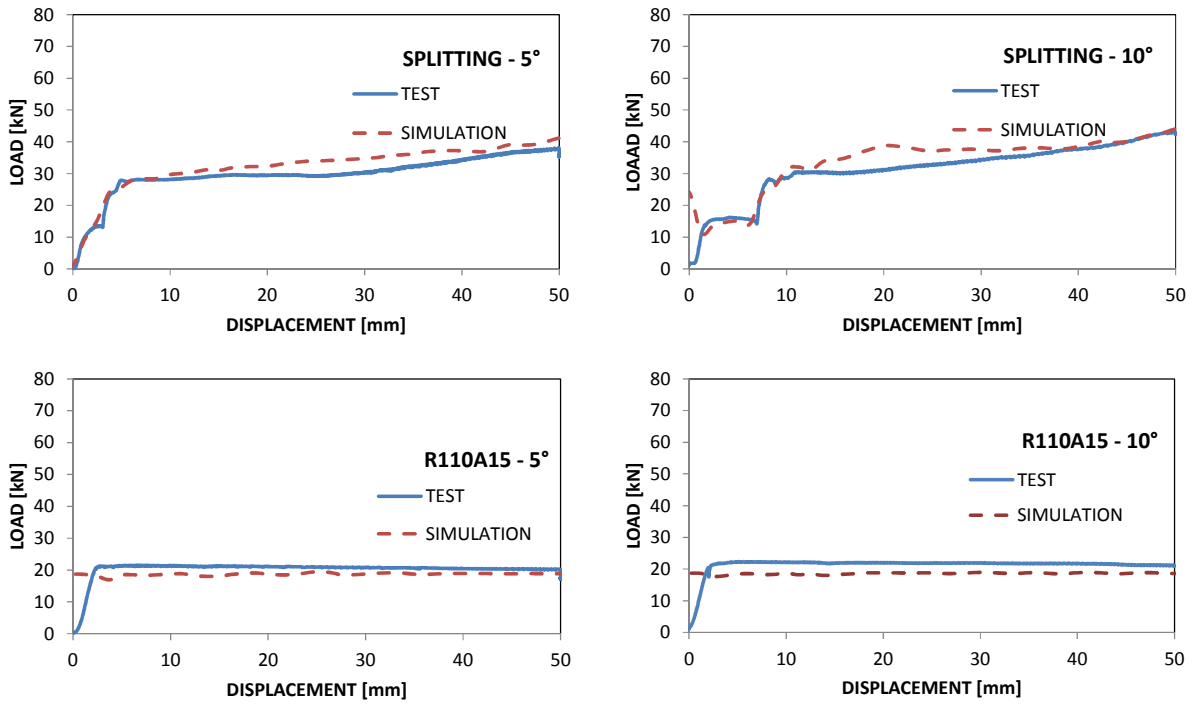

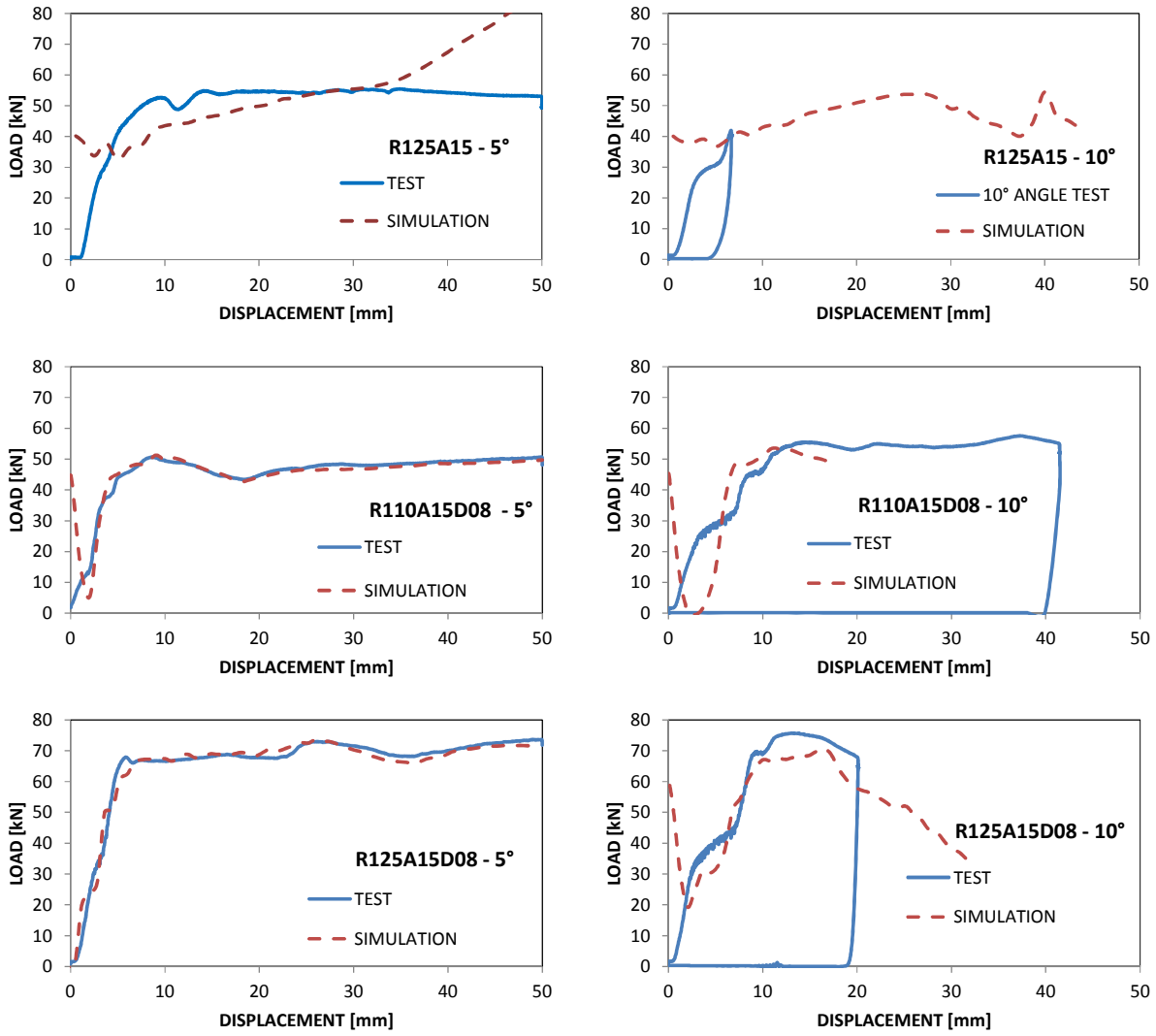

Figure 77: Load-displacement properties comparison between quasi-static test and simulation results of tubes subjected to oblique loading

		ENERGY (kJ)		
	SPECIMEN	**TEST**	**SIMULATION**	**VARIATION (%)**
SPLITTING	SPLITTING 5°	1.272	1.328	4.4
	SPLITTING 10°	1.396	1.508	8.0
EXPANSION	R110A15 5°	0.830	0.751	-9.5
	R110A15 10°	0.870	0.745	-14.4
	R125A15 5°	2.161	2.368	9.6
	R125A15 10°	-	2.412	-
HYBRID	R110A15D08 5°	1.915	1.887	-1.5
	R110A15D08 10°	-	-	-
	R125A15D08 5°	2.687	2.788	3.8
	R125A15D08 10°	-	-	-

Table 25: Energy absorbed by the specimens tested under the 5° and 10° inclined plates and the energy absorption predicted by their numerical models

7 Discussion

7.1 Literature Review

The literature highlighted that there are many commercial energy absorbers available in the railway industry. There is no consensus about which energy absorbing mechanism is the most suitable for the crash conditions present in a collision between railway vehicles. The review highlighted that there is scope for improving the existing designs or creating new concepts.

The scientific literature review highlighted that several characteristics of the underlying energy absorption mechanisms are not fully understood yet. That is particularly the case of splitting tubes. There is a lack of information in the literature about the simulation methods to predict the splitting of tubes. In particular, three critical parameters, which are necessary to accurately predict the behaviour of splitting tubes, are not fully understood.

- Static and dynamic friction coefficients between the splitting tube and the die
- The value of the fracture strain of the tube material as it splits under the loading of the die
- The stress state of the material as it fractures

For a potentially improved railway energy absorber including splitting of the material, these parameters have to be studied, in order to predict the performance of the energy absorber, as required by the regulations.

7.2 Hybrid Tubes

The combination of expansion and splitting of tubes, was identified as a potentially improved solution to the requirements of crashworthiness of railway vehicles. These tubes appeared to combine the benefits of each of the underlying energy absorption mechanisms. They could exhibit high force efficiency, typical of expansion tubes, and high stroke efficiency, typical of splitting tubes.

There are not yet any commercial products based on the expansion-splitting technology. They have not been researched in any detail, and their performance is still largely unknown. Therefore, this project demonstrated that hybrid tubes can present an improved solution over the existing commercial expansion and splitting tubes for the first time.

7.3 Experimental and Simulation Methodology

The quasi-static and dynamic testing was performed following accepted methods, including compression testing and drop tower testing. The results, whether quasi-static or dynamic, were very repeatable, which adds confidence onto the method employed. Unfortunately, the dynamic load-displacement data measured by the drop tower equipment experienced an artificially induced uncertainty in the form of a harmonic fluctuation of the load. This effect prevented the assessment of the force efficiency of the specimens under dynamic conditions.

The use of inclined plates to induce a transverse load into the specimens has been extensively used and is considered an acceptable way of performing oblique loading testing. The methodology used to evaluate the performance of the tubes under the oblique loading has not been used before. The consistency of the results and the fact that most of the specimens exhibited an increase of the load as the plate angle was increased, appear to justify this methodology. More research into the oblique loading performance of energy absorbers, different of crumple columns, is recommended.

A new proposed methodology (section 4.7) attempts to provide an accurate way of measuring the fracture strain and stress state at the tip of the crack of splitting tubes. New contributions to this topic in the literature would be very useful, to confirm the benefits of this methodology, or otherwise.

The knowledge of the stress state also suggests that the determination of the fracture strain data for a splitting tube, made from different materials, could be performed with the sole assistance of plane-strain tensile specimens. This feature could simplify greatly the calibration of finite element numerical models of splitting tubes.

Due to the lack of knowledge from the fracture locus of the E355 steel, the numerical model had to be modified to ensure the deleting of elements of the tube along a straight path, as observed experimentally. A seam line part, separate from the tube main body part, was included for that purpose. The validation of the FEA results performed in section 6.4 confirmed that the numerical models were able to accurately predict the experimental results, from where it can be inferred that the methodology is acceptable. Section 6.5 further asserted that this methodology is suitable even to predict the behaviour of tubes

subjected to oblique loading. In this case, the applicability of the method, could have been doubted as the splitting crack may not propagate in a straight line. However, observation and the fact that the model can simulate the results with accuracy suggest that the path of the crack follows a straight path even under oblique loading conditions.

7.4 Maximum Limit Load of the Tubes (Submission 6)

The standard BS EN 12663 specifies the maximum loads which energy absorbers may transmit. Therefore, an ideal energy absorber would exhibit a mean load as close as possible to the maximum load permitted by the railway vehicle, without exceeding it. (Ahn et al., 2008) stated that expansion tubes experienced buckling when a certain load, which depended on the dimensions and the material of the tube, was reached. Following the methodology of (Ahn et al., 2008), the critical global buckling load of the tubes used in the present experiments was calculated as 68 kN. The experimental work, section 5.3, showed that the tubes in this study experienced global buckling when the axial load reached the magnitude of 70 kN and more than 75 kN, for quasi-static and dynamic conditions respectively. Therefore, both tubes using expansion and expansion-splitting mechanisms can reach these loads without buckling. Splitting tubes however may not be able to reach similar high loads. This was described by (Reid, 1993), who showed the transition from tube splitting to tube inversion as the flaring radius of the die was reduced in order to increase the resistive axial load.

Thus the expansion and hybrid tubes exhibit flexibility, not matched by the splitting tubes, to modify their axial load up to the maximum load permissible (given by the critical global buckling load of the tube).

7.5 Comparison of the Force Efficiency of the Splitting, Expansion and Hybrid Tubes (Submission 6)

The force efficiency (ratio of mean load to peak load) measures the conformity of the device to the ideal type I energy absorber identified by (Calladine and English, 1984). Expansion tubes tend to exhibit quasi-ideal type I load-displacement properties. Splitting and hybrid tubes exhibit a pronounced initial peak, corresponding to the moment when the tube fractures and splits. As such, these two energy mechanisms are likely to deviate from the characteristics of the ideal absorber (as shown in Figure 2).

Table 26 summarises the force efficiency ratios of the three different energy absorbing mechanisms tested based on the results of the quasi-static testing. Due to the filtering of the measured load applied to the data, as stated in section 4.4, the peak load could not be inferred for the dynamic testing. Note that, in the calculation of the force efficiency, the initial stroke was not included (the stroke before the steady-state stage was reached). The reason for this is not to penalise the expansion and hybrid tubes which use more stroke to reach the steady-state stage. In practise, energy absorbers would be pre-crushed, in order to avoid this effect.

It can be observed from the data, that the force efficiency of the expansion tubes approximates that of the ideal energy absorber. As expected, both splitting and expansion-splitting mechanisms present a lower efficiency with the hybrid tubes being the higher of the two. Figure 78 shows that the axial load exhibited by the hybrid tubes is the addition of the axial loads exhibited by their underlying expansion and splitting mechanisms working independently. Therefore, the higher efficiency of the expansion stage increases the efficiency of the hybrid tubes.

MECHANISM	TYPE	FORCE EFFICIENCY (%)
SPLITTING		81.6
EXPANSION	R110A15	97.7
	R110A30	98.7
	R125A15	98.7
	R125A30	99.7
HYBRID	R110A15D08	85.5
	R110A15D12	83.0
	R125A15D08	92.8
	R125A15D12	87.1

Table 26: Force efficiency of the different energy absorbing mechanisms

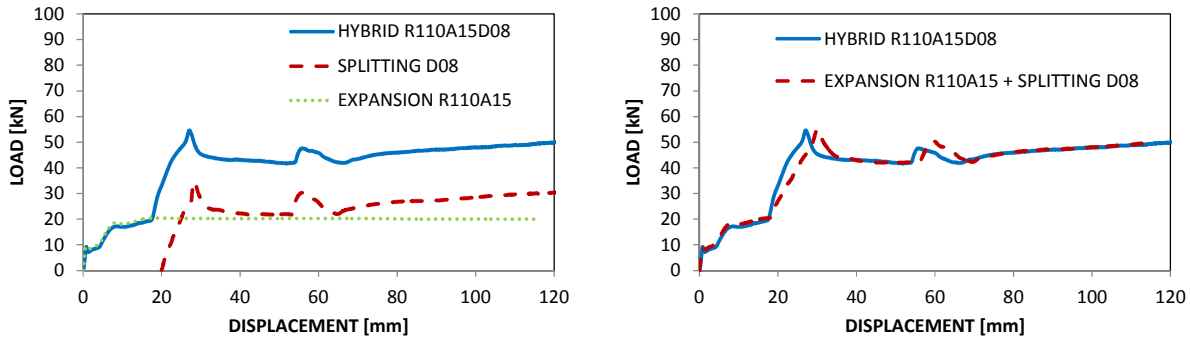

Figure 78: Generic load-displacement properties of splitting, expansion and hybrid tubes (left); and generic load-displacement properties of the hybrid tube compared to the addition of the load of the individual expansion and splitting tubes (right)

7.6 Comparison of the Stroke Efficiency of the Splitting, Expansion and Hybrid Tubes (Submission 6)

Chapter 2 highlighted the poor stroke efficiency performance of expansion tubes. This is caused by the inability of the tube to collapse, which limits its stroke efficiency to 50%. In practice, due to the overlap between the die and the tube, its stroke efficiency is likely to be even smaller. Figure 79 shows a representation of the expansion, splitting and hybrid tubes, their total length and their stroke. The stroke of the expansion tube is noticeably shorter by comparison to its total length.

Table 27 shows the stroke efficiency of the tubes tested. The stroke efficiency of hybrid tubes is approximately 7% lower than that of the splitting tubes due to the inclusion of the expansion die. However, the stroke efficiency of the expansion tubes is 30% lower than that of the splitting tubes. As a result, the working design of a splitting or hybrid tube could be much shorter than that of the expansion tube. Alternatively, for a similar total length, splitting and hybrid tubes would dissipate more energy, even if not so efficiently, as shown in section 7.5.

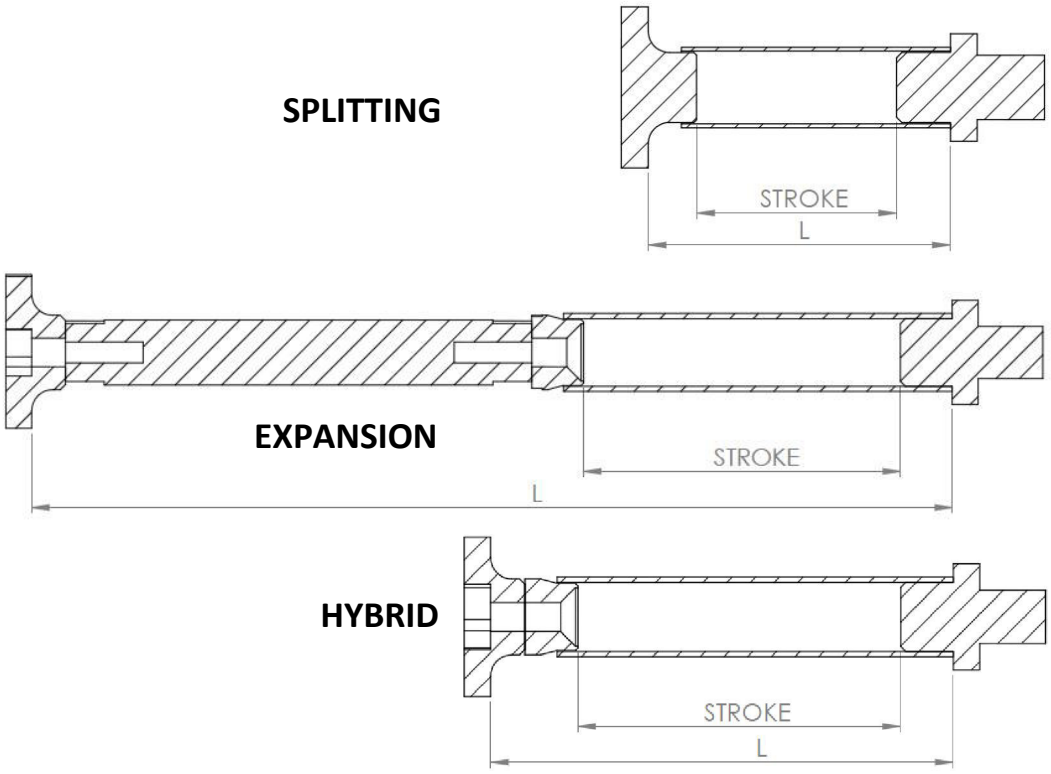

Figure 79: Schematic representation of the stroke and the length of the splitting, expansion and hybrid devices

MECHANISM	TYPE	STROKE	LENGTH	EFFICIENCY (%)
SPLITTING		160	208	77
EXPANSION		160	360	44
HYBRID	R110A15D08	160	224	71
	R110A15D12	160	228	70
	R125A15D08	160	231	69
	R125A15D12	160	235	68
	R125A30D08	160	225	71
	R125A30D12	160	229	70

Table 27: Stroke efficiency of the different specimens tested

7.7 Energy Absorption Efficiency Comparison Activity (Submission 6)

An overall energy absorption efficiency comparison may be accomplished using the force and stroke efficiency found above, for the dimension of tubes used in this research. Figure 80 illustrates the comparison of load-displacement properties of an ideal energy absorber and the splitting, expansion and hybrid tubes studied. As stated in section 7.4 the maximum buckling load the tubes can reach is 70 kN. Figure 80 shows the load-displacement properties of an ideal energy absorber of length 200 mm, 100% force efficiency (70 kN) and 100% stroke efficiency (200 mm of stroke). The load-displacement properties of the

splitting, expansion and hybrid tubes are plotted for comparison, where their stroke and force efficiencies found in sections 7.5 and 7.6 have been applied. As stated previously, the splitting specimens are not able to reach the critical global buckling load of 70 kN. Submission 1 showed that splitting tubes are limited in their energy absorption capabilities by a transition from a splitting to a tube inversion process. Numerical simulation showed that the smallest flaring ratio of the splitting die which achieves the splitting of the tube is D = 5 mm, smaller than this, inversion is predicted. The mean load at D = 5 mm was 50 kN. Therefore, the energy absorption capability of the splitting tube was re-assessed using this magnitude of the mean load (included in Figure 80). Figure 81 shows the comparative energy properties of the researched splitting, expansion and hybrid tubes, when the maximum mean load for the splitting tube is 50 kN. Note that the energy absorption efficiency of the hybrid tubes is 11% and 40% higher than that of the splitting and expansion tubes respectively, for any given stroke of the devices. This important result clearly identifies the potential of the hybrid tubes for improved energy absorption.

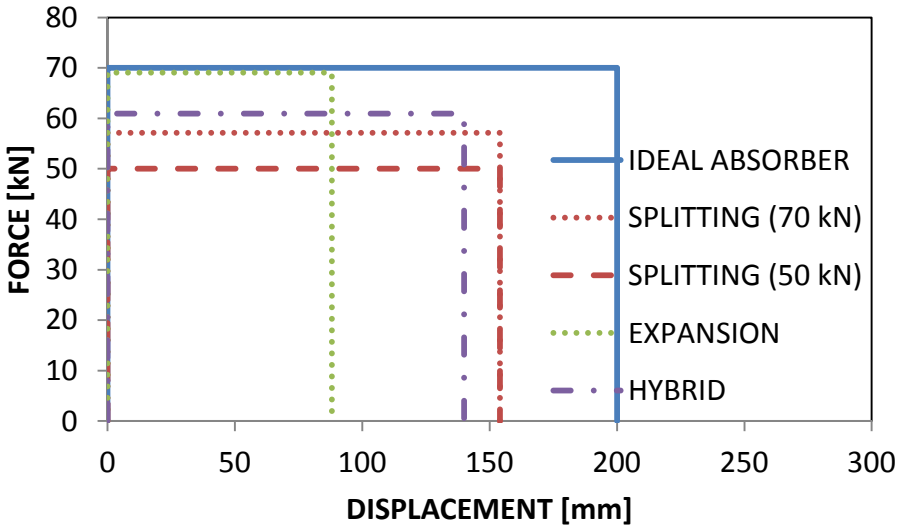

Figure 80: Illustrative comparison of load-displacement properties of an ideal energy absorber and the studied splitting, expansion and hybrid tubes

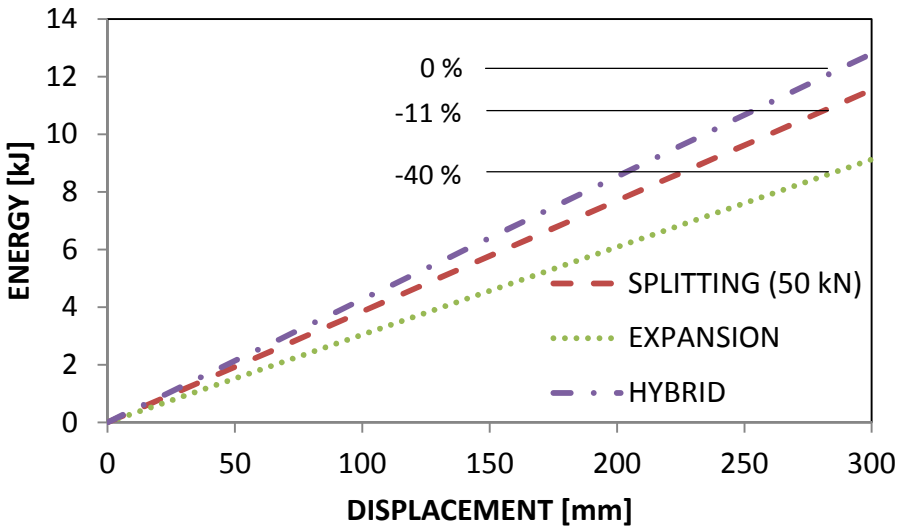

Figure 81: Illustrative comparison of energy properties of the researched splitting, expansion and hybrid tubes, when the maximum mean load for the splitting specimen is 50 kN

7.8 Oblique Loading Performance of the Splitting, Expansion and Hybrid Tubes (Submission 7)

7.8.1 Discussion of the Quasi-static Oblique Testing

The results shown in section 5.4 confirm the assertion that type I energy absorbers (splitting, expansion, and hybrid tubes) increase their mean load as they are subjected to oblique loading. As shown in section 4.6, a new methodology to evaluate the performance of type I energy absorbers was used. This consisted of plotting the mean load under oblique conditions versus the mean load under axial conditions for each specimen. Figure 82 shows the results from the quasi-static testing. As stated in section 5.3.1, the critical global buckling load for these tubes is 70 kN under quasi-static conditions. Ideally tubes would not deviate from ideal behaviour.

The splitting tubes exhibit a large deviation from the ideal behaviour (greater than 11% as shown in Table 20) for a low mean load (approximately 30 kN). A possible explanation for this can be found in the incipient strip merging displayed by the splitting tubes (top strips), shown in Figure 83. In submission 3 it was acknowledged that the effect of strip merging is to increase the energy absorption capacity of splitting tubes.

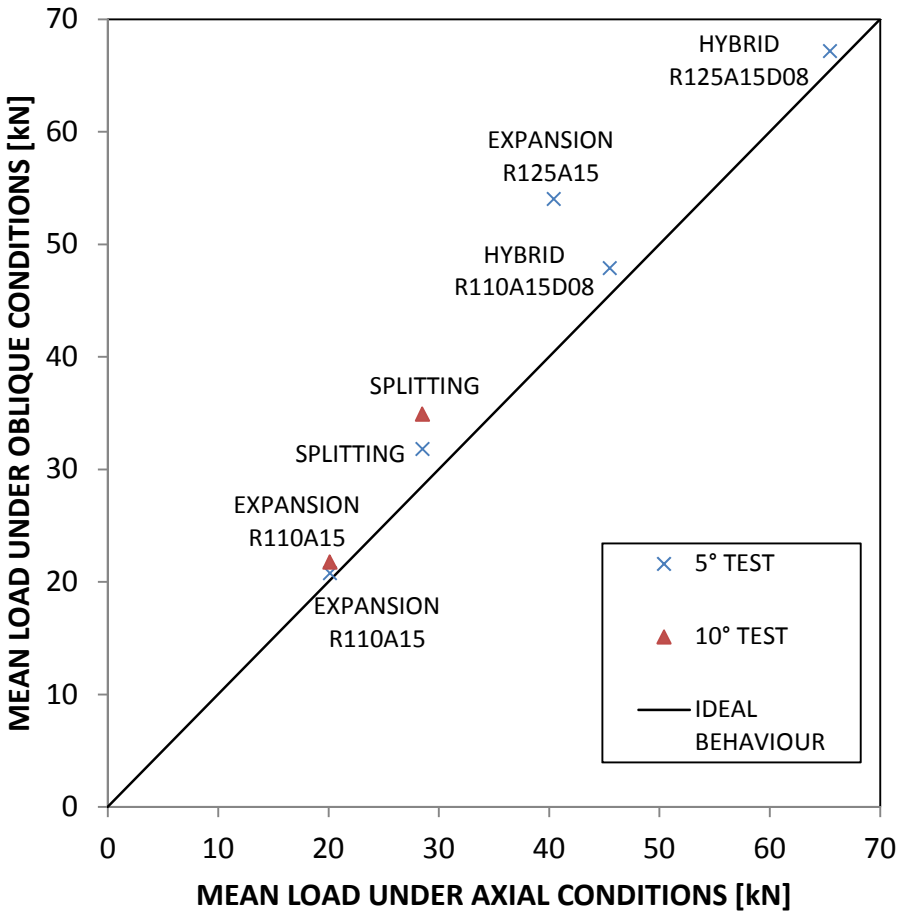

Figure 82: Mean load under oblique conditions vs. mean load under axial conditions for all the specimens, crushed by the 5° and 10° inclined plates under quasi-static conditions

The expansion R110A15 tubes exhibit a quasi-ideal behaviour. Instead, the expansion R125A15 tubes exhibit a large deviation from the ideal behaviour (greater than 33% as shown in Table 20). The reason for this behaviour could be caused by the deformation distortion created by the conformity of the R125A15 die to the inclined plate, shown in Figure 63. This behaviour does not occur for the R110A15 die, which remains vertical as it is supported by the deformation tube. Thus, for oblique loading of expansion tubes, there appears to be a critical mean load (between 20 and 40 kN) at which the efficiency of the expansion tube deteriorates rapidly.

The hybrid tubes exhibit a low deviation from the ideal behaviour in both cases. It can be inferred that, under a plate angle of up to 5° and quasi-static conditions, the hybrid tubes are largely insensitive to the oblique loading, for any mean load up to the global buckling critical load of 70 kN.

The splitting and expansion R110A15 specimens, tested under the 10° inclined plate, confirm that a larger transverse loading, induced by a larger inclined angle, have the effect of increasing the deviation from the ideal behaviour.

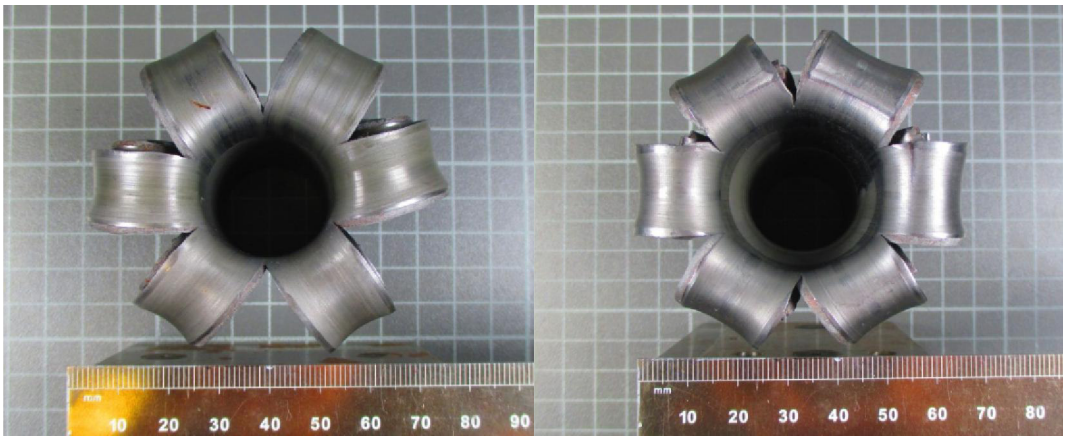

Figure 83: Top view of splitting (left) and hybrid R125A15D08 tubes (right) showing strip merging in the splitting specimen (top strips)

7.8.2 Discussion of the Dynamic Oblique Testing

Figure 84 shows the mean load under oblique conditions versus the mean load under axial conditions for all the specimens under dynamic oblique testing conditions. The critical global buckling load is 75 kN in dynamic conditions. Figure 84 presents a similar trend to that from Figure 82 for the specimens crushed under the 5° incline plate, although the magnitude of the deviation from the ideal behaviour is generally smaller.

The performance of the splitting and expansion R110A15 tubes tested under the 10° inclined plate shows a smaller deviation from ideal behaviour than the tubes tested under the 5° inclined plate, contrary to the quasi-static results, shown in Figure 82. The results of the hybrid R110A15D08 tubes are consistent with the quasi-static results.

The quasi-static results suggested that the hybrid tubes, unlike splitting and expansion, are largely insensitive to the application of a transverse loading. The hybrid tubes are more efficient than expansion or splitting tubes under quasi-static oblique loading.

However, the dynamic results cannot confirm this assertion, since the performance of the splitting and expansion tubes improved with increasing transverse loading. In order to confirm these results, it would be desirable to perform more testing, using splitting and

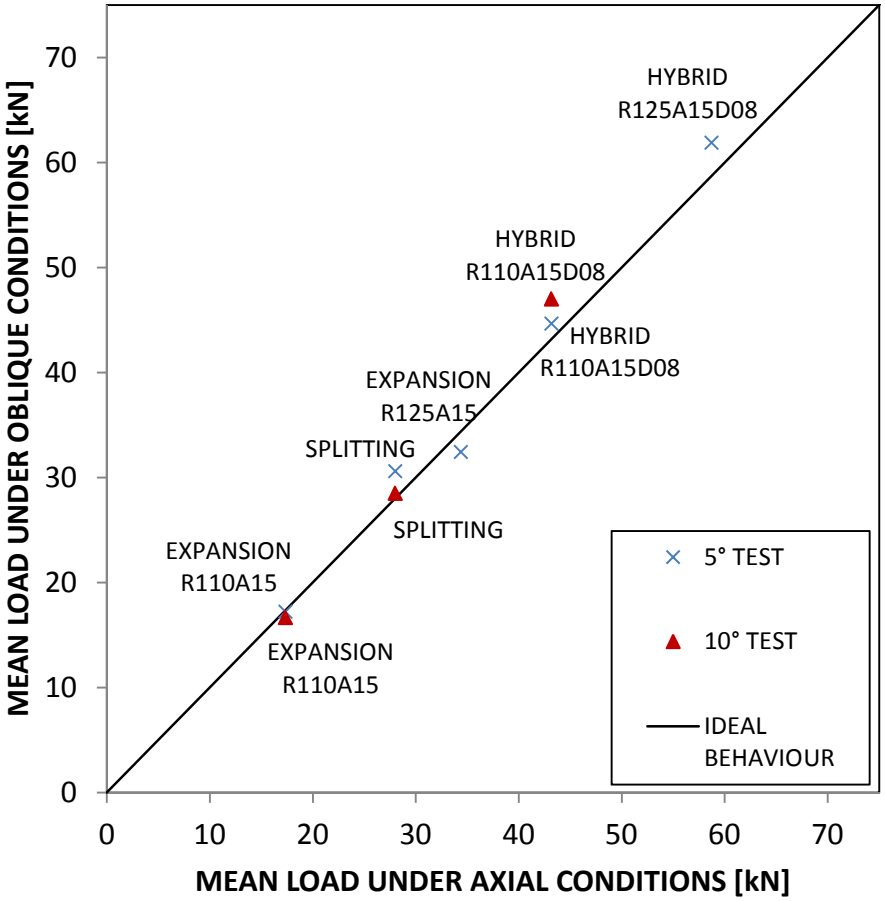

Figure 84: Mean load under oblique conditions vs. mean load under axial conditions for all the specimens, crushed by the 5° and 10° inclined plates under dynamic conditions

7.9 Fracture Strain and Stress State at the Tip of the Crack of the Splitting Tubes (Submission 4)

Section 5.5 showed the results of the fracture strain measurements for seamless splitting tubes made of E355 steel, $\varepsilon_f \approx 0.60$. This value is consistent with the fracture value of $\varepsilon_f \approx 0.61$, found by (Gruben et al., 2012) for cold-rolled dual-phase steel Docol 600DL. This value is a necessary requirement for the numerical model to accurately predict the tube deformation as it is being plastically deformed and split under the compression of the die. The accurate prediction of the tube deformation is a required in order to infer the coefficient of friction between the die and the tube. It will be shown in the next section, that the coefficient of friction inferred in this manner agrees with those stated by the literature for the friction conditions present in the expansion tubes.

The average axial distance between the last data node (see section 4.7) before the GOM facet disappears and the tip of the crack is 0.23 mm and 0.18 mm for the six and four notches respectively. The distances are very similar in both cases and are approximately half of a facet length, measured as 0.44 mm. From Figure 37, it could be argued that extrapolation of the von Mises strain for a distance of 0.20 mm may introduce a significant uncertainty, since the strain grows rapidly. However, the consistency of the results found for the splitting tubes with four and six notches, shown in Table 22, gives an indication of the accuracy of the values found. Additional support for the fracture strain value found comes from the fact that the coefficient of friction which allows the simulation to be accurate coincides for the simulation of the splitting tube with both four and six notches.

In addition, the methodology identified the stress state present at the tip of the crack as under plane strain conditions. The strain ratio α at the tip of the crack was measured as α = -0.11 and α = -0.03 for the six and four notches specimens respectively. This data suggests that the determination of the fracture strain data for splitting tube, made from different materials, could be performed with the sole assistance of plane-strain tensile specimens. This feature could simplify greatly the calibration of finite element numerical models of splitting tubes.

7.10 Calibration of the Numerical Models of the Splitting and Expansion Tubes under Quasi-static Conditions (Submissions 4 and 5)

The inclusion of a fracture strain value $\varepsilon_f \approx 0.60$ led to the determination of a friction value of μ = 0.07 for the splitting tubes. This allows the simulations of the splitting specimens with four and six notches to accurately predict the results given by the quasi-static test, as the energy absorption estimate is within 1% of the test results. This value of friction is outside the range (μ = 0.1-0.5) of values quoted in the published work for splitting tubes, as shown in section 2.2.6. However, it coincides with the typical value quoted in the literature (section 2.2.7) for the radial expansion of tubes. This suggests that the friction conditions under the splitting and the radial expansion mechanisms may be much more similar than previously acknowledged.

The simulation of the expansion tubes allowed inferring of the coefficient of friction between the tube and the conical die as μ = 0.07 and μ = 0.09-0.11 for the tubes with expansion R = 1.10 and R = 1.25 respectively. The deformation of the expansion tubes allows

for the easy measurement of the outer diameter and length of the exhausted tubes, which, in turn allows for simple calibration of the numerical model which accurately reproduced the deformed shape of the tested tubes. Therefore, the coefficients of friction inferred in this manner are deemed to be accurate, as no fracture is present in the expansion event. The difference between the values of the coefficients for different expansion ratios highlights the sensitivity of the contact regime subjected to high pressures.

7.11 Calibration of the Splitting and Expansion Tubes Numerical Models under Dynamic Conditions (Submission 3, 4 and 5)

The simulation of the dynamic crush of the splitting and expansion tubes requires the knowledge of the strain rate sensitivity of the material, steel E355. Experimental data was not available to the author. (Keeler and Kimchi, 2014) provided data such as the increase in yield stress vs. strain rate for a range of different grades of steel, Figure 85.

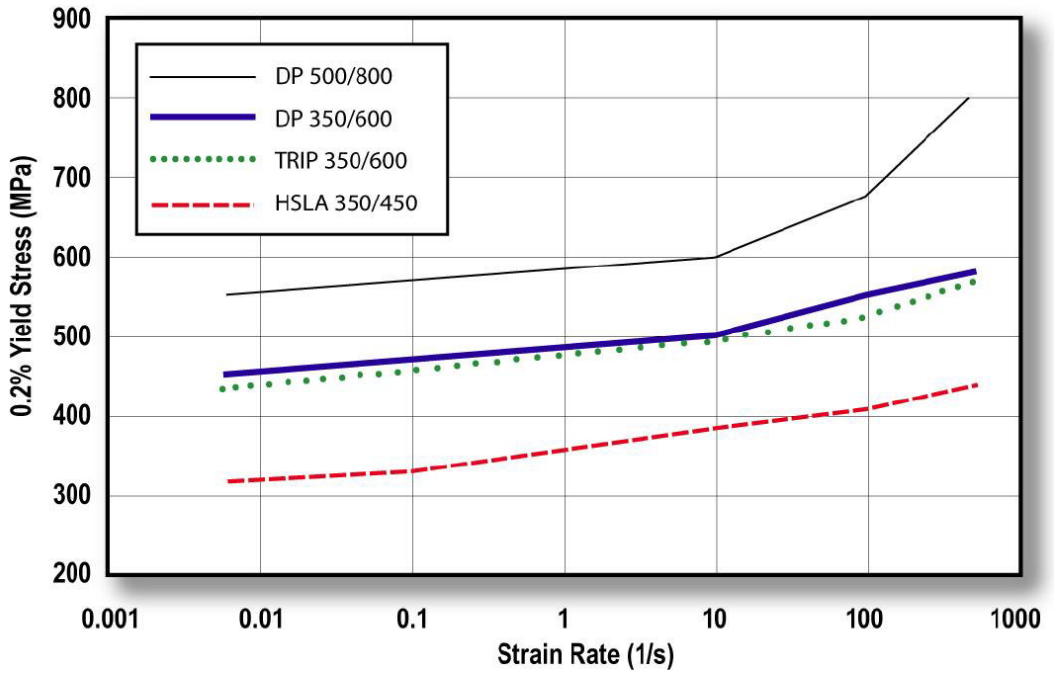

Figure 85: Yield stress vs. strain rate for a range of different steel grades (Keeler and Kimchi, 2014)

The yield stress of the available material, E355 steel, is 380 MPa. Submissions 3 and 5 estimated the average strain rate on the splitting and expansion tubes as 300 s^{-1} and 100 s^{-1} respectively, under the dynamic test conditions specified in section 4.4. The increase in yield stress of a material which exhibited a yield stress of 380 MPa can be interpolated from the plot in Figure 85, for strain rates 100 s^{-1} and 300 s^{-1}. The estimated increase in yield stress

for E355 steel is 22% and 29%, for strain rates 100 s^{-1} and 300 s^{-1} respectively. It may be assumed that the axial load exhibited by the tubes increases proportionally to the yield stress. If that was the case, the effect of strain rate on the axial load (+ 22-29%) would be larger than the effect of dynamic friction (- 12-28%, as shown in sections 6.2 and 6.3). This appears to contradict the dynamic test results, where the expansion tubes exhibited a smaller axial load under dynamic conditions. This could suggest that, using the estimated strain rate model, may somewhat over-predict the effect of the strain rate.

7.12 Validation of the Numerical Models of the Hybrid Tubes (Submission 6)

The methodology of the validation of the numerical models (section 4.8) was performed by including the fracture strain and coefficients of friction that were found into the numerical models of the hybrid tubes. The numerical models of the quasi-statically tested tubes predicted their behaviour accurately. The conclusion is thus that the numerical models that were developed are an adequate tool to predict the quasi-static performance of the hybrid tubes.

In particular, for the modelling technique (section 4.8.1), the inclusion of an additional part to separate the path of the fracture line from the main deforming body of the tube, appears to offer an appropriate modelling solution when the full fracture locus of the material is unknown.

7.13 Validation of the Oblique Loading Simulation (Submission 7)

The numerical models of the oblique loading tests reveal the complexity of the non-axial events. The numerical models of the splitting and hybrid, R110A15D08 and R125A15D08, reasonably predict the results of testing. These results suggest that, despite the limitations of the numerical model, i.e. the inclusion of a seam line part to constrain the deletion of elements to a straight path, they can be used to predict the performance of tubes undergoing tearing under oblique loading conditions. However, the numerical models of the expansion R110A15 and R125A15 tubes under-predict the axial mean load observed in test by 10-15%, for which a satisfactory explanation could not be found.

7.14 Cost Comparison

The production costs (set-up and machining, hourly rate and raw materials) were estimated with the help of the Oleo International production department. Table 28 shows a summary

of the production costs of the splitting, expansion and hybrid tubes, per manufactured unit. The costs of the splitting tubes and the hybrid tubes are 21% and 73% higher than the cost of the expansion tubes, respectively. It was expected that the inclusion of an additional die would result in a large increase of cost of the tube.

	MACHINING TIME (hours)	HOURLY RATE (£/hour)	MACHINING COST (£)	RAW MATERIAL (£)	TOTAL (£)
TUBE	3.31	40	132.4	60.0	192
EXPANSION DIE	4.56	40	182.4	30.0	212
SPLITTING DIE	5.01	40	200.4	95.0	295
SPLITTING TUBE	-	-	-	-	488
EXPANSION TUBE	-	-	-	-	405
HYBRID TUBE	-	-	-	-	700

Table 28: Production costs of the splitting, expansion and hybrid tubes, per unit manufactured

8 Conclusions

The aim of the project was to investigate the possibility of an innovative energy absorbing device with improved performance compared to that of the existing designs, for the sponsor company Oleo International. Proof of any improvement had to be provided by means of physical testing. The constrains, in terms of energy absorption, limiting maximum loads and railway vehicles overriding protection, were given by the BS EN 15227 (British Standards, 2010b) and BS EN 12663 (British Standards, 2010a) standards. In addition, the BS EN 15227 (British Standards, 2010b) stipulates accurate simulation of the energy absorbers. Therefore, a numerical model, calibrated against the results from test, had to be provided to Oleo International.

An appropriate selection process was employed to identify a potentially improved design of an energy absorber for railway vehicles. An innovative hybrid energy absorber was proposed combining two existing energy absorption mechanisms. Testing provided the physical evidence for improvements exhibited by the energy absorber concept. The testing provided the means to calibrate the numerical models built to simulate the performance of the proposed energy absorber.

8.1 Impact

8.1.1 Quasi-static Test of Demonstrator at Oleo International (Submission 8)

A full-scale demonstrator of the hybrid tube concept was tested quasi-statically at Oleo International facilities on 26 March 2015. Figure 86 shows the assembly drawings of the hybrid demonstrator (made by an Oleo International design engineer). Figure 87 shows the assembly of the demonstrator prior to test. The outer diameter of the full-scale demonstrator was OD = 166 mm. Therefore, the tube was scaled up approximately 5.5 times.

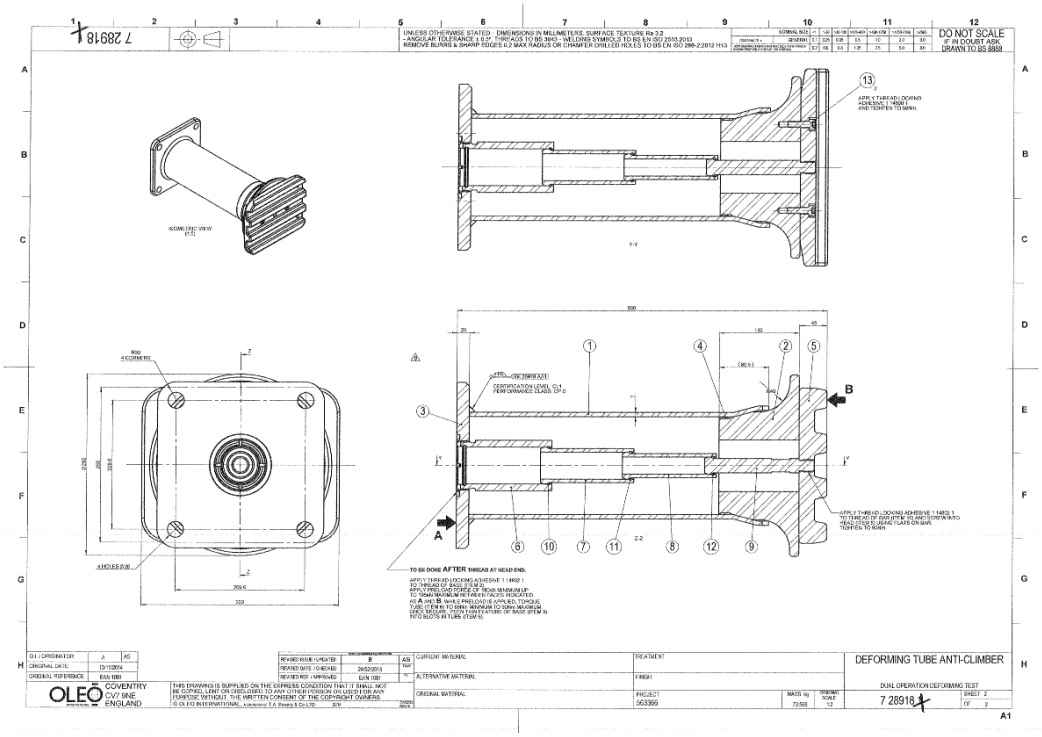

Figure 86: Oleo International drawings of the hybrid demonstrator

Figure 87: Assembly of the demonstrator prior to test

The quasi-static test was conducted in a press at a rate of 5 mm/s for a stroke of 400 mm. The test did not proceed as expected in that the neat formation of the strips observed in the testing of the scaled tubes above did not occur. Figure 88 shows the image series of the testing. The strip formation was prevented by fast fracture (see the formation of the petal to the left of the tube) and branching and diagonal progress of the crack (see crack located at the centre of the tube). These effects caused excessive tearing on one side of the tube and immediate strip merging on the opposite side of the tube.

Figure 88: Image series of the quasi-static testing of the hybrid demonstrator

The two main differences between the scaled tubes used by the present author and the full-scale demonstrator are the following:

- The dimensions of the hybrid die
- The dimensions of the splitting notches

The hybrid demonstrator had the scaled dimensions of a R110A15D08 hybrid tube except for the length of the hybrid die. The transition from the expansion stage to the splitting stage is much shorter in the case of the demonstrator, as shown in Figure 89. In the case of the demonstrator under loading, the expansion stage is not fully complete before the tube comes into contact with the flaring radius. Figure 39 showed that splitting tubes are under compressive state of stress (negative strain ratio α) ahead of cracking as when the tube enters the flaring radius of the splitting die. This is thought to be the case in the hybrid tubes tested during this project. In the case of the demonstrator, the tube is still being stretched under the loading of the expansion die, when tube enters the flaring radius of the splitting

die. Therefore, the demonstrator may not be under compressive state of stress when it starts flaring. As a result, the opening of the cracks is enhanced by the stretching of the tube, rather than being prevented from growing further by the compression state of the tube. This effect may have caused the fast fracture event and unstable collapse of the tube observed during the test, Figure 88.

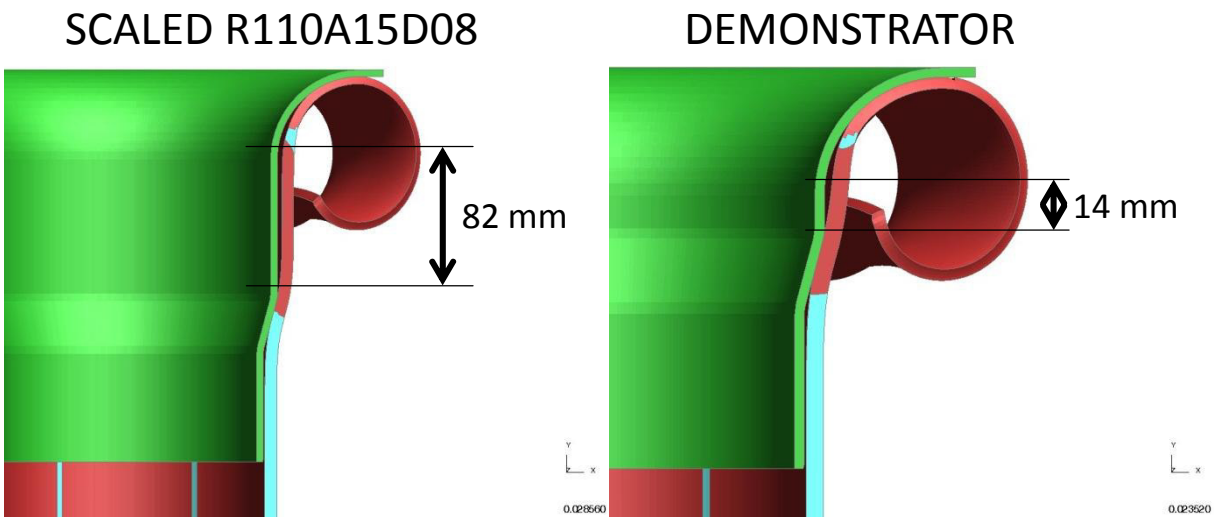

Figure 89: Comparison of the dimensions of the scaled R110A15D08 tube and the demonstrator

In addition, the dimensions of the notches were not proportional to the notches cut into the scaled tubes. In order to be proportional, the notches on the demonstrator had to be wider than 4 mm. The notches were serrated with a hand saw on the demonstrator. As a result, the notches were too narrow. This effect may have caused the observed tendency of the cracks to branch during the quasi-static test of the demonstrator. Inadequate triggering of the tubes has been observed previously, during the initial stages of the present project. Figure 90 shows a failure caused by fast fracture on a hybrid R125A15D08 specimen, due to inadequate triggering of the tube.

The combined effect of these two deviations from the previous methodology may have caused the poor performance of the demonstrator. Therefore, the test highlighted two areas which must be accounted for when designing new hybrid tubes. Further demonstrator tests are in planning.

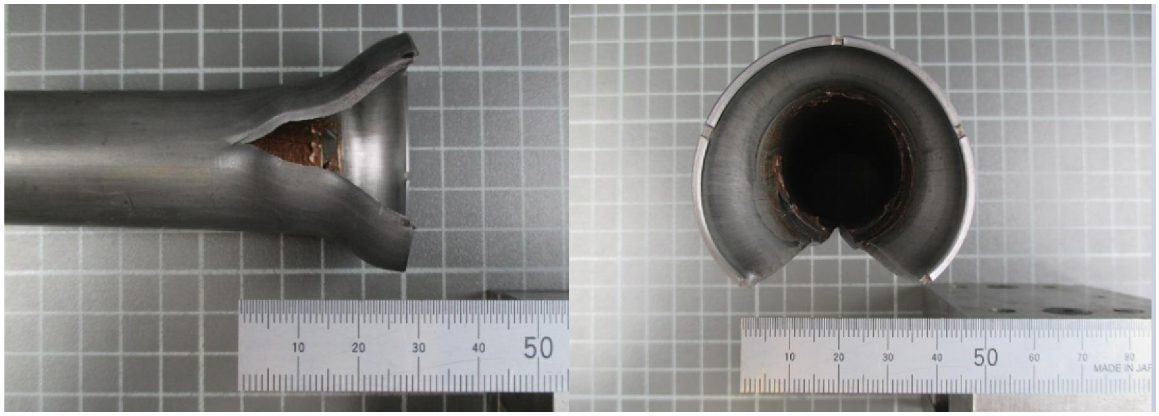

Figure 90: Failure caused by fast fracture on a hybrid R125A15D08 specimen

8.1.2 Patent

A patent application of the hybrid tube with various claims (patent application number 1505331.7) has been requested (date 27 March 2015).

The European Patent Office offers an online patent search service at (European Patent Office, 2015) where all the filed patents are made available to the public. This service offers the Cooperative Patent Classification system to assist the patent search. This classification uses an alphanumeric system as the one shown below:

B 61 G 11 / 16

In the example above, B stands for Transporting, 61 stands for Railways, G 11 for buffers and /16 for absorbing shocks by permanent deformation of buffer element.

Relevant searches could be conducted under the classification numbers stated in Table 29.

CLASSIFICATION	DESCRIPTION	ENERGY ABSORBING MECHANISM
B61G11/16	Transporting/ railways/ buffers/ absorbing shocks by permanent deformation of buffer element	Expansion tubes
B61D15	Transporting/ railways/ body details or kind of railway vehicles/ adaptations of vehicles for use on railways	Splitting tubes
B61D17	Transporting/ railways/ body details or kind of railway vehicles/ construction details of vehicle bodies	Crash columns
B60R19	Transporting/ vehicles general/ vehicle parts/ fitting damping bouncing force in collisions	Taper and flaring tubes
B60R21	Transporting/ vehicles general/ vehicle parts/ fittings on vehicles for protecting or preventing injuries to occupants or pedestrians in case of accidents or other traffic risks	Splitting tubes
B23B29	Performing operations/ machine tools and metal working/ turning and boring/ holders for non-rotary cutting tools	Cutting-chipping tubes

Table 29: Relevant searches under the Cooperative Patent Classification system

None of the searches showed an energy absorbing device which combined radial expansion of cylindrical tubes with splitting of the same tube.

8.1.3 Numerical Models for Compliance with BS EN 15227 Standard

This project has provided Oleo International with the simulation capability necessary to accurately predict the performance of tubes subjected to splitting. A calibrated numerical model of the energy absorbing device is a requirement of the standard BS EN 15227 (British Standards, 2010b).

8.1.4 Publications

Two peer-reviewed scientific outputs have been made. (Moreno et al., 2015) and IMechE Stephenson Conference papers have been published to disseminate knowledge acquired during the project realisation.

8.2 Achievements

The activities carried out for the duration of this project led to a number of contributions to knowledge. These are listed below.

- The determination of the fracture strain magnitude and stress state conditions at which fracture occurs for seamless cold drawn E355 steel tubes. The results were published in (Moreno et al., 2015).
- The determination of the static friction coefficient between the dies and the E355 steel tubes, subjected to splitting.
- The development of a methodology, using a digital image correlation technique, to assess the fracture strain and stress state conditions at the tip of the crack of a splitting tube. The DIC technique is not capable of measuring strains right up to the edge of a specimen, such as the tip of the crack location in a splitting tube (Moreno et al., 2015).
- Description and explanation of the behaviour of the splitting tubes after self-contact of the strips with the tube, provided in submission 3.
- The development of a FEA modelling technique, capable of predicting accurately the tearing of the tube with the sole knowledge of the fracture strain at the tip of the splitting crack. This technique is particularly useful when the fracture locus of the material is unknown.

The experimental and simulation work, together with the contributions to knowledge stated above, led to deliverables to Oleo International which could potentially give a competitive advantage. These innovations are:

- The identification of a radial expansion-splitting (hybrid) energy absorbing mechanism concept with improved performance over existing commercial products. This concept was proven to offer potential overall improvements in comparison to the existing energy absorbers based on tubes.
- The provision of a finite element numerical model, capable of accurately predicting the tearing of the tube and, consequently, the resistive force and the energy absorbed.
- Establishing a methodology to assess the behaviour and performance of type I energy absorbers subjected to oblique loading.

The innovations from this report have lead Oleo International to test a full-scale demonstrator and apply for a patent.

8.3 Limitations of the Research and Further Work

This section highlights the limitations of the research undertaken during this project and suggests further work to improve the understanding of the hybrid mechanism and application as a commercial product.

8.3.1 Limitations and Further Work from the Methodology

Fracture strain and stress state

The methodology used to find the fracture strain and stress state at the tip of the splitting crack is completely new. The results, in terms of fracture strain magnitude, were shown to be similar to those results obtained for grades of similar steel, as it was stated in section 7.9. However, it was also shown that, due to the utilization of extrapolation, large errors of the fracture strain may be obtained if appropriate care was not taken. Therefore, more research performed following this methodology or similar to understand the limitations of the DIC methodology would be very useful to assess the applicability of the methodology and the accuracy of results, such as fracture strain and stress state.

Oblique loading performance

Another novel technique was introduced in section 4.6 in order to carry out a valid assessment of the oblique loading performance of type I energy absorbers studied during this project. The assessment of the results (section 7.8) shows that there was a lack of data to carry out a complete comparison of the oblique loading performance of the splitting, expansion and hybrid tubes. In particular, more splitting and expansion tubes, featuring higher axial mean loads, have to be tested in order to assess their performance near the limits of the tube energy absorption capabilities.

8.3.2 Limitations and Further Work from the Experimental Activity

The main limitation of the work was the dimensions of the tubes tested. The tubes were significantly smaller than the typical size of a railway vehicle energy absorbing tube. Some of the parameters found during the completion of this project, parameters such as the fracture strain, coefficients of friction, peak and mean loads, may differ for tubes with different dimensions. In particular, the force efficiency measured and the oblique loading performance assessment may be different, leading to different conclusions from those

stated above. Therefore, the scalability of the results should be researched. This could be accomplished by performing a dimensional analysis, such as in the case of the axial mean loads. Alternatively, testing of tubes with different dimensions could be performed. In that case, different test equipment must be used as the equipment during this project is limited as specified in chapter 4. The effect of the dimensions on the fracture strain, since a 'thin' wall stress state assumption was taken, must be studied using experimental methods. Therefore, an extension to this project could be the study of the fracture strain of large tubes which may not be assumed to be thin enough to be under stress state conditions.

The friction regime was quantified by means of numerical simulation. The assumption used was that, if the numerical simulation produces the correct shape of the plastically deformed tube, the coefficient of friction which correctly predicts the energy absorption must be the actual value. It could be interesting whether the coefficient of friction could be inferred using experimental methods, in order to evaluate the accuracy of the coefficients of friction found in this document. However, as stated in section 4.8.5, popular methods, such as the ring compression test, have been found inadequate (Almeida et al., 2006). Alternative adequate methods have not been found.

The effect of the notch dimension, as shown by the demonstrator, needs further investigation.

Section 4.4 highlighted the necessity to filter the measured load from the dynamic testing, due to artificial load fluctuation induced by the drop tower. This effect prevented the determination of the force efficiency of the energy absorbers under dynamic conditions. It is therefore important to confirm the results obtained under quasi-static conditions, by means of dynamic testing of the tubes using equipment which allows a more accurate measurement of the dynamic peak load.

As stated in the previous section, the evaluation of the different energy absorbers under oblique loading conditions was not fully researched as splitting and expansion tubes featuring high axial mean loads were not tested. Their performance prediction could be carried out using numerical simulation. However, experimental tests must be performed to confirm the simulation results. Therefore, different splitting and expansion dies would have to be designed, featuring smaller flaring radius (splitting) or larger expansion ratios (expansion) to reach larger mean loads.

8.3.3 Limitations and Further Work from the Simulation Activity

The main limitations of the numerical models were the lack of information about the material fracture locus and the effect of the strain rate sensitivity of the material under dynamic conditions. This prompted the alternative solution of including an additional seam line part. A more realistic solution would include a fracture locus, in which case the seam line part would be unnecessary. Without this part, there would be no concerns about the path followed by the propagating crack for the prediction of the specimens subjected to oblique loading. This solution would require the testing of different tensile specimens as specified in (Bao and Wierzbicki, 2004) or (Wierzbicki et al., 2005).

The strain hardening of the material due to its strain rate sensitivity was observed in submissions 3, 4, 5 and 6, from the results of the dynamic testing. Under dynamic conditions, the mean load reduction due to the smaller dynamic friction coefficient was partially offset by the strain rate sensitivity. The strain rate of the material needs to be assessed in order to find the proportion of the discrepancy of the energy absorption attributable to the strain rate sensitivity, under dynamic conditions.

References

ABRAMOWICZ, W. & JONES, N. 1997. Transition from initial global bending to progressive buckling of tubes loaded statically and dynamically. *International Journal of Impact Engineering,* 19**,** 415-437.

AHN, K., KIM, J. S. & HUH, H. The effects of local buckling on the crash energy absorption of thin-walled expansion tubes. Numisheet 2008, 1/09/2008 2008 Interlaken, Switzerland.

ALEXANDER, J. M. 1960. An approximate analysis of the collapse of thin cylindrical shells under axial loading. *The Quarterly Journal of Mechanics and Applied Mathematics,* 13**,** 10-15.

ALGHAMDI, A. A. A. 2001. Collapsible impact energy absorbers: an overview. *Thin-Walled Structures,* 39**,** 189-213.

ALMEIDA, B. P. P., ALVES, M. L., ROSA, P. A. R., BRITO, A. G. & MARTINS, P. A. F. 2006. Expansion and reduction of thin-walled tubes using a die: Experimental and theoretical investigation. *International Journal of Machine Tools and Manufacture,* 46**,** 1643-1652.

AXTONE. *Review of crash products - AX-ZKL1 Crash Buffer* [Online]. Crash Technology Railway Components. Available: http://www.crashtechnology.eu/crash-technology/ax-zkl1.html [Accessed 18 September 2012 2012].

BAO, Y. & WIERZBICKI, T. 2004. On fracture locus in the equivalent strain and stress triaxiality space. *International Journal of Mechanical Sciences,* 46**,** 81-98.

BØRVIK, T., HOPPERSTAD, O. S., REYES, A., LANGSETH, M., SOLOMOS, G. & DYNGELAND, T. 2003. Empty and foam-filled circular aluminium tubes subjected to axial and oblique quasi-static loading. *International Journal of Crashworthiness,* 8**,** 481-494.

BRITISH STANDARDS 2009. Metallic materials - Tensile testing - Part 1: Method of test at room temperature (ISO 6892-1:2009). *BS EN 6892-1:2009*

BRITISH STANDARDS 2010a. Railway applications - Structural requirements of railway vehicle bodies. Part 1: Locomotives and passenger rolling stock (and alternative method for freight wagons). *BS EN 12663-1:2010.*

BRITISH STANDARDS 2010b. Railway applications — Crashworthiness requirements for railway vehicle bodies. *BS EN 15227:2008+A1:2010.*

BRITISH STANDARDS 2011. Steel tubes for precision applications - Technical delivery conditions - Part 4: Seamless cold drawn tubes for hydraulic and pneumatic power systems. *BS EN 10305-4:2011.*

CALLADINE, C. R. & ENGLISH, R. W. 1984. Strain-rate and inertia effects in the collapse of two types of energy-absorbing structure. *International Journal of Mechanical Sciences,* 26**,** 689-701.

CHENG, Q. & ALTENHOF, W. 2005. Load/displacement and energy absorption performances of AA6061-T6 tubes under cutting defotmation mode. *International Journal of Crashworthiness,* 10**,** 624-633.

CHOI, H. H., HWANG, S. M., KANG, Y. H., KIM, J. & KANG, B. S. 2002. Comparison of Implicit and Explicit Finite-Element Methods for the Hydroforming Process of an Automobile Lower Arm. *The International Journal of Advanced Manufacturing Technology,* 20**,** 407-413.

CHUNG KIM YUEN, S., ALTENHOF, W., OPPERMAN, C. J. & NURICK, G. N. 2013. Axial splitting of circular tubes by means of blast load. *International Journal of Impact Engineering,* 53**,** 17-28.

COTTERELL, B. & REDDEL, J. K. 1977. The essential work of plane stress ductile fracture. *International Journal of Fracture,* 13**,** 267-277.

EUROPEAN PATENT OFFICE. 2015. *Patent Search* [Online]. Available: http://worldwide.espacenet.com/ [Accessed 27 September 2015].

FISCHER, F. D., RAMMERSTORFER, F. G. & DAXNER, T. 2006. Flaring—An analytical approach. *International Journal of Mechanical Sciences,* 48**,** 1246-1255.

GOM 2013. ARAMIS User Manual - Software. *ARAMIS v6.3 and higher.* Braunschweig, Germany: GOM mbH.

GRUBEN, G., HOPPERSTAD, O. S. & BØRVIK, T. 2012. Evaluation of uncoupled ductile fracture criteria for the dual-phase steel Docol 600DL. *International Journal of Mechanical Sciences,* 62**,** 133-146.

HALLQUIST, J. O. 2006. LS-DYNA Theory Manual. Livermore, California: Livermore Software Technology Corporation.

HAN, D. C. & PARK, S. H. 1999. Collapse behavior of square thin-walled columns subjected to oblique loads. *Thin-Walled Structures,* 35**,** 167-184.

HEXCEL. 2012. *HexWeb Honeycomb Energy Absorption Systems - Design Data* [Online]. Available: http://www.hexcel.com/products/aerospace/ [Accessed 20 September 2012 2012].

HUANG, X., LU, G. & YU, T. X. 2002a. Energy absorption in splitting square metal tubes. *Thin-Walled Structures,* 40**,** 153-165.

HUANG, X., LU, G. & YU, T. X. 2002b. On the axial splitting and curling of circular metal tubes. *International Journal of Mechanical Sciences,* 44**,** 2369-2391.

HUANG, X., LU, G. & YU, T. X. 2002c. A theoretical model for axial splitting and curling of circular metal tubes. *In:* CHAN, S. L., TENG, J. G. & CHUNG, K. F. (eds.) *Advances in Steel Structures (ICASS '02).* Oxford: Elsevier.

HUSS, P. 2005. Anti-climbing phenomena: comparison between test and numerical simulations. *Passive Safety of Rail Vehicles - 5th International Symposium.* IFV Bahntechnik.

INSTRON 2005. 2525-800 Series - Load Cells.

JIN, S. Y., MAJUMDER, A., ALTENHOF, W. & GREEN, D. 2010. Axial cutting of AA6061-T6 circular extrusions under impact using single- and dual-cutter configurations. *International Journal of Impact Engineering,* 37**,** 735-753.

JOHNSON, G. R. & COOK, W. H. 1985. Fracture characteristics of three metals subjected to various strains, strain rates, temperatures and pressures. *Engineering Fracture Mechanics,* 21**,** 31-48.

JOHNSON, W. & MAMALIS, A. G. 1978. *Crashworthiness of Vehicles,* London, Mechanical Engineering Publications Limited.

JONES, N. 1997. *Structural Impact*, Cambridge University Press.

KARAGIOZOVA, D. & JONES, N. 2008. On the mechanics of the global bending collapse of circular tubes under dynamic axial load—Dynamic buckling transition. *International Journal of Impact Engineering,* 35**,** 397-424.

KARRECH, A. & SEIBI, A. 2010. Analytical model for the expansion of tubes under tension. *Journal of Materials Processing Technology,* 210**,** 356-362.

KEELER, S. & KIMCHI, M. 2014. Advanced High-Strength Steels - Application Guidelines Versions 5.0 [Online]. Available: http://www.worldautosteel.org/projects/advanced-high-strength-steel-application-guidelines/ [Accessed 27 November 2015].

KO, Y., AHN, K., HUH, H., CHOI, W., JUNG, H. & KWON, T. 2011. Evaluation of Crash Energy Absorption Capacity of a Tearing Tube. *In:* PROULX, T. (ed.) *Experimental and Applied Mechanics, Volume 6.* Springer New York.

KO, Y. K., LEE, J. S., HUH, H., KIM, H. K. & PARK, S. H. 2007. Prediction of fracture in hub-hole expanding process using a new ductile fracture criterion. *Journal of Materials Processing Technology,* 187–188**,** 358-362.

LU, G. 2002. Energy absorption requirement for crashworthy vehicles. *Journal of Rail and Rapid Transit,* 216**,** 31-39.

LU, G., FAN, H. & WANG, B. 1998. An experimental method for determining ductile tearing energy of thin metal sheets. *Metals and Materials,* 4**,** 432-435.

LU, G., ONG, L. S., WANG, B. & NG, H. W. 1994. An experimental study on tearing energy in splitting square metal tubes. *International Journal of Mechanical Sciences,* 36**,** 1087-1097.

LU, G. & YU, T. 2003. *Energy Absorption of Structures and Materials,* Cambridge, England, Woodhead Publishing Limited.

LU, Y.-H. 2004. Study of tube flaring ratio and strain rate in the tube flaring process. *Finite Elements in Analysis and Design,* 40**,** 305-318.

MAI, Y. W. & COTTERELL, B. 1984. The essential work of fracture for tearing of ductile metals. *International Journal of Fracture,* 24**,** 229-236.

MAMALIS, A. G. & JOHNSON, W. 1983. The quasi-static crumpling of thin-walled circular cylinders and frusta under axial compression. *International Journal of Mechanical Sciences,* 25**,** 713-732.

MAYVILLE, R. 2001. Sleeved column system for crashworthiness of light rail vehicles. *In:* ADMINISTRATION, F. R. (ed.). Transportation Research Board.

MORENO, C., BEAUMONT, R., HUGHES, D. J., WILLIAMS, T. & DASHWOOD, R. 2015. Determination of the fracture behaviour of axial splitting tubes and the numerical prediction of their energy absorption capabilities. *International Journal of Crashworthiness,* 20**,** 191-199.

MULLUR, A. A., MATTSON, C. A. & MESSAC, M. 2003. Pitfalls of the Typical Construction of Decision Matrices for Concept Selection. *41st aerospace Sciences Meeting and Exhibit.* Reno, NV.

NAGEL, G. M. & THAMBIRATNAM, D. P. 2006. Dynamic simulation and energy absorption of tapered thin-walled tubes under oblique impact loading. *International Journal of Impact Engineering,* 32**,** 1595-1620.

OLABI, A. G., MORRIS, E. & HASHMI, M. S. J. 2007. Metallic tube type energy absorbers: A synopsis. *Thin-Walled Structures,* 45**,** 706-726.

PAVLINA, E. J. & VAN TYNE, C. J. 2008. Correlation of Yield Strength and Tensile Strength with Hardness for Steels. *Journal of Materials Engineering and Performance,* 17**,** 888-893.

PRIOR, A. 1994. Applications of implicit and explicit finite element techniques to metal forming. *Journal of Materials Processing Technology,* 45**,** 649-656.

PUGH, S. 1990. *Total design: integrated methods for successful product engineering,* Wokingham, Addison-Wesley.

REDDY, T. Y. & REID, S. R. 1986. Axial splitting of circular metal tubes. *International Journal of Mechanical Sciences,* 28**,** 111-131.

REID, S. R. 1993. Plastic deformation mechanisms in axially compressed metal tubes used as impact energy absorbers. *International Journal of Mechanical Sciences,* 35**,** 1035-1052.

RICE, J. R. & TRACEY, D. M. 1969. On the ductile enlargement of voids in triaxial stress fields. *Journal of the Mechanics and Physics of Solids,* 17**,** 1201-17.

ROWELL, L. F., BRAUN, R. D., OLDS, J. R. & UNAL, R. 1999. Multidisciplinary Conceptual Design Optimization of Space Transportation Systems. *Journal of Aircraft,* 36**,** 218-226.

SCHNEIDER, S. 2002. Design concept and application of highly integrated and lightweight crash components. EST - Eisenbahn-systemtechnik.

SCHOLES, A. 1987. Railway passenger vehicle design loads and structural crashworthiness. *Proceedings of the Institute of Mechanical Engineers,* 201.

SHAKERI, M., SALEHGHAFFARI, S. & MIRZAEIFAR, R. 2007. Expansion of circular tubes by rigid tubes as impact energy absorbers: experimental and theoretical investigation. *International Journal of Crashworthiness,* 12**,** 493-501.

STRONGE, W. J., YU, T. X. & JOHNSON, W. 1983. Long stroke energy dissipation in splitting tubes. *International Journal of Mechanical Sciences,* 25**,** 637-647.

THAKKER, A., JARVIS, J., BUGGY, M. & SAHED, A. 2009. 3DCAD conceptual design of the next-generation impulse turbine using the Pugh decision-matrix. *Materials & Design,* 30**,** 2676-2684.

WIERZBICKI, T. & ABRAMOWICZ, W. 1983. On the crushing mechanics of thin-walled structures. *Journal of Applied Mechanics,* 50**,** 727-734.

WIERZBICKI, T., BAO, Y., LEE, Y.-W. & BAI, Y. 2005. Calibration and evaluation of seven fracture models. *International Journal of Mechanical Sciences,* 47**,** 719-743.

WOOLLEY, M., SCALAN, J. & EVESON, W. 2000. The use of Formal Design Techniques in the Development of a Medical Device. *In:* WILEY (ed.) *Design for excellence: engineering design conference.*

XUE, L. 2007. Damage accumulation and fracture initiation in uncracked ductile solids subject to triaxial loading. *International Journal of Solids and Structures,* 44**,** 5163-5181.

YANG, J., LUO, M., HUA, Y. & LU, G. 2010. Energy absorption of expansion tubes using a conical–cylindrical die: Experiments and numerical simulation. *International Journal of Mechanical Sciences,* 52**,** 716-725.

YI JIN, S., ALTENHOF, W. & KAPOOR, T. 2006. An experimental investigation into the cutting deformation mode of AA6061-T6 round extrusions. *Thin-Walled Structures,* 44**,** 773-786.

ZHANG, X. W., SU, H. & YU, T. X. 2009. Energy absorption of an axially crushed square tube with a buckling initiator. *International Journal of Impact Engineering,* 36**,** 402-417.